HOKKAIDO UNIVERSITY

Title	Relationship between actin plate formation and cytokinesis progression in apical cells of the brown alga Sphacelaria rigidula
Author(s)	青木, 日向子
Degree Grantor	北海道大学
Degree Name	博士(環境科学)
Dissertation Number	甲第15722号
Issue Date	2024-03-25
DOI	https://doi.org/10.14943/doctoral.k15722
Doc URL	https://hdl.handle.net/2115/94531
Type	doctoral thesis
File Information	Hinako_Aoki.pdf

Hokkaido University Collection of Scholarly and Academic Papers : HUSCAP

Relationship between actin plate formation and cytokinesis progression in apical cells of the brown alga *Sphacelaria rigidula*

（褐藻ワイジガタクロガシラ頂端細胞における
アクチンプレート形成と細胞質分裂進行の関係性について）

Hinako Aoki

Division of Biosphere Science,

Graduate School of Environmental Science,

Hokkaido University

Table of contents

Acknowledgement.....2

General Introduction.....4

Chapter 1. Reexamination of cytokinesis with the simultaneous observation of actin plate and new cell partition membrane in *Sphacelaria rigidula* (Sphacelariales, Phaeophyceae)

Introduction.....12

Materials and Methods.....18

Results.....25

Discussion.....33

Chapter 2. Time-lapse observation of actin plate and new cell partition membrane formation in *Sphacelaria rigidula* (Sphacelariales, Phaeophyceae) sporophytes

Introduction.....41

Materials and Methods.....46

Results.....51

Discussion.....62

Summary.....69

Table.....74

References.....75

Plate legends.....86

Acknowledgement

I would like to express my gratitude to many people for their guidance and cooperation in conducting this research.

First of all, I would like to give sincere thanks to my supervisor, Prof. Chikako Nagasato, Muroran Marine Station, Field Science Center for Northern Biosphere, Hokkaido University. She gave me the opportunity to initiate this interesting research, provide knowledge and experiment guidance. I always received warm encouragements from her.

I would like to appreciate to Prof. Yoichiro Hoshino, Field Science Center, for Northern Biosphere, Hokkaido University, Associate Prof. Ryota Uehara, Faculty of Advanced Life Science, Hokkaido University, Assistant Prof. Kensuke Ichihara, Field Science Center for Northern Biosphere, Hokkaido University for their valuable suggestion and critical reading of this thesis.

I would like to appreciate to emeritus Prof. Taizo Motomura and Project Assistant Prof. Yusuke Horinouchi in Muroran Marine Station. They gave me kind discussion and essential advice through this research.

I would like to express my gratitude to Dr. Christos Katsaros, National and Kapodistrian University of Athens, for kindly providing me with the *Sphaceralia rigidula* female gametophytes used in this study.

I appreciate the staff in Muroran Marine Station, Mr. Teruo Tomioka, Ms. Saeko Kitabayashi and Ms. Izumi Tonozaki.

Finally, I would like to express my sincere gratitude to my family who have supported me throughout my student life.

General Introduction

Multicellularity has independently evolved in the five lineages, i.e., animal and fungi in Opisthokonta, green plants including land plants and a part of green algae, red algae in Archaeplastida, and brown algae in Stramenopiles (Cock et al. 2010). For multicellular organisms, cell division at an appropriate position is critical for morphogenesis, and they have developed their own cytokinesis machinery. This contrasts with the process of chromosome replication to segregation, which is largely conserved among various organisms. In animal cells, the equator of a microtubule (MT) array, called a central spindle formed by the mitotic spindle, is coincident with the cell division plane, and cytokinesis progresses from the outside to the inside, relying on a contractile ring mainly composed of actin and myosin (Green et al. 2012). In animal cells, RhoA-GTP contributes to the establishment of the contractile ring through the downstream effectors formin and Rho kinase. Formin forms polymerized nuclei of actin filaments and promotes actin filament growth. Rho kinase phosphorylates the myosin II regulatory light chains to yield myosin II. The actin filaments and myosin II form a contractile ring (Verma et al. 2019). In fungi, the septum is completed by an ingrowth of the plasma membrane, which has been replaced inside the cell by contraction of the actin-myosin ring. In *Neurospora crassa*, a widely used model organism, the anillin-like protein bud site selection protein 4 (BUD-4) functions upstream of the Rho-GTPase RHO-4 and its effectors. BUD-4 is localized as a punctate ring on

the plasma membrane at the site of septum formation and functions in the correct positioning of RHO-4. BUD-3 activates RHO-4, which promotes localization and activation of formin BNI-1 to form contractile rings (Berepiki et al. 2011). In land plant cells, there is no contractile ring, and cytokinesis progresses depending on the phragmoplast, which is composed mainly of MTs and is formed between two separated daughter cells. Cytokinesis progresses as the cell plate formed within the phragmoplast expands from the inside to the outside (Livanos and Müller 2019). In land plant cells, the cytokinesis site corresponds to the position of the preprophase band (PPB) of MTs that appears during the G2 phase (Mineyuki et al. 1988, Gunning and Sammut 1990, Mineyuki 1999, Buschmann and Zachgo 2016). In the Ulvophyceae multicellular algae, cytokinesis is finished by the ingrowth of a furrow of the plasma membrane (Lokhorst and Star 1983, Sluiman et al. 1983). Observation of cytokinesis in vegetative cells of *Urospora neglecta* and *Urospora wormskioldii* using a transmission electron microscope revealed the presence of phycoplast-like MT structures at the leading edge of the invaginating plasma membrane. It is thought that MTs guide the direction of invagination or provide physical strength and protect its tip (Lokhorst and Star 1983). On the other hand, when observing cytokinesis in vegetative cells of *Ulothrix zonata* and *Ulothrix tenuissima* using a transmission electron microscope, MT structures such as phragmoplast and phycoplast were not observed, indicating that MTs are not

involved in the invagination of the plasma membrane (Sluiman et al. 1983). In multicellular and multinucleate green algae, cytokinesis proceeds by the ingrowth of a furrow of the plasma membrane, and the MT band leads to the edge of the furrow (Aruga et al. 1996, Sekida and Okuda 2022). In red algae, cytokinesis proceeds from an ingrowth of the plasma membrane (Ueki et al. 2008). It is not clear what apparatus controls the progression of cytokinesis, but an area densely packed with actin filaments is present beneath the cell membrane before cytokinesis in *Griffithsia pacifica* (Garbary et al, 1992). It is likely that this region is related to cytokinesis.

Brown algae are marine multicellular organisms, and cytokinesis, which is important for maintaining their structure, is driven by MTs and actin. In brown algae, centrosomes have a crucial role in the formation of the bipolar spindle and segregation of daughter chromosomes similar to in animal cells (Bisgrove et al. 1998, Nagasato et al. 1999). During cytokinesis, a plate-like actin structure (actin plate) appears where MTs from the centrosome intersect with each other in the intermediate region between daughter nuclei (Katsaros and Galatis 1992, Nagasato and Motomura 2002a, Bisgrove and Kropf 2004, Nagasato and Motomura 2009). In brown algae, cytokinesis does not proceed when inhibitors that promote depolymerization (cytochalasin B, D, latrunculin B) or stabilization (jasplakinolide) of actin are used, and thus it is clear that actin is involved in cytokinesis (Kropf 1992, Bisgrove and Kropf 1998, Karyophyllis et al. 2000, Hable

et al. 2003, Nagasato and Motomura 2009, Nagasato et al. 2010). MTs may be involved in transporting Golgi vesicles to the division plane during cytokinesis in brown algae (Nagasato and Motomura 2002a), but the role of actin remains unclear.

It had not been defined how cytokinesis proceeds in brown algae, until the process was only clarified in the 2000s by ultrastructural observations using rapid freezing and freeze substitution (Nagasato and Motomura 2002a). Ultrastructural observation using conventional chemical fixation, cytokinesis in brown algae had been reported to proceed by invagination of the cell membrane in *Pylaiella littoralis* (Markey and Wilce 1975), *Fucus vesiculosus* (Brawley et al. 1977), *Mutimo cylindricus* (La Claire 1981), *Sphacelaria tribuloidesi* (Katsaros et al. 1983), and by outgrowth of a new cell partition membrane in *Ascophyllum nodosum* (Rawlence 1973). With the conventional chemical fixation of brown algae, it has been difficult to capture the state of cytokinesis because plasma separation tends to occur, and the internal membrane structure is not preserved well (Nagasato et al. 2018). The state of cytokinesis in brown algae was clarified by using the rapid freeze-substitution method, in which the water inside the cells is replaced with acetone while the cells are instantly freeze-fixed at extremely low temperatures. In the zygotes of *Scytosiphon lomentaria* (Nagasato and Motomura 2002a) and *Silvetia babingtonii* (Nagasato et al. 2010), the apical meristem of *Dictyota dichotoma* (Terauchi et al. 2012), and apical cells of

Halopteris congesta (Nagasato et al. 2017), new cell partitions arise from inside the cell. In contrast, in the apical cells of *Sphacelaria rigidula*, the cell membrane at the dividing plane invaginates into the cell interior, and vesicles are observed to fuse with the invagination (Katsaros et al. 2009). This observation indicates that the ingrowth of the furrow progresses with a supply of vesicles, which differs from other eukaryote's cytokinetic pattern that uses a contractile ring.

Transmission electron microscopy and indirect fluorescence microscopy have revealed that cytokinesis in brown algae (except for *S. rigidula*) proceeds as follows. First, after nuclear division is complete, the intersection of MTs extending from the centrosome near the daughter nucleus becomes the cytokinetic plane (Nagasato and Motomura 2002b, Bisgrove et al. 2003). Golgi vesicles and flat cisternae (flat membrane structures involved in cytokinesis) accumulate at the division plane and fuse to form a membrane, which is the partition of new cells (Nagasato et al. 2010). Cytokinesis is completed by extending the new cell partition membrane to the parent cell wall (Nagasato and Motomura 2002a, Nagasato et al. 2010, Nagasato et al. 2014). A plate-like actin structure (actin plate) appears where MTs from the centrosome intersect with each other in the intermediate region between daughter nuclei (Katsaros and Galatis 1992, Nagasato and Motomura 2002a, Bisgrove and Kropf 2004, Nagasato and Motomura 2009). Pharmacological experiments indicate that actin plate has a crucial role in the progression of cytokinesis in brown

algae (Kropf 1992, Bisgrove and Kropf 1998, Karyophyllis et al. 2000, Hable et al. 2003, Nagasato and Motomura 2009, Nagasato et al. 2010). However, it has not been possible to visualize actin filaments under the electron microscope in brown algae, so it remains unclear how the actin plate is involved in the process of cytokinesis. The reason for this is that actin and new cell partition membrane formation cannot be observed simultaneously. Alternative means are required to observe both actin plate and new cell partition membrane simultaneously.

The dynamics of MTs and actin during cytokinesis of land plants are observed in transformants expressing fluorescent protein-fused tubulin and actin and membrane-staining reagents (Murata et al. 2013, Arima et al. 2018). The following new findings were made: phragmoplasts are composed of MTs of different stability, and it causes a change of MT array according to the development of cell plate (Murata et al. 2013), and actin may work for guidance the phragmoplast to the correct division position memorized by the PPB (Arima et al. 2019). These insights are derived from observations of living cells, and live cell imaging can be an important analytical tool that provides new insights.

In this study, the relationship between the actin plate and the progression of cytokinesis in brown algae was examined to understand the function of the actin plate. *S. regidula*, an apically growing filamentous brown alga, was chosen as the material because the

apical cells in this species show relatively frequent of cytokinesis among brown algae. This species shows a life cycle with an alternation of generation between isomorphic gametophyte and sporophyte (Plate 1: van den Hock and Flinterman 1968). In Chapter 1, the female gametophyte of *S. regidula* (Plate 1f) was used because it divides more frequently than the male gametophyte (Plate 1g).

S. regidula is the only brown alga in which cell membrane invagination at the division plane was observed using the rapid freeze-substitution method and observed using a transmission electron microscope (Katsaros et al. 2009). Chapter 1 first reexamined the directionality of cytokinesis in *S. regidula* using transmission electron microscopy and membrane staining. After establishing the direction of cytokinesis in *S. regidula*, co-staining of the actin plate and membranes was performed in fixed cells to evaluate the relationship between the actin plate and membrane. Based on the results, the function of actin in cytokinesis of brown algae is discussed. Chapter 1 mainly reports the results obtained from fixed cells, but these lacked time-scale information. Therefore, in Chapter 2, time-lapse observations of cytokinesis in living cells were performed. In Chapter 2, *S. regidula* sporophytes were selected (Plate 1a, 1b). Although there is no major external difference between the gametophyte and sporophyte of *S. regidula*, the filament diameter is larger in the sporophyte (van den Hock and Flinterman 1968). In Chapter 2, to observe

cytokinesis in living cells over time, fluorescent probes that label actin and MTs were injected into cells. Sporophytes were selected because they are larger, which would be advantageous when performing microinjections. There are few reports of observing cytokinesis over time in living cells of brown algae, and therefore which fluorescent probes should be used was considered. By observing actin, MTs, and membranes during cytokinesis over time, we were able to clarify the detailed process of cytokinesis.

Chapter 1. Reexamination of cytokinesis with the simultaneous observation of actin plate and new cell partition membrane in *Sphacelaria rigidula* (Sphacelariales, Phaeophyceae)

Introduction

Cytokinesis is the process of physically dividing a cell into two parts to separate the daughter nuclei. The cytokinetic apparatus driving this process consists of the cytoskeleton that has actin and microtubules (MTs) as components. The direction of cytokinesis is one of its important characteristics, as it is closely related to the orientation of the cytoskeleton during division. In animal cells, a contractile ring consisting of actin and myosin is the cytokinesis apparatus, and division progresses centripetally by contraction of this ring at the division plane (Plate 2) (Green et al. 2012). In animal cells, astral and central MTs from centrosomes are involved in determining the division plane (Plate 2a). Astral MTs inhibit furrow formation in areas other than the division plane and allow the cortex at the equatorial plane to contract. The central spindle signals to the cortex at the division plane, promoting furrow invagination (Glotzer 2005, D'Avino et al. 2005, von Dassow 2009). A contractile ring is formed at the division plane, and cytokinesis progresses with its constriction (Plate 2b). As invagination progresses, the midbody, a structure consisting of densely packed antiparallel MTs, is formed at the intercellular bridge and performs the final cell abscission (Plate 2c, d, Glotzer 2009, Green et al. 2012). At this time, the cell partition is

completed not only by constriction of the cell membrane but also by a supply of vesicles.

In land plant cells, the cytokinesis plane coincides with the position of the preprophase band (PPB) that appears in the G2 phase (Plate 3a; Mineyuki et al. 1988, Gunning and Sammut 1990, Mineyuki 1999). PPB is a bundle-like structure of MTs that appears just below the plasma membrane, and actin is also present in this region (Takeuchi et al. 2016). Clathrin-coated pits and vesicles are observed more frequently than in non-PPB regions (Karahara et al. 2009). PPB disappears before nuclear division, and acentrosomal spindles showing barrel-shaped are formed. Cytokinesis progresses through a phragmoplast that appears between daughter nuclei at the late stage of nuclear division (Plate 3b). The phragmoplast consists of MTs and actin that develop perpendicular to the plane of cytokinesis, and Golgi vesicles containing cell wall materials are supplied to construct the cell plate that serves as a partition for new cells (Plate 3b, 3c; Livanos and Müller 2019). The cell plate is formed from the center of the phragmoplast, expands toward the area where the PPB was once located, and completes cytokinesis when it reaches the parent cell wall (Plate 3d). It is speculated that frequent endocytosis in the PPB area may generate a "negative memory" by locally removing membrane proteins (Karahara et al. 2009).

Similar to animals and land plants, actin and MTs play a central role in cytokinesis in brown algae (Plate 4). MTs radially extend from the centrosomes associated with the daughter

nuclei after mitosis toward the cell surface and cytokinetic plane (Nagasato and Motomura 2002b, Bisgrove et al. 2003). The division plane coincides with the intersection of MTs extending from the centrosomes (Plate 4a). At the MT intermingled region, the formation of a plate-like actin structure (actin plate) has been confirmed by indirect immunofluorescence using anti-actin antibodies and fluorescent-conjugated phalloidin (Plate 4b, 4c; Katsaros and Galatis 1992, Karyophyllis et al. 2000, Nagasato and Motomura 2002a, Bisgrove and Kropf 2004, Nagasato and Motomura 2009). Actin is essential for cytokinesis because it does not proceed when cells are treated with actin depolymerizing agents (cytochalasin B and D and latrunculin B) or stabilizing agents (jasplakinolide) (Bisgrove and Kropf 1998, Karyophyllis et al. 2000, Hable et al. 2003, Nagasato and Motomura 2009, Nagasato et al. 2010). However, because actin inhibitors affect all actin filaments, all actin-related cellular activities are disrupted, and it is not possible to evaluate only the function of the actin plate during cytokinesis. After completion of cytokinesis, the actin plate disappears (Plate 4d).

There are two reports on the progression of cytokinesis in brown algae. Progression of cytokinesis by invagination of the plasma membrane has been reported in the plurilocular gametangia of *Pylaiella littoralis* (Markey and Wilce 1975), the zygote of *Fucus vesiculosus* (Brawley et al. 1977), and the apical cell of *Sphacelaria tribuloidesi* (Katsaros et al. 1983). On

the other hand, it has been reported that in vegetative cells of *Ascophyllum nodosum* (Rawlence 1973), cytokinesis progresses by forming a cell plate from inside the cell. These studies were performed using transmission electron microscopy (TEM) and chemically fixed samples . Chemical fixation of a TEM sample often induced detachment between the plasma membrane and cell wall in brown algal cells, and leakage of phenolic compounds from the physodes prevents good preservation of intracellular structures (Clayton and Beaks 1983; Nagasato et al. 2018). Therefore, detailed observation of the membrane structure during cytokinesis using TEM is difficult, and thus the progression of cytokinesis in brown algae is controversial. In 2002, a rapid freezing and freeze-substitution method for TEM samples was established for brown algae, and detailed membrane formation during cytokinesis was revealed (Nagasato and Motomura 2002a, b, Katsaros et al. 2009, Nagasato et al. 2010, Nagasato et al. 2014, Terauchi et al. 2012, Nagasato et al. 2017). Using this method, zygotes of *Scytosiphon lomentaria* (Nagasato and Motomura 2002a), zygotes of *Silvetia babingtonii* (Nagasato et al. 2010, Nagasato et al. 2014), the apical meristem of *Dictyota dichotoma* (Terauchi et al. 2012), and the apical cells of *Halopteris congesta* (Nagasato et al. 2017), showed new cell partition membranes forming from within the cell. TEM observation using the rapid freezing and freeze-substitution method revealed that Golgi vesicles and flat cisternae (flat membrane structures found only in brown algae) fuse at the cytokinetic

plane, forming a new cell partition membrane from inside the cell. However, in the apical cell of *Sphacelaria rigidula*, the plasma membrane at the division plane invaginates, and vesicles accumulate around the invagination (Katsaros et al. 2009). In this species, cytokinesis proceeds centripetally by growing a furrow.

Detailed analysis using electron tomography showed that flat cisternae may originate from the endoplasmic reticulum (ER) (Nagasato et al. 2014). Golgi vesicles and flat cisternae accumulate at the division plane, and the vesicles fuse to the edges of the flat cisternae, forming a membranous sac (MS) through a membranous network. MSs form at several sites in the cytokinetic plane, each fused and expanded to form a new cell partition membrane. Changes in membrane structure during cell plate formation in land plants have been analyzed using electron tomography (Otegui et al. 2001, Otegui and Staehelin 2004, Seguí-Simarro et al. 2004). In land plants, vesicles fuse in the division plane to form a tubulo-vesicular membrane network (TVN) (Otegui and Staehelin 2004; Seguí-Simarro et al. 2004). TVNs form island-like domains in the division plane and then connect to form a tubular network (TN), which forms a tight structure throughout the phragmoplast and expands (Seguí-Simarro et al. 2004). The membrane formation processes in brown algae and land plants share similarities in that membrane formation begins on the division plane and undergoes complex changes in membrane structure (Bisgrove and Kropf

2004, Nagasato et al. 2010, 2014).

The purpose of this study was to investigate the role of the actin plate in cytokinesis in brown algae and to reexamine the directionality of cytokinesis in *S. rigidula*. The role of the actin plate has not been elucidated because actin in brown algae has not been successfully observed at the ultrastructural level and its spatiotemporal relationship with the progression of cytokinesis has not been clarified. Furthermore, simultaneous observation of the actin plate and the division plane using specific fluorescent probes for actin and membrane structures has not been performed. Observing the development of the actin plate as cytokinesis progresses is essential for understanding its role in this process. Furthermore, it is necessary to determine how actin plates are formed in *S. rigidula*, as the cytokinesis pattern differs from that observed in other brown algae. Therefore, in this study, cytokinesis in the apical cells of *S. rigidula* was reexamined. Actin plate formation was observed through simultaneous visualization of the actin plate and the developing cytokinetic plane.

Materials and Methods

Culture

Female gametophytes of *S. rigidula* Kützing (obtained from Dr. Christos Katsaros, National and Kapodistrian University of Athens) were incubated in glass dishes with half-strength Provasoli's enriched seawater (PES) medium (Provasoli 1968) under white light-emitting diodes (LEDs; 20-40 μmol photons m^{-2} s^{-1}) at 15°C under long-day conditions (14 h light: 10 h dark). The medium was replaced once every 7 to 10 days.

Measuring division frequency by time of day

The number of nuclei in the apical cells was counted 2, 5, 8, and 11 h after the start of the light period, and 2, 5, 8, and 11 h after the start of the dark period. The cells were treated with a culture medium containing 10 μg mL^{-1} FM4-64FX (Molecular Probes, Thermo Fisher Scientific, Eugene, OR, USA; stock solution of 1 mg mL^{-1} in distilled water), which stains cell membranes, for 30 min. Subsequently, fixation and nuclear staining were performed using culture medium containing 4% paraformaldehyde (Electron Microscopy Sciences, PA, Hatfield, USA), 10 μg mL^{-1} FM4-64 FX, and 0.01% SYBR Green I (TaKaRa, Shiga, Japan). At each time point, 100 apical cells were randomly selected and the number of nuclei per cell was counted. The experiment was performed three times, and the average value of the three results was calculated. An Olympus epifluorescence

microscope (BX53; Olympus Optical, Tokyo, Japan) fitted with a CCD camera (AxioCam 305 color; Zeiss, Oberkochen, Germany) was used for observation.

Inhibitor treatment

Brefeldin A (BFA; Sigma, MO, St. Louis, USA) was used to delay cytokinesis progression. BFA inhibits the transport between ER and the Golgi apparatus. BFA was stored in ethanol at 5 mg mL^{-1}; it was diluted to 0.5 μg mL^{-1} with culture medium before use. The temperature and lighting conditions during inhibitor treatment were as previously mentioned, and cultivation with BFA was performed during the light period.

To determine the effective concentration of BFA for the progression of cytokinesis, *S. rigidula* filaments were cultured in a medium containing 0.1, 0.5, and 1.0 μg mL^{-1} BFA, and FM4-64 and SYBR green I staining was performed to evaluate the progress of mitosis and cytokinesis.

Membrane staining of living cells

To observe the course of cytokinesis, the cells were treated with culture medium containing 10 μg mL^{-1} FM4-64FX for 10 min. Images were captured at 1-min intervals using an Olympus epifluorescence microscope (BX53; Olympus Optical, Tokyo, Japan) fitted with a CCD camera

(AxioCam 305 color; Zeiss, Oberkochen, Germany).

Double staining of the actin plate and the new cell partition membrane

Double staining with Alexa Fluor 488-phalloidin (Invitrogen, Carlsbad, CA, USA) and FM4-64FX was performed to simultaneously observe actin plate development and cytokinesis progression. The cells were incubated in culture medium containing 10 μg mL^{-1} FM4-64FX for 30 min and then fixed with 4% paraformaldehyde (Electron Microscopy Sciences, Hatfield, UK) in culture medium containing 10 μg mL^{-1} FM4-64FX for 15 min. After fixation, the cells were incubated with 2.5% Alexa Fluor 488-phalloidin in culture medium containing 0.01% Triton X-100 (used to improve the permeability of phalloidin into cells) and 10 μg mL^{-1} FM4-64FX for 30 min. Finally, for the triple staining of actin, membrane structure, and nuclei, the cells were stained with 0.5% 4′,6-diamino-2-phenylindole (DAPI) in culture medium containing 10 μg mL^{-1} FM4-64FX for 10 min. Fluorescence of FM4-64FX may not be retained owing to immobilization or surfactant treatment. To resolve this issue, cell membranes were labeled with FM4-64FX before fixation. FM4-64FX was then added to all solutions used during fixation and nuclear staining.

The cells were observed under an Olympus epifluorescence microscope (BX53). Images

were captured using a CCD camera (AxioCam 305 color; Zeiss). Some samples were observed using confocal laser scanning microscopy (TCS-SPE; Leica, Wetzlar, Germany). In confocal laser microscopy (TCS-SPE; Leica), DAPI, Alexa Fluor 488, and FM4-64FX were excited at 488, 532, and 635 nm, respectively, and detected in the ranges of 420–470, 500–550, and 560–650 nm, respectively. The acquired digital images were converted to tiff format. Image processing was performed using ImageJ (Fiji, Schindelin et al. 2012).

Transmission electron microscopy

Cryofixation and freeze-substitution were performed as previously described (Nagasato and Motomura 2002a). Gametophytes were cut into short filaments using a razor before fixation. The shortened filaments with the apical region were placed on a gel support film (ATTO, Tokyo, Japan) and cut into triangles with sides of 1 cm. The samples on the gel support films were rapidly frozen by sinking them into liquid propane (precooled to −180°C using liquid nitrogen) and then immediately transferred into liquid nitrogen. They were then transferred into cooled acetone (−85°C) containing 2% osmium tetroxide in serum tubes and were stored at −85°C for 2 days. Next, samples were incubated at −20°C for 2 h and at 4°C for 2 h. Finally, the temperature of the fixative was gradually allowed to rise to room temperature. Samples detached from the films were

washed several times with acetone at room temperature and infiltrated with Spurr's low-viscosity epoxy resin (Polysciences, Warrington, PA, USA). The resin-infiltrated samples were placed on aluminum foil dishes at 60°C overnight for polymerization. Serial sections were prepared using an Ultracut ultramicrotome (Reichert-Jung, Vienna, Austria) and mounted on formvar-coated slot copper grids. The sections were stained using an EM Stainer (Nisshin EM, Tokyo, Japan) and lead citrate (Reynolds 1963). Observations were made using a JEM-1011 electron microscope (JEOL, Tokyo, Japan).

Indirect immunofluorescence microscopy

A fixative solution was prepared by adding 0.1% glutaraldehyde (TAAB Laboratory Equipment, Aldermaston, Berkshire, UK), 3% paraformaldehyde (Electron Microscopy Sciences), and 4% NaCl to the PHEM buffer: 60 mM PIPES (piperazine-1,4-bis (2-ethanesulfonic acid)), 25 mM HEPES (2-[4- (2-hydroxyethyl) -1-piperazinyl] ethanesulfonic acid)), 10 mM EGTA (ethylene glycol tetraacetic acid), and 2 mM $MgCl_2$, pH 7.5. A washing solution was prepared by mixing PHEM buffer containing 2% NaCl and phosphate-buffered saline (PBS; 137 mM NaCl, 2.7 mM KCl, 4.9 mM Na_2PO_4, and 1.5 mM KH2PO4, pH7.4; Sigma) at a ratio of 1:1.

Samples were fixed in a fixative solution for 30 min at room temperature. The samples

were then washed with washing solution. Subsequently, the samples were treated with 0.5% *Trichoderma reesei*-derived cellulase (Sigma) in washing solution. Samples were washed after cellulase treatment and mounted on a 1 mg mL^{-1} poly-L-lysine (Sigma) coated cover glass. The sample was slightly crushed between a coverslip and a glass slide to facilitate antibody penetration. Samples were then treated with PBS containing 5% Triton X-100 for 30 min at room temperature and washed three times with PBS. To prevent nonspecific fluorescence of glutaraldehyde, samples were treated in 0.1% $NaBH_4$ diluted by PBS for 20 min at room temperature and washed three times with PBS. The samples were then incubated in blocking solution (2.5% skim milk, 5% normal goat serum, and 0.05% NaN_3 in PBS) for 30 min at room temperature. Afterward, samples were incubated for 90 min at room temperature with a mixture of anti-α-tubulin polyclonal antibody (rabbit; Sigma; diluted 1:200 in PBS) and anti-actin monoclonal antibody (mouse; C4; MP Biomedicals Inc., Solon, Ohio, USA; diluted 1:400 in PBS) and rinsed in PBS. Samples were incubated for 60 min at room temperature with FITC-conjugated goat anti-mouse IgG and rhodamine-conjugated goat anti-mouse IgG (Sigma; diluted 1:50 in PBS). Samples were washed with PBS several times, stained for 10 min at room temperature with DAPI (0.5 μg mL^{-1} in PBS), and rinsed with PBS. Samples were finally mounted with Mowiol 4-88 mounting medium (Osborn and Weber 1982) containing 0.2% p-phenylenediamine.

The cells were observed under an Olympus epifluorescence microscope (BX53). Images were captured using a CCD camera (AxioCam 305 color; Zeiss). Some samples were observed using confocal laser scanning microscopy (TCS-SPE; Leica). In confocal laser microscopy (TCS-SPE; Leica), DAPI, FITC, and rhodamine were excited at 488, 532, and 635 nm, respectively, and detected in the ranges of 420–470, 500–550, and 560–650 nm, respectively. The acquired digital images were converted to tiff format. Image processing was performed using ImageJ (Fiji, Schindelin et al. 2012).

Results

Morphological analysis of S. rigidula

S. rigidula showed a branched filament form (Plate 5a) with a large dividing cell at the tip (Plate 5b, 5c, 5d). An apical cell contains more chloroplasts than other cells. Cytokinesis was observed using time-lapse observation in the apical cell and the second cell from the apex (Plate 6). Both the apical cell and the second cell from the apex had one nucleus (Plate 6a, asterisks). At 40 min after Plate 6a, the second cell from the apex underwent nuclear division and had two nuclei (Plate 6b). At 180 min after Plate 6b, nuclear division occurred in the apical cell, resulting in a cell with two nuclei (Plate 6c). At this time, a division plane was formed in the second cell from the apex (Plate 6c, white arrow). At 270 min after Plate 6c, a division plane was formed in the apical cell (Plate 6d, white arrowhead), and cytokinesis was completed in the second cell from the apex (Plate 5d, white arrow). At 660 min after Plate 6d, cytokinesis was completed in the apical cell (Plate 6e, white arrow). The cells at the apical part including the first and second cells from apex of *S. rigidula* were used for subsequent experiments because they were actively dividing.

Frequency of cytokinesis by time of day

To increase the efficiency of the work, it was important to determine the time of day when cytokinesis was frequent under the culture conditions. The number of nuclei within the cells was

counted using SYBR Green I and FM4-64 FX was simultaneously used for confirming the cell boundary (Plate 7). When a membrane labeled with FM4-64FX was observed between the nuclei, the case was counted as a cell at the one-nucleus stage (Plate 7a-7c). The cells in which no membrane structure labeled with FM4-64FX was observed and each cell had two nuclei were counted as cells in the two-nuclear stage (Plate 7d-7f). In addition, there were cells in which a membrane structure in the process of formation was observed on the division plane (Plate 7g-7i). Because these cells were in the process of cytokinesis, they were counted as binucleate cells. This experiment revealed that, regardless of the light and dark periods, approximately 60% of the cells had one nucleus (Plate 8, black area), and the remaining had two nuclei (Plate 8, gray area). The frequency of cytokinesis remained the same regardless of when the experiment was carried out.

Formation of a new cell partition in living cells observed by time-lapse microscopy

Cytokinesis in *S. rigidula* proceeds centrifugally by invagination of the plasma membrane (Katsaros et al 2009). To reinvestigate the directionality of cytokinesis in *S. rigidula*, the formation of a new cell partition membrane was observed over time using FM4-64FX in living cells (Plates 9, 10; n = 3). A FM4-64FX-labeled membrane was found on both sides of the cytokinetic plane throughout the observations (Plate 9b, 9e, 9h, Plate 10b, 10e, 10h). However,

this area remained within the cortical region. In addition to the plasma membrane, accumulation of FM4-64FX-labeled membranes was observed on the left (Plates 9a-9c), center (Plate 9d-9f, 1 min later), and right (Plate 9g-9i, 2 min later) of the division plane. In another cell (Plate 10), a faint accumulation of FM4-64FX-labeled membranes other than the plasma membrane was observed in the division plane (Plate 10a-10c). The fluorescent intensity increased and spread over the entire division plane (Plate 10d-10f, 3 min later; Plate 10g-10i, 6 min later).

Ultrastructural observation of a new cell separation membrane in the cytokinetic plane

The progression of cytokinesis was observed using TEM (Plates 11, 12). Consistent with a previous study, plasma membrane furrowing was observed at the plasma membrane around the cytokinesis plane (Katsaros et al. 2009; Plate 11a, 11b, 11e, 11g, 11h). Small MSs formed by the fusion of flat cisternae and Golgi vesicles were observed in the middle of the cytokinetic plane (away from the furrowing), and Golgi vesicles and flat cisternae were lined up around them (Plate 11a, 11c, 11d). Plate 11e-11h shows another section of the same cell as in Plate 11a-11d. A large MS with many perforations was surrounded by numerous Golgi vesicles and flat cisternae (Plate 11e, 11f). The junction of MS and the invagination was not detected even when observing consecutive sections. In contrast to observations in a previous study (Katsaros et al, 2009), no

accumulation of Golgi vesicles and flat cisternae was observed near the furrowing (Plate 11a, 11b, 11e, 11g,11 h). A lack of connection between the furrow and the MS was also observed in another cell (n = 2).

BFA inhibits the transport between the ER and the Golgi apparatus, suppressing the supply of Golgi vesicles to the cytokinetic plane. In brown algae, inhibition of cytokinesis has been observed in the zygotes of *Fucus distichus* (Shaw and Quatrano 1996, Belanger and Quatrano 2000), *Scytosiphon lomentaria* (Nagasato and Motomura 2009), and *Silvetia babingtonii* (Nagasato and Motomura 2019) by BFA treatment.

Cytokinesis was observed using BFA at a concentration and treatment time that did not completely inhibit cytokinesis (Plate 12). This experiment was conducted to determine whether membrane furrowing development occurs when membranous structure formation is delayed. MSs with many membrane perforations were observed in the middle of the division plane, surrounded by several Golgi vesicles (Plate 12a–12d). The degree of division progression differed according to the position observed. Plate 12e and 12f show areas with further expansion and fusion of MSs compared to Plate 12a–12d of the same cell. At an advanced cytokinesis level, the number of membrane perforations on the MSs decreased, and the MSs became flat with some tubular microchannels remaining (Plate 12e, 12f). These channels corresponded to pre-plasmodesmata

(Terauchi et al. 2012, Nagasato et al. 2017). In contrast to untreated cells (Plate 11), the number of flat cisternae observed around the cytokinetic plane decreased. Although furrows of the plasma membrane arose on both sides of the cytokinetic plane (Plate 12a, 12c, 12e, 12f), inward growth was not observed even when cytokinesis was delayed by BFA treatment. One more cell showing the same condition as in Plate 12 was observed.

Ultrastructural analysis of cytokinesis in untreated and BFA-treated cells revealed that inward development of membrane furrowing did not occur, and MSs were formed from inside the cells and spread over the cytokinetic plane. These results are consistent with the results obtained by time-lapse observation of membrane formation in living cells using FM4-64 FX (Plates 9, 10).

Observation of cytokinesis using indirect immunofluorescence microscopy

To observe the orientation of the cytoskeleton during cytokinesis, indirect immunofluorescence was performed using anti-α-tubulin and anti-C4 actin antibodies (Plate 13). In interphase cells, centrosomes were positioned at opposite sides of the nucleus, and MTs emanated from the two centrosomes over the cytoplasm (Plate 13a-13c). In metaphase, MTs from the centrosomes were concentrated in the spindle region (Plate 13d-13f). When the nuclear division was completed, MTs from the two centrosomes radiated toward the cortical region or intersected in the

intermediate region of the daughter nuclei (Plate 13g-13i). Structures that positively reacted with anti-C4 actin antibody were not observed until completion of mitosis. An actin plate was then formed at the MTs crossing region (Plate 13j-13l). The actin plate disappeared after cytokinesis.

In cells treated with 0.5 $\mu g\,mL^{-1}$ BFA, the orientation of the cytoskeleton during cytokinesis was investigated using indirect immunofluorescence microscopy (Plate 14). The orientation pattern of MTs and the timing of actin plate appearance were the same as in control cells. However, in BFA-treated cells, many cells showing actin plates that had not reached the mother cell wall were observed, which was hardly seen in the untreated sample (Plate 15). In those cases, the MTs were connected to the edges of the actin plate in the process of expansion (Plate 15a-15c). This is thought to result from the inhibitor slowing down cytokinesis by disrupting the supply of Golgi vesicles needed to build a new cell separation membrane. The same cell as in Plate 15a-15c was observed using confocal laser scanning microscopy, and the MT array toward the actin plate was confirmed (Plate 15d-15f). MTs were tightly bound to the edges of the developing actin plate.

Simultaneous observation of actin plate and new cell partition membrane

To investigate the relationship between actin plate development and new cell partition membrane

formation, simultaneous visualization of actin plate and new cell partition membrane using Alexa Fluor 488-phalloidin and FM4-64FX was performed. Immediately after mitosis and before the onset of cytokinesis, no fluorescent signals from actin or labeled FM4-64FX indicating membrane structures were observed (Plate 16a-16c). At a later stage of cytokinesis, a small actin plate appeared between the two daughter nuclei, and a membrane structure of the same size as the actin plate appeared in the same position (Plate 16d-16f). At advanced stages of cytokinesis, the actin plate and new cell partition membrane expanded (Plate 16g-16i). The actin plate and new cell partition membrane in the process of formation were also observed in three other cells. The structures did not develop uniformly in a circular shape, but the time to reach the cell wall varied depending on their location. Eventually, the actin plate and new cell partition membrane expanded across the division plane, completing the new cytokinetic plane (Plate 16j-16l). To investigate the possibility that Alexa Fluor 488-phalloidin or FM4-64FX fluorescence leaked into different fluorescent cubes, staining with Alexa Fluor 488-phalloidin or FM4-64FX alone was performed. This experiment confirmed that the signals of Alexa Fluor 488-phalloidin and FM4-64FX did not overlap (data not shown).

The formation of the actin plate and the development of a new cytokinetic plane were also observed in BFA-treated cells whose membrane formation was inhibited (Plate 17). After

treatment with BFA, cells with actin plates of different sizes and new cell partition membranes were frequently observed (Plate 17). Epifluorescence microscopy analysis often showed that the actin plate was slightly larger than the membrane structure labeled with FM4-64FX (n = 24). However, under confocal laser scanning microscopy observation, the Alexa Fluor 488-phalloidin fluorescence signal and FM4-64FX-labeled membrane structure appeared to be of similar size (Plate 18). In addition, the actin plate did not expand across the division plane without new cell partition membrane formation.

Discussion

Actin plate and flat cisternae are characteristic structures during cytokinesis in brown algae (Nagasato and Motomura 2002a, Katsaros and Galatis 1992, Bisgrove and Kropf 2004, Nagasato and Motomura 2009). Inducing actin depolymerization and stabilization inhibits the progression of cytokinesis (Kropf 1992, Bisgrove and Kropf 1998, Karyophyllis et al. 2000, Hable et al. 2003, Nagasato and Motomura 2009, Nagasato et al. 2010) and the formation of flat cisternae (Nagasato and Motomura 2009, Nagasato et al. 2010). Two types of membrane structures, Golgi vesicles and flat cisternae, are involved in the formation of the cytokinetic plane in brown algae, and a new cell partition membrane formation is initiated by the fusion of Golgi vesicles with the edges of the flat cisternae (Nagasato et al. 2010, Nagasato et al. 2014). Electron tomography showed that flat cisternae form from the ER, and that MTs oriented parallel to the ER may be involved in the process. In addition, actin is thought to participate in the formation of flat cisternae (Nagasato et al. 2014). However, actin inhibitors block not only actin plate formation but also the function of actin filaments throughout the cell, and thus other analytical methods were needed to reveal actin plate function. Therefore, in this study, cytokinesis was observed in cells treated with BFA, a membrane formation inhibitor (Shaw and Quatrano 1996, Belanger and Quatrano 2000, Nagasato and Motomura 2009, 2019). In addition to the functional analysis of actin plate, the cytokinesis pattern of *S. rigidula* was investigated by observing cytokinesis during BFA treatment.

Establishment of a synchronous cell cycle system leads to improved experimental efficiency in the study of cytokinesis. In tobacco (*Nicotiana tabacum*) BY-2 cells, treatment with aphidicolin, a specific inhibitor of DNA polymerase α, synchronizes the cell cycle at a high rate of approximately 70% (Nagata and Kumagai 1999). Cell cycle synchronization of *S. rigidula* with aphidicolin treatment was attempted but was unsuccessful (data not shown). However, the present study was conducted because cell division occurred in *S. rigidula* regardless of light and dark periods.

In this study, the pattern of cytokinesis (centripetal or centrifugal) in *S. rigidula* was investigated by live cell imaging of membrane formation and ultrastructural observation by TEM. Plate 19 shows the cytokinetic patterns of brown algae in the zygotes of *Scytosiphon lomentaria* (Nagasato and Motomura 2002a), the zygotes of *Silvetia babingtonii* (Nagasato et al. 2010, Nagasato et al. 2014), the apical meristem of *Dictyota dichotoma* (Terauchi et al. 2012), the apical cells of *H. congesta* (Nagasato et al. 2017), (Plate 19a-19e) and *S. rigidula* (Plate 19f-19j). In *S. rigidula*, the furrow appears in the plasma membrane at the cytokinetic plane at the beginning of cytokinesis (Plate 19f). However, the ingrowth of the cleavage furrow was not observed. Cytokinesis in *S. rigidula* was achieved by the growth of MS, originating from a membranous network formed by the fusion of Golgi vesicles and flat cisternae (Plate 19g-19i), as observed in

other brown algae by rapid freezing and freeze-substitution (Nagasato and Motomura 2002a, Katsaros et al. 2009, Nagasato et al. 2010, Terauchi et al. 2012, Nagasato et al. 2017).

In *S. rigidula*, vesicle accumulation and fusion at the edge of furrows lead to the inward development of the cytokinetic plane (Katsaros et al. 2009). In this study, time-lapse observation of cells stained with FM4-64FX (Plates 9, 10) showed that the cleavage furrow was stained compared to other regions of the plasma membrane. Therefore, the furrow was formed by the fusion of vesicles to the plasma membrane. However, the cleavage furrow did not develop inward through cytokinesis. Ultrastructural analysis showed the occurrence of small MSs in the cytokinetic plane, and fusion was not uniform across the cytokinetic plane (Plates 11, 12). AS observed in a previous study (Katsaros et al. 2009), a portion of the MS formed near the edge of the cytokinetic plane may have fused into the furrow. Time-lapse observations using FM4-64FX and double staining of actin plates and new cell partition membrane using fluorescent phalloidin and FM4-64FX during cytokinesis support this result. In the present study, it was confirmed that cytokinesis in brown algae proceeded by centrifugal expansion as observed by TEM using the rapid freeze-substitution method (Nagasato and Motomura 2002a, Katsaros et al. 2009, Nagasato et al. 2010, Terauchi et al. 2012, Nagasato et al. 2017). The cytokinesis apparatus and membrane components to build a new division plane in brown algae differ from those in land plants

(Nagasato and Motomura 2002a, Otegui and Staehelin 2004, Seguí-Simarro et al. 2004, Nagasato et al. 2010, 2014, Smertenko et al. 2017). However, there are common features between the two groups, such as the transportation of Golgi vesicles via MTs and changes in membrane configuration to form a new cell partition plane. The present study showed that there are currently no exceptions to this scenario in brown algae.

To reveal the function of the actin plate, a structure specific to cytokinesis in brown algae, the spatiotemporal relationship between the new cell partition membrane and the actin plate was investigated (Plates 16-18). Alexa Fluor 488-phalloidin and FM4-64FX were employed simultaneously to evaluate the actin plate and new cell partition membrane. Phalloidin only penetrates fixed cells and labels actin filaments. Although there have been reports of the morphology of actin plates in brown algae using fluorescent phalloidin and anti-actin antibodies (Brawley and Robinson 1985, Kropf et al. 1989, Bouget et al. 1996, Alessa and Kropf 1999, Karyophyllis et al. 2000, Hable et al. 2003, Bisgrove and Kropf 2004), this study is the first to simultaneously observe actin plate and formation of the new cell partition membrane. The results showed that the actin plate arose at the center of the cytokinetic plane before the formation of a new cell partition membrane. Expansion of actin plates synchronously progressed according to the outgrowth of a new cell partition membrane. There are two possible functions of actin plates

during cytokinesis. The first is to fuse Golgi vesicles and flat cisternae for the development of MS. The second is to guide the developing MS to the mother cell wall and complete cytokinesis. The results of the present study support at least the latter.

In land plants and brown algae, cytokinesis proceeds by membrane fusion from inside the cytokinetic plane. The phragmoplast, composed of MTs, actin, and Golgi vesicles, expands toward the parent cell wall as the cell plate grows. Disruption of actin filaments by bistheonellide A, an actin depolymerizer, delays cell plate growth (Higaki et al. 2008). However, cytokinesis is eventually completed. Actin cables connecting the cortical division zone (where the PPB is located) and the phragmoplast were observed in centrifuged cells (Arima et al. 2018). This structure may be involved in the expansion of the cell plate toward the cortical division zone. Although the distribution of actin differs between brown algae and land plants, its functions may be similar.

BFA inhibits vesicle transportation between the ER and Golgi cisternae, which affects the Golgi apparatus' structure and function. In land plants treated with BFA, the supply of Golgi vesicles to the cytokinetic plane is insufficient, and the formation of the cell plate is delayed (Yasuhara et al. 1995, Yasuhara and Shimaoka 2000, van Oostende-Triplet et al. 2017). In the present study, cytokinesis was observed in *S. rigidula* under BFA treatment, confirming that even

if cytokinesis was delayed owing to an insufficient supply of Golgi vesicles, inward development of furrowing did not occur. In brown algae, the effects of BFA on cytokinesis have been reported in *Scytosiphon lomentaria* zygotes and fucoid zygotes (Belanger and Quatrano 2000, Nagasato and Motomura 2009, Nagasato and Motomura 2019). In *Scytosiphon lomentaria* zygotes, cytokinesis progresses even under BFA treatment, but no deposition of cell wall components is observed (Nagasato and Motomura 2009). On the other hand, ultrastructural studies of *Silvetia babingtonii* zygotes under BFA treatment showed that no or only some membrane fusion occurs to form new cell cross walls (Nagasato and Motomura 2019). The purpose of BFA treatment in the present study was the following two points: ⅰ) delay cytokinesis and observe more dividing cells and ⅱ) confirm that furrowing does not grow inward under any conditions. In *S. rigidula* cells treated with BFA for 6 h, cytokinesis progressed more slowly than in untreated cells, and some cells showed incomplete cytokinesis. Cytokinesis progressed gradually during BFA treatment likely because Golgi vesicles were supplied to the cytokinetic plane before treatment. Therefore, membrane fusion to form a new cell partition membrane had progressed to some extent. However, the amount supplied was insufficient to complete the cytokinesis plane, and partial formation was observed.

In land plants, the phragmoplast, which is composed of MTs and actin, serves as the

division apparatus and is involved in the formation and expansion of the cell plate. Phragmoplast has a cylindrical shape when Golgi vesicles that have accumulated at the cytokinetic plane begin to fuse. As the fusion of Golgi vesicles progresses and the cell plate develops, the MTs inside the phragmoplast depolymerize and change into a donut shape surrounding the cell plate (Smertenko 2018). During cytokinesis in brown algae, no significant changes in MT orientation associated with new cell partition membrane expansion were observed. However, when new cell partition membrane formation was delayed in BFA-treated cells, MTs were linked to the edge of the expanding actin plate (Plate 15). This phenomenon has also been observed in *S. babingtonii* zygotes treated with BFA (Nagasato and Motomura 2019). This result indicates that actin plates and MTs are associated and that the orientation of MTs changes as the actin plate expands. In this study, changes in the orientation of the cytoskeleton and the relationship between the actin plate and the new cell partition membrane during cytokinesis were observed in fixed cells. Time-lapse observation of cytokinesis in living cells may reveal changes in the orientation of MTs associated with the development of the actin plate and new cell partition membrane.

In this study, the cytokinesis pattern of *S. rigidula* was re-examined and shown that cytokinesis proceeded by the outgrowth of a new cell partition membrane, similar to other brown algae. The occurrence of a plasma membrane furrow was also confirmed; however, further inward

progression of cytokinesis was not observed. No structure causing furrowing of the plasma membrane, such as actin, was found. At present, this is the only described example of a furrow initially formed but not further developed during brown algae cytokinesis. A similar cytokinesis pattern is observed in the evolution of aquatic streptophyte algae to terrestrial plants (Buschmann and Zachgo 2016). In the green alga *Spirogyra* sp., cytokinesis is accomplished by ingrowing furrows and developing a cell plate (Fowke and Pickett-Heaps 1969). In *Coleochate scutata*, cytokinesis is completed by the fusion of small cell plates to the furrows (Marchant and Pickett-Heaps 1973). Furrows were not observed in *Halopteris congesta*, which belongs to Sphacelariales (Nagasato et al. 2017). Further investigation is needed to determine whether furrows are a remnant of the primitive character of cytokinesis in brown algae or are a specific feature of the *Sphacelaria* genus.

Chapter 2. Time-lapse observation of actin plate and new cell partition membrane formation in *Sphacelaria rigidula* (Sphacelariales, Phaeophyceae) sporophytes

Introduction

Brown algal cells have a pair of centrioles throughout the life cycle. In vegetative cells, MTs mainly elongate from the periphery of the centrosome. During mitosis, centrosomes are positioned at the poles of the nucleus and participate in the bipolar spindle and the separation of daughter nuclei (Bisgrove et al. 1998, Nagasato et al. 1999). The cytokinesis plane of brown algae coincides with the intersection of MTs extending from the centrosome near the daughter nucleus (Nagasato and Motomura 2002b, Bisgrove et al. 2003). Golgi vesicles necessary for the formation of a new cell partition membrane are transported to the division plane by MTs (Nagasato and Motomura 2002a, Nagasato et al. 2010). During cytokinesis in brown algae, actin appears as an actin plate at the division plane (Katsaros and Galatis 1992, Nagasato and Motomura 2002a, Bisgrove and Kropf 2004, Nagasato and Motomura 2009). Actin plate is unique structure observed only in brown algal cytokinesis among eukaryotes. The function of the actin plate in brown algal cytokinesis has been unknown, however, simultaneous visualization of actin and membrane structure during cytokinesis in *Sphacelaria rigidula* showed that actin plate and new cell partition membrane co-localized, indicating that actin plate may be involved in new cell partition membrane formation (Plates 16-18; Aoki et al. 2023). Furthermore, in the zygotes of

Silvetia babingtonii (Nagasato and Motomura 2019) and the apical cell of *S. rigidula* (Plate 15; Aoki et al. 2023), MTs were observed to concentrate at the edges of the expanding actin plate when new cell partition membrane formation was delayed by BFA treatment. It has been suggested that MTs are involved in the formation of the actin plate.

Knowledge of cytokinesis in brown algae was mainly obtained from fixed cells, and there are few examples of time-lapse observation of living cells. In contrast, there are many examples of time-lapse observation of cytokinesis using living land plant cells. Murata et al. (2013) used tobacco (*Nicotiana tabacum*) BY-2 cells to observe the behavior of the phragmoplast during cytokinesis in living cells over time. This study focused on the morphological changes during phragmoplast expansion and revealed that MT stability is high at the leading edge of the phragmoplast and depolymerization rates are high at the trailing edge.

This is thought to contribute to improving the stability of the phragmoplast. In addition, Arima et al. (2018) observed cytokinesis after centrifuging tobacco (*N. tabacum*) BY-2 cells and shifting the position of the phragmoplast: an actin filament cable was observed connecting the edge of the phragmoplast and the cortical division zone (CDZ). Actin filaments accumulate in a band shape within the CDZ during the early stages of cytokinesis and disappear at the end of cytokinesis (Arima et al. 2018). This actin cable may guide the phragmoplast to the correct

position during division as determined by the PPB (Arima et al. 2018). As is clear from these previous studies, time-lapse observation using living cells is useful for observing detailed behavior, including the appearance and disappearance of actin and MTs during cytokinesis. In these previous studies, genetic recombination was used to express fluorescently labeled tubulin and fimbrin (a protein with an actin-binding domain that binds and labels actin filaments) to observe MTs and actin (Murata et al. 2013, Arima et al. 2018). However, the relevant promoter region in the brown algae genome has not been identified, and genetic recombination technology has not been established. Therefore, it is necessary to label the target structure using different methods.

To observe living cells over time, it is necessary to label target structures using a non-destructive method. Many labeling reagents are commercially available, but because brown algae have cell walls, few reagents can be used in living cells without permeabilization. Therefore, it is necessary to introduce reagents directly into cells. An MT dynamics loaded fluorescently labeled tubulin into the early zygotes of *Fucus serratus* by a hydraulic microinjection system (Corellou et al. 2005). Changes in the MT array during rhizoid formation and asymmetrical cell division occur in living cells. In land plant cells, cytokinesis has been observed by microinjecting fluorescent probes. In the endosperm cells of *Haemanthus katherinae*, actin reorganization during

cytokinesis was examined using fluorescently labeled phalloidin (Schmit and Lambert 1990), which revealed that actin is assembled *de novo* during cell plate formation. In *Tradescantia virginiana* stamen hair cells, MTs and filamentous actin (F-actin) were observed in the PPB during prophase using fluorescently labeled tubulin or phalloidin, and PPB disappears just before the breakdown of the nuclear envelope (Cleary et al. 1992). Furthermore, F-actin remains in all cortical regions except the division plane.

Recently, studies using a laser-assisted thermal-expansion microinjection system in brown algae were conducted. For investigation of symplastic translocation via plasmodesmata, fluorescein isothiocyanate (FITC)-dextrans with different sizes were injected into the zygotes of *Fucus distichus* (Nagasato et al. 2015) and the apical cells of *Halopteris congesta* (Nagasato et al. 2017). A laser-assisted thermal-expansion microinjection system was used, making microinjection possible with a small glass needle tip diameter, which reduces damage to the injected cells compared to the hydraulic microinjection. This microinjection system should allow the observation of actin and tubulin behavior during cytokinesis in a less stressful situation for cells.

To observe cytokinesis in living cells over time in brown algae, injecting fluorescent probes into cells using microinjection is considered effective. In this study, actin, MTs, and

membrane structures were observed during cytokinesis by microinjecting fluorescent probes for actin and tubulin and staining membrane structures with FM4-64FX to examine the relationship among actin plates, MTs, and new cell partition membranes. This is the first study to describe the dynamics of cytokinesis in living brown algae cells.

Materials and Methods

Culture

Sporophytes of *S. rigidula* Kützing (KU-1314 strain; purchased from Kobe University Macroalgal Culture Collection) were incubated in glass dishes with half-strength Provasoli's enriched seawater (PES) medium (Provasoli 1968) under white light-emitting diodes (LEDs; 20-40 μmol photons m^{-2} s^{-1}) at 15°C under long-day conditions (14 h light: 10 h dark).

Indirect immunofluorescent antibody

Cryofixation was performed as previously described (Nagasato and Motomura 2002a, Nagasato et al. 2018, 2022). In preparation for immunofluorescence microscopy, Omnipore membrane filters (Merck KGaA, Darmstadt, Germany) were cut into triangles and mounted on 0.3% agarose gels in seawater. Samples were cut apically and placed on the top of Omnipore membrane filters with a drop of culture medium. Before cryofixation, excess water on the Omnipore membrane filter was removed using filter paper, and the samples were quickly frozen using liquid propane that had been previously cooled to −180°C with liquid nitrogen. The samples were then immediately transferred to liquid nitrogen. Subsequently, the samples were substituted in methanol at −80°C for 1 week. Samples were left at room temperature and gradually transferred from methanol to PBS (pH 7.4, Sigma). The Omnipore membrane filters were removed, and the

detached samples were placed on a cover glass coated with poly-L lysine (Sigma). Samples were gently squashed between the slide glass and coverslip to facilitate antibody penetration. These samples were treated with PBS containing 5% Triton X-100 for 30 min at room temperature and washed several times with PBS. Samples were incubated in blocking solution (PBS containing 2.5% skim milk, 5% normal goat serum, and 0.05% NaN_3) for 30 min at 35°C. Then, the samples were incubated with anti-α-tubulin (rabbit; Sigma; diluted 1:200 in PBS) and anti-actin (mouse; C4; MP Biomedicals; diluted 1:400 in PBS) antibodies. After that, free antibodies were washed away with PBS. Samples were incubated with FITC-conjugated goat anti-mouse IgG and rhodamine-conjugated goat anti-mouse IgG (Sigma; diluted 1:50 in PBS) for 60 min at 35°C. Samples were washed several times with PBS. DAPI (0.5 μg mL^{-1} in PBS) staining was performed for 10 min at room temperature and rinsed with PBS. Samples were finally mounted with Mowiol 4-88 mounting medium (Osborn and Weber 1982) containing 0.2% *p*-phenylenediamine. Samples were observed using an Olympus epifluorescence microscope (BX50WI-FLA; Olympus Optical, Tokyo, Japan) equipped with differential interference contrast (DIC). Photographs were taken using a CCD camera (AxioCam, Zeiss, Oberkochen, Germany). Image processing was performed using ImageJ (Fiji; Schindelin et al. 2012).

Microinjection of fluorescent probes using laser-assisted thermal-expansion microinjection

Alexa Fluor 488, Alexa Fluor 555, and rhodamine phalloidin (Invitrogen, USA) were dissolved in methanol, which was evaporated at room temperature for 50 min. It was then diluted with injection solution (20 mM HEPES, 150 mM potassium chloride, pH 7.0; Badis et al. 2021, Shen et al. 2023) to 6.0 μM. Rhodamine-conjugated actin (Cytoskeleton, Denver, CO, USA) was diluted to 0.01 mg mL^{-1} and Fluorescent HiLyte 488-conjugated tubulin (Cytoskeleton, USA) and rhodamine-conjugated tubulin were diluted to 0.65 mg mL^{-1}, respectively, using chilled injection solution to prevent polymerization. All fluorescent probes used for microinjection were centrifuged (16,000 × *g*, 10 min) before loading into glass needles and the supernatant was used. The combinations of fluorescent probes used and the objects observed are shown in Table 1.

A thin glass needle was prepared for injection by pulling a glass capillary (GDC-1; Narishige, Tokyo, Japan) over a micropipette puller (PV-97; Sutter Instrument, USA). Fluorescent probes, silicone oil (Shin-Etsu Chemical, Tokyo, Japan), WF-25 laser absorber (NepaGene, Chiba, Japan), and UV absorber (A-1428; Tesk, Tokyo, Japan) were sequentially loaded into the microinjection needle. The procedure for loading the needle with fluorescent probes was performed at room temperature for phalloidin and on ice for actin and tubulin to prevent polymerization.

The injection equipment has been previously described (Nagasato et al. 2015, 2017, Badis et al. 2021, Shen et al. 2023). The micromanipulator, consisting of an MN-4 coarse manipulator (Narishige) and a MO-202 three-axis joystick oil hydraulic micromanipulator (Narishige), was installed on an Olympus IX71 inverted microscope (Olympus Optical, Tokyo, Japan). Microinjection was performed using a laser thermal microinjector LTM-1000 (NepaGene). After microinjection, cells were stained in culture medium containing 10 μg mL^{-1} FM4-64FX or PlasMem Bright Green (DOJINDO LABORATORIES, Kumamoto, Japan) for 10 min as needed.

Cells were sequentially observed after introduction of the fluorescent probe. Observations were performed in a chamber made with double-sided adhesive tape (Nichiban, Tokyo, Japan) between the glass slide (Fine Frost; Matsunami Glass, Osaka, Japan) and the coverslip (Micro Cover Glass 20 × 20mm; Matsunami Glass) to prevent cell damage (Kinoshita et al. 2016). The culture medium was dropped between the double-sided tape, and the filament containing the microinjected cells was placed into the drop. To prevent drying, the drop of culture medium was surrounded with mineral oil (Sigma) and gently covered with a cover glass (Matsunami Glass). The cells were observed under an Olympus epifluorescence microscope (BX53). Images were captured using a CCD camera (AxioCam 305 color; Zeiss). Some cells were observed using confocal laser scanning microscopy (TCS-SPE; Leica, Wetzlar, Germany).

In confocal laser microscopy, Alexa Fluor 488 and Fluorescent HiLyte 488 were excited at 532 mm and detected in the 500-550 mm range. FM4-64FX and rhodamine were excited at 635 mm and detected in the 560-650 mm range. Image processing was performed using ImageJ (Fiji; Schindelin et al. 2012).

Results

Selection of cells used for microinjection

S. rigidula alternates between isomorphic gametophyte and sporophyte (van den Hock and Flinterman 1968, Plate 1). However, according to van den Hock and Flinterman (1968), the diameter of the filaments differs slightly, with the diameter of the gametophyte being 13.5 to 31 μm, whereas that of the sporophyte is 19 to 41 μm. Microinjection was performed to introduce fluorescent probes to label tubulin and actin and observe the behavior of the cytoskeleton during cytokinesis in living cells. I expected that it might be better to use larger cells to achieve this. The filament thickness between the sporophyte (KU-1314, Plate 20a-20c) and the female gametophyte used in Chapter 1 (Plate 20d-20f) was compared. The results showed that the average diameter of sporophytes (KU-1314) was 36.0 ± 0.84 μm (n = 8) and the average diameter of female gametophytes was 27.2 ± 0.77 μm (n = 8). The sporophyte showed a significantly larger cell diameter than the female gametophyte ($p < 0.05$).The larger diameter of sporophytes was consistent with previous study (van den Hock and Flinterman 1968). Sporophytes were therefore selected for microinjection. Similar to gametophytes, sporophytes possess a large, actively dividing apical tip cell (Plate 20a-20c). This cell contains many chloroplasts in the apex, and the autofluorescence of chloroplasts may interfere when observing fluorescent probes injected into the cell. The frequency of division in the second cell is also higher (Plate 6) and, therefore, the

second cell from the apical end was targeted for microinjection.

Observation of actin and MT orientation during cytokinesis by indirect immunofluorescent microscopy

To determine whether the orientation of the cytoskeleton during cytokinesis in the sporophyte was the same as in the female gametophyte, it was observed using anti-C4 actin and anti-α-tubulin antibodies (Plates 21, 22). In addition to the first apical cell (Plate 21), the cytoskeleton was also observed in the subapical cell (Plate 22). In interphase, MTs extended from the two centrosomes near the nucleus over the cytoplasm (Plates 21a-21c, 22a-22c). After mitosis, MTs from the centrosomes associated with daughter nuclei intersected in the middle of the cell (Plates 21d-21f, 22d-22f). During cytokinesis, actin plates were formed at the locations where MTs intersect (Plate 21g-21i, 22g-22i). The orientation of the cytoskeleton in the first and second apical cells of the sporophyte was similar to that observed in the gametophytes (Plate 13).

Actin plate formation during cytokinesis in living cells

To simultaneously observe actin plates and new cell partition membranes, Alexa Fluor 488-phalloidin was microinjected into cells, which were stained with FM4-64FX to label the plasma

membrane (Plates 23-25, Table 1 No. 1). First, the concentration of phalloidin was determined and its effect on cells was evaluated. Because *S. rigidula* subapical cells take approximately 3 to 4 h to undergo cytokinesis (Plate 6), cytotoxicity was examined in cells injected with phalloidin during this period. Microinjection of Alexa Fluor 488-phalloidin at a concentration of 12 μM or higher inhibited the progression of cytokinesis, and nuclear division did not occur in interphase cells. In cells injected with 6.0 μM Alexa Fluor 488-phalloidin, no delay in cytokinesis was observed compared to the time-lapse imaging results of the second cell from the apex (Plate 5). Fluorescence of Alexa Fluor 488-phaloidin and FM4-64FX was observed in three cells (Plates 23-25).

Plate 23 shows Alexa Fluor 488-phaloidin and FM4-64FX fluorescence immediately after injection in the first series (Plate 23a-23c). Plate 23d-23f, 23g-23i, 23j-23l, and 23m-23o shows the signals 30, 46, 52, and 56 min after the observation in Plate 23a-23c. The fluorescence of Alexa Fluor 488-phalloidin was intensely detected around the injection site, especially the nuclear periphery on one side (Plate 23b, white arrow). Formation of an actin plate was observed near the center of the division plane (Plate 23d-23f, yellow arrowhead). A membrane was formed in the location of the actin plate (Plate 23g-23i, yellow arrow). Expansion of the actin plate and the membrane occurred (Plate 23j-23l), spreading across the division plane (Plate 23m-23o).

Plate 24 shows Alexa Fluor 488-phaloidin and FM4-64FX fluorescence in the second series. Plate 24d-24f, 24g-24i, 24j-24l and 24m-24o shows the signals 60, 100, 120, and 140 min after the observation in Plate 24a-24c. Immediately after injection (Plate 24a-24c), the fluorescence of Alexa Fluor 488-phalloidin was intensely detected around the injection site (Plate 24b, white arrowhead), especially in the nuclear periphery on one side (Plate 24b, white arrow). At the beginning of the observation, the actin plate was already formed at the division plane (Plate 24a-24c, yellow arrowhead) and remained at the division plane (Plate 24d-f) until a membrane was formed from the same position (Plate 24g-24i, yellow arrow). Expansion of the actin plate and the membrane then occurred (Plate 24j-24l). Finally, the actin plate and membrane spread across the division plane (Plate 24m-24o).

Plate 25 shows Alexa Fluor 488-phaloidin and FM4-64FX fluorescence in the third series. Plate 25d-25f, 25g-25i, 25j-25l, 25m-25o, and 25p-25r shows the signals 10, 30, 50, 60, and 70 min after the observation in Plate 25a-25c. Immediately after injection (Plate 25a-25c), the fluorescence of Alexa Fluor 488-phalloidin was intensely detected around the injection site (Plate 25b, white arrowhead), especially in the nuclear periphery on one side (Plate 25b, white arrow). Actin plate formation had not yet started. Formation of an actin plate was observed near the center of the division plane (Plate 25d-25f, yellow arrowhead). A membrane was formed from

the same position as the actin plate (Plate 25g-25i, yellow arrow). The fluorescence of Alexa Fluor 488-phalloidin and FM4-64FX spread faintly across the division plane (Plate 25j-l) but had high intensity at the division plane (Plate 25m-25r).

The morphology of the actin plate and the new cell partition membrane was consistent with the results of simultaneous observation of actin plate and membrane in fixed cells (Plate 16; Aoki et al. 2023). However, microinjected Alexa Fluor 488-phalloidin in living cells labeled the nuclear periphery in addition to the actin plate (Plate 23-25, white arrows), and such images were not observed in fixed cells using Alexa Fluor 488-phalloidin and FM4-64FX (Plate 16; Aoki et al. 2023).

Confocal laser microscopy was used to observe the morphology of the actin plate and membrane inside the cell (Plate 26). The cell observed with an epifluorescent microscope (Plate 26a-26c) was analyzed with a confocal laser scanning microscope (Plate 26d-26k). The scanning images were picked up at 0 μm (Plate 26d, 26e), 2.5 μm (Plate 26f, 26g), 4.0 μm (Plate 26h, 26i), and 5.0 μm (Plate 26j, 26k). The actin plate and the new cell partition membrane were present at the same location inside the living cell (Plate 26d-26k), with the actin plate covering a slightly larger area than the new cell partition membrane (Plate 26j, 26k).

MT orientation during cytokinesis in living cells

To examine the changes in MT orientation during cytokinesis and its contribution to the formation of the new cell partition membrane, HiLyte 488-conjugated tubulin was microinjected into cells, which were stained with FM4-64FX to show the development of a new cell partition membrane (Plates 27, 28; Table 1 No. 2). Simultaneous observation of MTs and membranes using HiLyte 488-conjugated tubulin was performed in two cells. In cells injected with HiLyte 488-conjugated tubulin, no delay in cytokinesis was observed compared to the time-lapse imaging results of the second cell from the apex (Plate 6). HiLyte 488-conjugated tubulin fluorescence was prominently observed in MTs emanating from the centrosomes, and this orientation pattern was similar to that observed in fixed cells (Plates 21, 22). In other words, fluorescent tubulin was polymerized with endogenous tubulins. This method was useful for live cell observations in this species. Immediately after microinjection, no fluorescence was observed around the injection site (Plates 27b, 28b, white arrowheads), and MTs near both centrosomes showed similar fluorescence intensities (Plates 27b, 28b).

Plate 27 shows the first series of observing HiLyte 488-conjugated tubulin and FM4-64FX. Immediately after injection, no membrane structure was observed (Plates 27a-27c). Plate 27d-27f, 27g-27i, 27j-27l, and 27m-27o shows the signals 45, 60, 65, and 70 min after the

observation in Plate 27a-27c. MT plus ends from the centrosomes intermingled at the cytokinetic plane before the formation of the new cell partition membrane (Plate 27d-27i, white arrows). In addition, partial invagination of the division plane was observed (Plate 27f, 27i, yellow arrow). The orientation of MTs extending towards the plasma membrane at the cytokinesis plane was observed (Plates 27e, 27h, 27k, yellow arrowheads). MTs parallel to the division plane were also observed (Plates 27h, 27k). The new membrane formed from the division plane where the MTs were attached, and the new cell partition membrane formed across the division plane (Plate 27j-27l). MTs from each centrosome were detached from the division plane after completion of the new cell partition membrane (Plate 27m-27o).

Plate 28 shows the second series of observing HiLyte 488-conjugated tubulin and FM4-64FX. Plate 28d-28f, 28g-28i, 28j-28l, and 28m-28o shows the signals 30, 50, 60, and 70 min after the observation in Plate 28a-28c. Immediately after injection, no membrane structure was observed (Plate 28a-28c). MTs extending toward the division plane were observed (Plate 28b, 28e, 28h, white arrows) before formation of the new cell partition membrane; however, a partial invagination of the division plane was observed (Plate 28f, 28i, yellow arrows). An orientation of MTs extending towards the plasma membrane at the cytokinesis plane was observed (Plate 28h, 28k, yellow arrowheads). A new membrane was formed from the division plane where the MTs

were bound, and a new cell partition membrane formed across the division plane (Plate 28j-28l). The signal of the formed membrane became clearer (Plate 28m-28o). The MT and terminal connections from each centrosome were resolved after the completion of the new cell partition membrane (Plate 28p-28r).

To investigate the relationship between membrane formation and MTs, rhodamine-conjugated tubulin was microinjected into cells, which were then stained with PlasMem Bright Green (Plate 29; Table 1 No. 3). Plate 29 shows different cells injected with rhodamine-conjugated tubulin. MTs labeled with rhodamine-conjugated tubulin differed from those labeled with HiLyte 488-conjugated tubulin and were not used in the experiment because they were strongly localized near the centrosome and at the division plane.

Formation and development of actin plate and change in MT orientation during cytokinesis

To simultaneously observe actin and MT orientation during cytokinesis, rhodamine-conjugated actin and HiLyte 488-conjugated tubulin were microinjected (Plates 30-32; Table 1 No. 4). First, the concentrations of HiLyte 488-conjugated tubulin and rhodamine-conjugated actin were determined. HiLyte 488-conjugated tubulin did not inhibit cytokinesis or mitosis even when injected into cells at 0.65 mg mL^{-1} or higher. In contrast, when rhodamine-conjugated actin was

injected into cells at 0.04 mg mL^{-1} or higher, the progression of mitosis and cytokinesis was inhibited, probably because of an excess of actin inside cells.

In cells injected with rhodamine-conjugated actin and HiLyte 488-conjugated tubulin, no delay in cytokinesis was observed compared to the time-lapse imaging results of the second cell from the apex (Plate 6). The fluorescence of rhodamine-conjugated actin and HiLyte 488-conjugated tubulin was observed in three cells. HiLyte 488 tubulin fluorescence was observed in MTs from the centrosomes and those appearing parallel to the cytokinesis plane, similar to when it was injected alone. Rhodamine-conjugated actin was observed in intracellular granular structures and was located near the microinjection site, indicating that rhodamine-conjugated actin was not diffused throughout the cell (Plates 31-33c).

Plate 30 shows the first series of observing rhodamine-conjugated actin and HiLyte 488-conjugated tubulin. Plate 30d-30f, 30g-30i, 30j-30l, and 30m-30o shows the signals 20, 30, 35, and 50 min after the observation in Plate 30a-30c. No actin plate was observed at the start of observation (Plate 30a-30c). Even before actin plate formation, MTs were elongating toward the division plane (Plate 30b, white arrow). Rhodamine-conjugating actin molecules appeared to accumulate around the cell membrane at the division surface (Plate 30d-30f, yellow arrowheads). The actin plate formed at the division plane (Plate 30g-30i, yellow arrow) and spread across the

division plane (Plate 30j-30l), and the MT plus end was no longer bound to the division plane (Plate 30m-30o).

Plate 31 shows the second series of observing rhodamine-conjugated actin and HiLyte 488-conjugated tubulin. Plate 31d-31f, 31g-31i, 31j-31l, and 31m-31o shows the signals 30, 50, 70, and 90 min after the observation in Plate 31a-31c. No actin plate formed at the start of observation (Plate 31a-31c). MTs were elongating toward the division plane (Plate 31e, white arrow), and rhodamine-conjugated actin fluorescence was observed throughout the division plane (Plate 31f). The actin plate formed from the center of the division plane (Plate 31i, yellow arrow) and MTs extending toward it (Plate 31h). The actin plate spread across the division plane, and the connection of the MT plus end to the division plane was broken (Plate 31m-31o).

Plate 32 shows the third series of observing rhodamine-conjugated actin and HiLyte 488-conjugated tubulin. Plate 32d-32f, 32g-32i, 32j-32l, and 32m-32o shows the signals 20, 60, 80, and 120 min after the observation in Plate 32a-32c. MTs were elongating toward the formed actin plate (Plate 32e, 32f, white arrow), and expansion of the actin plate was observed. The position of the actin plate appeared to have shifted downward compared to Plate 32i (Plate 32l). The actin plate spread across the division surface, and the connection of the MT plus end to the division surface was broken (Plate 32m-32o).

To observe the actin plate and MTs, the combination of Alexa Fluor 555-phaloidin- and HiLyte 488-conjugated tubulin was used (Plate 33; Table 1 No. 5). However, unlike Alexa Fluor 488-phaloidin, Alexa Fluor 555-phaloidin bound nonspecifically within cells and could not be used for observation (Plate 33). When Alexa Fluor 488-phalloidin alone was microinjected, no granules were observed, suggesting that the fluorescent probe took longer to diffuse into the cells (Plates 23-25). When microinjected with rhodamine-conjugated actin, granular structures were observed within cells (Plates 30-32). Over time, the number of granules decreased. A similar image to that of Alexa Fluor 555-phalloidin was observed when rhodamine phalloidin was microinjected (data not shown).

Discussion

In this study, to investigate the tripartite relationship among the formation of new cell partition membrane, actin plates, and MTs in brown algal cytokinesis, double staining in the following combinations was performed and observed over time with live apical cells of *S. rigidula*: (1) fluorescently labeled phalloidin and FM4-64FX, (2) fluorescently labeled actin and tubulin, and (3) fluorescently labeled tubulin and FM4-64FX. In brown algae, only one study described MT orientation in living cells of *Fucus* zygotes using rhodamine-conjugated tubulin (Corellou et al. 2005), and MT arrays during rhizoid formation and asymmetrical division were examined. No studies have focused on cytokinesis and observed multiple structures by double staining in living cells.

To observe actin filaments in cytokinesis, 6.0 μM Alexa Fluor 488-phalloidin (Plates 23-25), Alexa Fluor 555-phalloidin (Plate 33), or 0.01 mg mL^{-1} rhodamine-conjugated actin (Plate 30-32) were injected into the subapical cell. Live imaging of actin orientation requires the selection of probes that do not interfere with actin dynamics (Melak et al. 2017). In this study, cytokinesis and nuclear division were inhibited in cells microinjected with 12 μM or higher of Alexa Fluor 488-phalloidin and 0.65 mg mL^{-1} or higher rhodamine-conjugated actin. Phalloidin promotes actin polymerization, and it may disrupt intracellular actin dynamics and adversely affect cells (Coluccio and Tilney 1984, Visegrády et al. 2004, Wehland et al. 1977). In addition,

rhodamine-conjugated actin has monomeric actin bound to rhodamine and has a different three-dimensional structure from that of the endogenous actin, and thus its incorporation into actin filaments may be inhibited. In the present study, the period required for cytokinesis in cells microinjected with Alexa Fluor 488-phalloidin (6.0 μM) and rhodamine-conjugated actin (0.01 mg mL^{-1}) was not very different from that observed under the light microscope, and thus the concentrations used would have little effect on the dynamics of endogenous actin. In *S. rigidula,* rhodamine-labeled actin formed granular structures in the cytoplasm near the injection site (Plates 30-32). The number of granules decreased when the actin plate was formed. Using Alexa Fluor 488-phalloidin, a bias of fluorescent intensity in the cytoplasm was observed just after microinjection, but no granular structure. Therefore, it is thought that the granular structure signal is not from actin filaments but from aggregates of injected rhodamine-conjugated actin. When Alexa Fluor 555 phalloidin and rhodamine phalloidin were microinjected, only the granular structure was observed without labeling actin. Therefore, these fluorescent probes were not used for actin visualization in this species (Plate 33). Similarly with fluorescently labeled tubulin, the images were different between Alexa Fluor 488 and rhodamine. MT arrays shown by Alexa Fluor 488 tubulin were similar to those observed in fixed cells (Plates 21, 22). However, rhodamine-conjugated tubulin did not show the individual filaments in detail (Plate 29). The correct selection

of probe and fluorescence combination for observation in living cells was therefore essential to capture the orientation of the cytoskeleton.

Double staining using Alexa Fluor 488-phalloidin delivered by microinjection and FM4-64FX allowed the observation of the formation of actin and the development of new the cell partition membranes in living cells. The observation showed that the actin plate was formed before the new cell partition membrane, which formed from the same position as the actin plate (Plates 23-25). The observed relationship between actin plate and new cell partition membrane is consistent with the results obtained in fixed cells using Fluor 488-phalloidin and FM4-64FX (Plates 16-18 Aoki et al. 2023), and live cell observation added new temporal information. In tobacco BY-2 cells, actin filaments may play an important role in localizing primary aggregation and vesicle fusion in cell plate formation (van Oostende-Triplet et al. 2017). In brown algae, the actin plate is formed before the formation of a membrane structure, which is restricted within the range of the actin plate (Plates 23-25). In brown algae, as in land plants, actin filaments may also function to localize vesicles, promote vesicle fusion, and expand a new cell partition membrane.

In this study, the dynamics of MTs during the formation of new cell partition membrane was investigated for the first time in brown algae. Observation using HiLyte 488-conjugated tubulin delivered by microinjection and membrane staining with FM4-64FX showed that the new

cell partition membrane arose at the concentrated area of crossing MTs on the division plane. The relationship between the starting position of a new cell partition membrane and the orientation of MTs was newly revealed by observation over time in live cells. When the new cell partition membrane grew outwardly, the MT array changed its association with the periphery of the membrane structure (Plates 27, 28). In land plants, phragmoplast MTs change from cylindrical to donut-like shapes as the cell plate develops (Murata et al. 2013, Miart et al. 2013). Additionally, phragmoplast MTs transport Golgi vesicles, which are necessary for cell plate formation, to the division plane (Smertenko 2018). In brown alga *Scytosiphon lomentaria* zygotes, MTs transport Golgi vesicles to the division plane (Nagasato and Motomura 2002a). The changes in MT arrays associated with the development of a new cell partition membrane observed in this study may supply Golgi vesicles to the edges of the expanding new cell partition membrane similar to land plants. However, conspicuous orientation changes of MTs observed in cell plate development in land plants are absent in brown algae. There are two possibilities: the first is that the formation of the new cell partition membrane occurs at several areas in the division plane, and the second is that a large supply of Golgi vesicles to the division plane is unnecessary. In brown algae, flat cisternae build new cell partition membranes with Golgi vesicles, unlike in land plant cells (Nagasato and Motomura 2002a, Nagasato et al. 2010, Nagasato et al. 2014).

The observations using microinjection of HiLyte 488-conjugated tubulin and rhodamine-conjugated actin showed that the actin plate arose in the concentrated area of crossing MTs on the division plane as in the beginning of the new cell partition membrane. Double staining using Fluor 488-phalloidin microinjection and FM4-64FX staining indicated that the actin plate formed before the new cell partition. The results showed that the orientation of MTs influenced the location of actin plate formation, that the actin plate promoted vesicle fusion for new cell partition formation, and that actin and MTs were involved in the expansion of the new cell partition membrane. MTs were bound to the edges of actin plates as shown by indirect immunofluorescence in BFA-treated cells (Plate 15; Nagasato and Motomura 2019). These results suggest a connection between the actin plate and MTs. Formin, an actin-related protein, acts on both actin and MTs (Fernández-Barrera and Alonso 2018). In mammalians, formin, a regulator of actin polymerization (Goode and Eck 2007), stabilizes MTs (Ishizaki et al. 2001, Bartolini and Gundersen 2010). Formin improves MT stability by reducing the exchange of tubulin subunits at the plus end of MTs (Palazzo et al. 2001). In brown algae, there is no information about the molecules' interaction with both actin and MTs. These molecules likely link MTs and actin plates and regulate the orientation of both in brown algae. Triple staining of MTs, actin, and membrane structure has not been performed in the present study. However, observations using different probe

combinations suggested that MTs, the formation of actin plates, and new cell partition membranes were related to each other.

Observations using HiLyte 488-conjugated tubulin microinjection showed MTs parallel to the division plane (Plates 27, 28, 30-32). In contrast, observations using Alexa Fluor 488-phalloidin microinjection showed co-localization of actin with the spindle MTs (Plates 23-25). Co-localization of actin filaments to the spindle MTs is observed also in fixed cells stained with fluorescent phalloidin (Karyophyllis et al. 2000). However, the function of the co-localization of actin and MTs in the spindle MTs or the actin plate is unclear. It may play an assistant role in cytokinesis.

In the present study, the relationship among actin, MTs, and membrane structures during cytokinesis was investigated by microinjection of fluorescent probes. Triple staining of MTs, actin and membrane structure has not been performed in this study, however, observations from different two probes combination suggested that MTs, formation of actin plate and new cell partition membrane were related to each other. Although this method was effective in brown algae for which genetic transformation technology has not yet been established, it may not be the best method when considering the efficiency and sustainability of the fluorescent signal. Genome analysis of many species of brown algae has been performed in recent years (Cock et al. 2010, Ye

et al. 2015, Nishitsuji et al. 2020), and genome editing technology using CRISPR-Cas9 has been established for the brown algae *Ectocarpus* species 7 (Badis et al. 2021) and *Saccharina japonica* (Shen et al. 2023). In the future, cytokinesis research in brown algae will advance by searching for cytokinesis-related proteins through genome analysis and gene knock-in based on genome editing technology. Identification of their functions will complement live cell imaging. In addition, by observing cytokinesis in many cells using genome editing technology, it will be possible to clarify the progress of cytokinesis with higher precision.

Summary

For multicellular organisms, the process of cytokinesis, which physically partitions daughter nuclei after nuclear division, is an important step for maintaining this system. The machinery involved in cytokinesis mainly consists of MTs and actin, but their orientation differs between phylogenetic groups and species. In animal cells belonging to the Opisthokonta lineage, an actin ring appears just below the cell membrane at the division plane. When the actin ring contracts inside the cell, the cell membrane is constricted and divides centripetally. In contrast, in land plants belonging to the Archaeplastida lineage, the phragmoplast, whose main components are MTs, appears between daughter nuclei. The phragmoplast is oriented perpendicular to the cell plate, the partition of the new cell, and is involved in the centrifugal expansion of the cell plate from inside the cell toward the parent cell wall. Brown algae are marine multicellular organisms that belong to the Stramenopile lineage, and the division plane is the intersection of MTs that extend from the centrosome near the daughter nucleus toward the space between the daughter nuclei. Golgi vesicles transported by MTs accumulate at the division plane, fuse with a membrane structure called flat cisternae, and a new cell partition membrane is formed from inside the cell, which develops centrifugally to complete cytokinesis. During cytokinesis in brown algae, an actin plate (a plate-like actin structure), which has not been observed in other eukaryotic cells, appears at the division plane. Previous studies have suggested that the actin plate is involved in vesicle

fusion and membrane development, but its formation and function remain poorly understood. One of the reasons for this is that it is difficult to simultaneously observe actin and membrane structures at the division plane, making it impossible to fully understand the spatiotemporal relationship between the two. Therefore, the purpose of this study was to clarify the relationship between actin plate development and new cell partition membrane formation using apically dividing cells of the brown alga *S. rigidula*. This enabled the simultaneous labeling of the actin plate and the new cell partition membrane, allowing detailed observations in fixed and live cells.

Cytokinesis in *S. rigidula* proceeds centripetally with an invagination of the cell membrane at the division plane, which is different from the previously described characteristics of cytokinesis in brown algae. However, despite the different division modes, actin plate formation at the division plane has been observed. To clarify the role of the actin plate in cytokinesis in brown algae, it was necessary to reexamine this process in *S. rigidula*. First, time-lapse observation of living cells using the membrane-bound dye FM4-64FX and ultrastructural observation using a transmission electron microscope were performed. Although invagination of the cell membrane at the division plane was observed, the invagination did not progress inward, and the new cell partition membrane formed independently from inside the cell. Even when new cell partition membrane formation was delayed using brefeldin A (BFA), which affects Golgi

function, no invagination was observed to develop. These results revealed that cytokinesis in *S. rigidula*, similar to other brown algae, is completed when the new cell partition membrane progresses centrifugally from inside the cell toward the parent cell wall. Next, to investigate the relationship between actin plate and new cell partition membrane formation and expansion, double staining of membrane structure and actin using FM4-64FX and fluorescently labeled phalloidin in fixed cells was performed. Actin plates and new cell partition membrane formation were observed in the same location and expanded together. Similarly, it was shown that inhibiting new cell partition membrane formation by BFA treatment also stopped actin plate expansion, confirming that actin plate and new cell partition membrane expansion were linked. In addition, the MT orientation was examined in cells whose cytokinesis was inhibited by BFA treatment, and MTs were found to be attached to the edges of the developing actin plate. This suggests that MTs may be involved in actin plate expansion. Next, to investigate the relationship between actin plates and MTs in new cell partition membrane formation and expansion, fluorescently labeled phalloidin, actin, and tubulin were microinjected into cells and observed over time in living cells. 1) The relationship between actin plate and new cell partition membrane formation was investigated using Alexa Fluor 488-labeled phalloidin and FM4-64FX. This observation revealed that actin plate appeared at the division plane earlier than the new cell partition membrane, the

formation of which was delayed and occurred at the site of actin plate formation. 2) The relationship between actin plate and MTs was investigated by simultaneously microinjecting rhodamine-conjugated actin and HiLyte Fluor 488-conjugated tubulin. The results showed that before the appearance of the actin plate, there was a bias in the crossing regions of MTs extending from the centrosome, indicating that the actin plate formed in the area where MTs were abundant. Furthermore, MTs were observed at the edges of the expanding actin plate. 3) The relationship between MTs and new cell partition membrane formation was investigated using HiLyte Fluor 488-conjugated tubulin and FM4-64FX. The results revealed that, similar to the appearance of the actin plate, new cell partition membrane formation occurred in regions where a relatively large number of MTs intersected. When the new cell partition membrane expanded, MTs were oriented around its edge. Once actin plate and new cell partition membrane expansions were complete, MTs moved away from the cytokinesis plane and the distance between daughter nuclei increased.

In this study, ultrastructural analysis of the progression of cytokinesis in the apical cells of *S. rigidula* showed that cytokinesis progresses by centrifugal expansion of the new cell partition membrane, similar to other brown algae. Furthermore, simultaneous observation of actin plate and new cell partition membrane in brown algae was made possible in fixed cells and live cells. In addition, the time-lapse observation of the behavior of actin plates and MTs during new cell

partition membrane formation was performed for the first time in living cells of brown algae. The results showed that the orientation of MTs influences the position where the actin plate appeared and that the formation of the actin plate initiated new cell partition membrane formation at that position. MTs supply Golgi vesicles, which are necessary for new cell partition membrane formation, to the division plane. The results of this study also suggested that MTs are involved in the formation and expansion of new cell partition membranes in cooperation with the actin plate.

Proteins that control changes in the orientation of actin and MTs during cytokinesis in animals and land plants have been reported, and research on the role of the cytoskeleton in cytokinesis is progressing through functional analysis of these proteins. Genome analysis of many species of brown algae has progressed in recent years, and genome editing technology using CRISPR-Cas9 has been established for *Ectocarpus* species 7 and *Saccharina japonica*. In the future, it is expected that research on cytokinesis in brown algae will advance by searching for cytokinesis-related proteins through genome analysis and by using genome editing technology for their functions and live cell imaging. In addition, such research may shed light on the evolutionary process behind the appearance of the actin plate during cytokinesis in only brown algae among eukaryotes.

Table

Table 1. List of fluorescent probe combination and fluorescence wavelength.

Target	No.	Fluorescent probe combination	
actin and membrane	1	Alexa Fluor 488-phalloidin (495/518)	FM4-64FX (565/744)
MT and membrane	2	HiLyte 488 conjugated tubulin (499/523)	FM4-64FX (565/744)
	3	Rhodamine conjugated tubulin (550/570)	PlasMem Bright Green (488/560)
actin and MT	4	Rhodamine conjugated actin (550/570)	HiLyte 488 conjugated tubulin (499/523)
	5	Alexa Fluor 555-phalloidin (555/565)	HiLyte 488 conjugated tubulin (499/523)

MT; microtubule. (excitation wavelength/emission wavelength)

References

Alessa, L., & Kropf, D. L. (1999). F-actin marks the rhizoid pole in living *Pelvetia compressa* zygotes. *Development*, *126*(1), 201-209.

Aoki, H., Katsaros, C., Motomura, T., & Nagasato, C. (2023). Simultaneous visualization of the actin plate and new cell partition membrane during cytokinesis in the brown alga *Sphacelaria rigidula* (Sphacelariales, Phaeophyceae). *Phycological Research*, *71*(2), 107-115.

Arima, K., Tamaoki, D., Mineyuki, Y., Yasuhara, H., Nakai, T., Shimmen, T., Yoshihisa, T. & Sonobe, S. (2018). Displacement of the mitotic apparatuses by centrifugation reveals cortical actin organization during cytokinesis in cultured tobacco BY-2 cells. *Journal of plant research*, *131*, 803-815.

Aruga, H., Motomura, T., & Ichimura, T. (1996). Immunofluorescence study of mitosis and cytokinesis in *Acrosiphonia duriuscula* (Acrosiphoniales, Chlorophyta). *Phycological research*, *44*(4), 203-213.

Badis, Y., Scornet, D., Harada, M., Caillard, C., Godfroy, O., Raphalen, M., Gachon, C., M. M. Coelho, S. M., Motomura, T., Nagasato, C. & Cock, J. M. (2021). Targeted CRISPR‐Cas9‐based gene knockouts in the model brown alga *Ectocarpus*. *New Phytologist*, *231*(5), 2077-2091.

Bartolini, F., & Gundersen, G. G. (2010). Formins and microtubules. *Biochimica et Biophysica Acta (BBA)-Molecular Cell Research*, *1803*(2), 164-173.

Belanger, K. D., & Quatrano, R. S. (2000). Membrane recycling occurs during asymmetric tip growth and cell plate formation in *Fucus distichus* zygotes. *Protoplasma*, *212*, 24-37.

Belin, B. J., Goins, L. M., & Mullins, R. D. (2014). Comparative analysis of tools for live cell

imaging of actin network architecture. *Bioarchitecture*, *4*(6), 189-202.

Berepiki, A., Lichius, A., & Read, N. D. (2011). Actin organization and dynamics in filamentous fungi. *Nature Reviews Microbiology*, *9*(12), 876-887.

Bisgrove, S. R., Henderson, D. C., & Kropf, D. L. (2003). Asymmetric division in fucoid zygotes is positioned by telophase nuclei. *The Plant Cell*, *15*(4), 854-862.

Bisgrove, S. R., & Kropf, D. L. (1998). Alignment of Centrosomal and Growth Axes Is a Late Event during Polarization of *Pelvetia compressa* Zygotes. *Developmental Biology*, *194*(2), 246-256.

Bisgrove, S. R., & Kropf, D. L. (2004). Cytokinesis in brown algae: studies of asymmetric division in fucoid zygotes. *Protoplasma*, *223*, 163-173.

Bouget, F. Y., Gerttula, S., Shaw, S. L., & Quatrano, R. S. (1996). Localization of actin mRNA during the establishment of cell polarity and early cell divisions in Fucus embryos. *The Plant Cell*, *8*(2), 189-201.

Brawley, S. H., Quatrano, R. S., & Wetherbee, R. (1977). Fine-structural studies of the gametes and embryo of *Fucus vesiculosus* L. (Phaeophyta): III. cytokinesis and the multicellular embryo. *Journal of Cell Biology*, *24*(1), 275-294.

Brawley, S. H., & Robinson, K. R. (1985). Cytochalasin treatment disrupts the endogenous currents associated with cell polarization in fucoid zygotes: studies of the role of F-actin in embryogenesis. *The Journal of cell biology*, *100*(4), 1173-1184.

Buschmann, H., & Zachgo, S. (2016). The evolution of cell division: from streptophyte algae to land plants. *Trends in Plant Science*, *21*(10), 872-883.

Clayton, M. N., & Beakes, G. W. (1983). Effects of fixatives on the ultrastructure of physodes in vegetative cells of *Scytosiphon lomentaria* (Scytosiphonaceae, Phaeophyta) 1. *Journal of Phycology*, *19*(1), 4-16.

Cleary, A. L., Gunning, B. E., Wasteneys, G. O., & Hepler, P. K. (1992). Microtubule and F-actin dynamics at the division site in living Tradescantia stamen hair cells. *Journal of Cell Science*, *103*(4), 977-988.

Cock, J. M., Sterck, L., Rouzé, P., Scornet, D., Allen, A. E., Amoutzias, G., Anthouard, V., Artiguenave, F., Aury, J., Badger, J. H., Beszteri, B., Billiau, K., Bonnet, E., Bothwell, J. H., Bowler, C., Boyen, C., Brownlee, C., Carrano, C. J., Charrier, B., Cho, G. Y., Coelho, S. M., Collén, J., Corre, E., Silva, C. D., Delage, L., Delaroque, N., Dittami, S. M., Doulbeau, S., Elias, M., Farnham, G., Gachon, C. M. M., Gschloessl, B., Heesch, S., Jabbari, K., Jubin, C., Kawai, H., Kimura, K., Kloareg, B., Küpper, F. C., Lang, D., Bail, A. L., Leblanc, C., Lerouge, P., Lohr, M., Lopez, P. J., Martens, C., Maumus, F., Michel, G., Miranda-Saavedra, D., Morales, J., Moreau, H., Motomura, T., Nagasato, C., Napoli, C. A., Nelson, D. R., Nyvall-Collén, P., Peters, A. F., Pommier, C., Potin, P., Poulain, J., Quesneville, H., Read, B., Rensing, S. A., Ritter, A., Rousvoal, S., Samanta, M., Samson, G., Schroeder, D. C., Ségurens, B., Strittmatter, M., Tonon, T., Tregear, J. W., Valentin, K., von Dassow, P., Yamagishi, T., Van de Peer Y. & Wincker, P. (2010). The *Ectocarpus* genome and the independent evolution of multicellularity in brown algae. *Nature*, *465*(7298), 617-621.

Coluccio, L. M., & Tilney, L. G. (1984). Phalloidin enhances actin assembly by preventing monomer dissociation. *The Journal of Cell Biology*, *99*(2), 529-535.

Corellou, F., Coelho, S. M., Bouget, F. Y., & Brownlee, C. (2005). Spatial re-organisation of cortical microtubules in vivo during polarisation and asymmetric division of *Fucus* zygotes. *Journal of Cell Science*, *118*(12), 2723-2734.

D'Avino, P. P., Savoian, M. S., & Glover, D. M. (2005). Cleavage furrow formation and ingression during animal cytokinesis: a microtubule legacy. *Journal of Cell Science*, *118*(8), 1549-1558.

Fernández-Barrera, J., & Alonso, M. A. (2018). Coordination of microtubule acetylation and the actin cytoskeleton by formins. *Cellular and Molecular Life Sciences*, *75*(17), 3181-3191.

Fowke, L. C., & Pickett-Heaps, J. D. (1969). Cell division in Spirogyra. ii. Cytokinesis. *Journal of Phycology*, *5*(4), 273-281.

Garbary, D. J., Mcdonald, A. R., & Duckett, J. G. (1992). Visualization of the cytoskeleton in red algae using fluorescent labelling. *New phytologist*, *120*(3), 435-444.

Glotzer, M. (2005). The molecular requirements for cytokinesis. *Science*, *307*(5716), 1735-1739.

Goode, B. L., & Eck, M. J. (2007). Mechanism and function of formins in the control of actin assembly. *Annual Review of Biochemistry*, *76*, 593-627.

Green, R. A., Paluch, E., & Oegema, K. (2012). Cytokinesis in animal cells. *Annual Review of Cell and Developmental Biology*, *28*, 29-58.

Gunning, B. E., & Sammut, M. (1990). Rearrangements of microtubules involved in establishing cell division planes start immediately after DNA synthesis and are completed just before mitosis. *The Plant Cell*, *2*(12), 1273-1282.

Hable, W. E., Miller, N. R., & Kropf, D. L. (2003). Polarity establishment requires dynamic actin in fucoid zygotes. *Protoplasma*, *221*, 193-204.

Higaki, T., Kutsuna, N., Sano, T., & Hasezawa, S. (2008). Quantitative analysis of changes in actin microfilament contribution to cell plate development in plant cytokinesis. *BMC Plant Biology*, *8*(1), 1-15.

Ishizaki, T., Morishima, Y., Okamoto, M., Furuyashiki, T., Kato, T., & Narumiya, S. (2001). Coordination of microtubules and the actin cytoskeleton by the Rho effector mDia1. *Nature cell biology*, *3*(1), 8-14.

Karahara, I., Suda, J., Tahara, H., Yokota, E., Shimmen, T., Misaki, K., Yonemura, S., Staehelin, L. & Mineyuki, Y. (2009). The preprophase band is a localized center of clathrin‐mediated endocytosis in late prophase cells of the onion cotyledon epidermis. *The Plant Journal*, *57*(5), 819-831.

Karyophyllis, D., Katsaros, C., Dimitriadis, I., & Galatis, B. (2000). F-actin organization during the cell cycle of *Sphacelaria rigidula* (Phaeophyceae). *European Journal of Phycology*, *35*(1), 25-33.

Katsaros, C., & Galatis, B. (1992). Immunofluorescence and electron microscopic studies of microtubule organization during the cell cycle of *Dictyota dichotoma* (Phaeophyta, Dictyotales). *Protoplasma*, *169*, 75-84.

Katsaros, C., Galatis, B., & Mitrakos, K. (1983). Fine structural studies on the interphase and dividing apical cells of Sphacelaria tribuloides (Phaeophyta) 1. *Journal of Phycology*, *19*(1), 16-30.

Katsaros, C., Motomura, T., Nagasato, C., & Galatis, B. (2009). Diaphragm development in cytokinetic vegetative cells of brown algae. *Botanica Marina*, *52*(2), 150-161

Kinoshita, N., Shiba, K., Inaba, K., Fu, G., Nagasato, C., & Motomura, T. (2016). Flagellar waveforms of gametes in the brown alga *Ectocarpus siliculosus*. *European journal of Phycology*, 51(2), 139-148.

Kropf, D. L. (1992). Establishment and expression of cellular polarity in fucoid zygotes. *Microbiological Reviews*, *56*(2), 316-339.

Kropf, D. L., Berge, S. K., & Quatrano, R. S. (1989). Actin localization during *Fucus* embryogenesis. *The Plant Cell*, 1, 191-200.

La Claire, J. I. (1981). Occurrence of plasmodesmata during infurrowing in a brown alga. *Biol Cell*, *40*, 139-142.

Livanos, P., & Müller, S. (2019). Division plane establishment and cytokinesis. *Annual Review of Plant Biology*, *70*, 239-267.

Lokhorst, G. M., & Star, W. (1983). Fine structure of mitosis and cytokinesis in Urospora (Acrosiphoniales, Chlorophyta). *Protoplasma*, *117*(2), 142-153.

Markey, D. R., & Wilce, R. T. (1975). The ultrastructure of reproduction in the brown alga *Pylaiella littoralis*: I. Mitosis and cytokinesis in the plurilocular gametangia. *Protoplasma*, *85*, 219-241.

Melak, M., Plessner, M., & Grosse, R. (2017). Actin visualization at a glance. *Journal of Cell Science*, *130*(3), 525-530.

Miart, F., Desprez, T., Biot, E., Morin, H., Belcram, K., Höfte, H., Gonneau, M., & Vernhettes, S. (2014). Spatio‐temporal analysis of cellulose synthesis during cell plate formation in Arabidopsis. *The Plant Journal*, *77*(1), 71-84.

Mineyuki, Y. (1999). The preprophase band of microtubules: its function as a cytokinetic apparatus in higher plants. *International Review of Cytology*, 187, 1-49.

Mineyuki, Y., Wick, S. M., & Gunning, B. E. S. (1988). Preprophase bands of microtubules and the cell cycle: kinetics and experimental uncoupling of their formation from the nuclear cycle in onion root-tip cells. *Planta*, *174*, 518-526.

Murata, T., Sano, T., Sasabe, M., Nonaka, S., Higashiyama, T., Hasezawa, S., Machida, Y. & Hasebe, M. (2013). Mechanism of microtubule array expansion in the cytokinetic phragmoplast. *Nature Communications*, *4*(1), 1967.

Nagasato, C., Inoue, A., Mizuno, M., Kanazawa, K., Ojima, T., Okuda, K., & Motomura, T. (2010). Membrane fusion process and assembly of cell wall during cytokinesis in the brown alga, *Silvetia babingtonii* (Fucales, Phaeophyceae). *Planta*, *232*, 287-298.

Nagasato, C., Kajimura, N., Terauchi, M., Mineyuki, Y., & Motomura, T. (2014). Electron tomographic analysis of cytokinesis in the brown alga *Silvetia babingtonii* (Fucales, Phaeophyceae). *Protoplasma*, *251*, 1347-1357.

Nagasato, C., Katsaros, C., & Motomura, T. (2018). Cryofixation of brown algae for transmission electron microscopy. *Protocols for macroalgae research. CRC Press, Boca Raton*, 381-390.

Nagasato, C., & Motomura, T. (2002a). Ultrastructural study on mitosis and cytokinesis in *Scytosiphon lomentaria* zygotes (Scytosiphonales, Phaeophyceae) by freeze-substitution. *Protoplasma*, *219*, 140-149.

Nagasato, C., & Motomura, T. (2002b). Influence of the centrosome in cytokinesis of brown algae: polyspermic zygotes of *Scytosiphon lomentaria* (Scytosiphonales, Phaeophyceae). *Journal of Cell Science*, *115*(12), 2541-2548.

Nagasato, C., & Motomura, T. (2009). Effect of latrunculin B and brefeldin A on cytokinesis in the brown alga *Scytosiphon lomentaria* (Scytosiphonales, Phaeophyceae). *Journal of Phycology*, *45*(2), 404-412.

Nagasato, C., & Motomura, T. (2019). Effect of brefeldin A and the dynamics of the actin plate on cytokinesis of zygotes in the brown alga, *Silvetia babingtonii* (Fucales, Phaeophyceae). *European Journal of Phycology*, *54*(1), 26-38.

Nagasato, C., Motomura, T., & Ichimura, T. (1999). Influence of centriole behavior on the first spindle formation in zygotes of the brown Alga *Fucus distichus* (Fucales, Phaeophyceae). *Developmental Biology*, *208*(1), 200-209.

Nagasato, C., Tanaka, A., Ito, T., Katsaros, C., & Motomura, T. (2017). Intercellular translocation of molecules via plasmodesmata in the multiseriate filamentous brown alga, *Halopteris congesta* (Sphacelariales, Phaeophyceae). *Journal of Phycology*, *53*(2), 333-341.

Nagasato, C., Terauchi, M., Tanaka, A., & Motomura, T. (2015). Development and function of plasmodesmata in zygotes of *Fucus distichus. Botanica Marina*, *58*(3), 229-238.

Nagata, T., & Kumagai, F. (1999). Plant cell biology through the window of the highly synchronized tobacco BY-2 cell line. *Methods in Cell Science*, *21*, 123-127.

Nishitsuji, K., Arimoto, A., Yonashiro, Y., Hisata, K., Fujie, M., Kawamitsu, M., Shoguchi, E., & Satoh, N. (2020). Comparative genomics of four strains of the edible brown alga, *Cladosiphon okamuranus*. *BMC genomics*, *21*, 1-12.

Otegui, M. S., Mastronarde, D. N., Kang, B. H., Bednarek, S. Y., & Staehelin, L. A. (2001). Three-dimensional analysis of syncytial-type cell plates during endosperm cellularization visualized by high resolution electron tomography. *The Plant Cell*, *13*(9), 2033-2051.

Otegui, M. S., & Staehelin, L. A. (2004). Electron tomographic analysis of post-meiotic cytokinesis during pollen development in *Arabidopsis thaliana*. *Planta*, *218*, 501-515.

Palazzo, A. F., Cook, T. A., Alberts, A. S., & Gundersen, G. G. (2001). mDia mediates Rho-regulated formation and orientation of stable microtubules. *Nature Cell Biology*, *3*(8), 723-729.

Provasoli, L. (1968). Media and prospects for the cultivation of marine algae. *Cultures and Collections of Algae. Proceedings of US-Japan Conference, Hakone, September 1966*. *Japan Society of Plant Physiology*. 63-75.

Rawlence, D. J. (1973). Some aspects of the ultrastructure of *Ascophyllum nodosum* (L.) Le Jolis (Phaeophyceae, Fucales) including observations on cell plate formation. *Phycologia*, *12*(1-2), 17-28.

Reynolds, E. S. (1963). The use of lead citrate at high pH as an electron-opaque stain in electron microscopy. *Journal of Cell Biology*, *17*(1), 208.

Schmit, A. C., & Lambert, A. M. (1990). Microinjected fluorescent phalloidin in vivo reveals the F-actin dynamics and assembly in higher plant mitotic cells. *The Plant Cell*, *2*(2), 129-138.

Seguí-Simarro, J. M., Austin, J. R., White, E. A., & Staehelin, L. A. (2004). Electron tomographic analysis of somatic cell plate formation in meristematic cells of Arabidopsis preserved by high-pressure freezing. *The Plant Cell*, *16*(4), 836.

Sekida, S. & Okuda, K. (2022). Septum formation and cytoskeleton in cladophoralean, coenocytic cladophoralean, coenocytic green algae. I. Septum formation of *Chaetomorpha moniligera. The Japanese journal of Phycology (Sourui)*, *70*(3), 167-176

Shaw, S. L., & Quatrano, R. S. (1996). The role of targeted secretion in the establishment of cell polarity and the orientation of the division plane in *Fucus* zygotes. *Development*, *122*(9), 2623-2630.

Shen, Y., Motomura, T., Ichihara, K., Matsuda, Y., Yoshimura, K., Kosugi, C., & Nagasato, C. (2023). Application of CRISPR-Cas9 genome editing by microinjection of gametophytes of *Saccharina japonica* (Laminariales, Phaeophyceae). *Journal of Applied Phycology*, *35*(3), 1431-1441.

Sluiman, H. J., Roberts, K. R., Stewart, K. D., & Mattox, K. R. (1983). Comparative cytology and taxonomy of the Ulvophyceae. IV. Mitosis and cytokinesis in *Ulothrix* (Chlorophyta). *Acta Botanica Neerlandica*, *32*(4), 257-269.

Smertenko, A. (2018). Phragmoplast expansion: the four-stroke engine that powers plant cytokinesis. *Current Opinion in Plant Biology*, *46*, 130-137.

Smertenko, A., Assaad, F., Baluška, F., Bezanilla, M., Buschmann, H., Drakakaki, G., Hauser, M., Jason, M., Mineyuki, Y., Moore, I., Müller, S., Murata, T., Otegui, M. S., Panteris, E., Rasmussen, C., Schmit, A., Šamaj, J., Samuels, L., Staehelin, L. A., Damme, D. V.,

Wasteneys, G. & Žárský, V. (2017). Plant cytokinesis: terminology for structures and processes. *Trends in cell biology*, *27*(12), 885-894.

Takeuchi, M., Karahara, I., Kajimura, N., Takaoka, A., Murata, K., Misaki, K., Yonemura, S., Staehelin, L. A. & Mineyuki, Y. (2016). Single microfilaments mediate the early steps of microtubule bundling during preprophase band formation in onion cotyledon epidermal cells. *Molecular Biology of the Cell*, *27*(11), 1809-1820.

Terauchi, M., Nagasato, C., Kajimura, N., Mineyuki, Y., Okuda, K., Katsaros, C., & Motomura, T. (2012). Ultrastructural study of plasmodesmata in the brown alga *Dictyota dichotoma* (Dictyotales, Phaeophyceae). *Planta*, *236*, 1013-1026.

Ueki, C., Nagasato, C., Motomura, T., & Saga, N. (2008). Reexamination of the pit plugs and the characteristic membranous structures in *Porphyra yezoensis* (Bangiales, Rhodophyta). *Phycologia*, *47*(1), 5-11.

van den Hoek, C., & Flinterman, A. (1968). The life-history of *Sphacelaria furcigera* Kutz. (Phaeophyceae). *Blumea: Biodiversity, Evolution and Biogeography of Plants*, *16*(1), 193-242.

van Oostende-Triplet, C., Guillet, D., Triplet, T., Pandzic, E., Wiseman, P. W., & Geitmann, A. (2017). Vesicle dynamics during plant cell cytokinesis reveals distinct developmental phases. *Plant Physiology*, *174*(3), 1544-1558.

Verma, V., Mogilner, A., & Maresca, T. J. (2019). Classical and emerging regulatory mechanisms of cytokinesis in animal cells. *Biology*, *8*(3), 55.

Visegrády, B., Lőrinczy, D., Hild, G., Somogyi, B., & Nyitrai, M. (2004). The effect of phalloidin and jasplakinolide on the flexibility and thermal stability of actin filaments. *FEBS letters*, *565*(1-3), 163-166

von Dassow, G. (2009). Concurrent cues for cytokinetic furrow induction in animal cells. *Trends in Cell Biology, 19*(4), 165-173.

Wehland, J., Osborn, M., & Weber, K. (1977). Phalloidin-induced actin polymerization in the cytoplasm of cultured cells interferes with cell locomotion and growth. *Proceedings of the National Academy of Sciences*, *74*(12), 5613-5617.

Yasuhara, H., & Shibaoka, H. (2000). Inhibition of cell-plate formation by brefeldin A inhibited the depolymerization of microtubules in the central region of the phragmoplast. *Plant and cell physiology*, *41*(3), 300-310.

Yasuhara, H., Sonobe, S., & Shibaoka, H. (1995). Effects of brefeldin A on the formation of the cell plate in tobacco BY-2 cells. *European Journal of Cell Biology*, *66*(3), 274-281.

Ye, N., Zhang, X., Miao, M., Fan, X., Zheng, Y., Xu, D., Wang, J., Zhou, L., Wang, D., Gao, Y., Wang, Y., Shi, W., Ji, P., Li, D., Guan, Z., Shao, C., Zhuang, Z., Gao, Z., Qi, J., & Zhao, F. (2015). *Saccharina* genomes provide novel insight into kelp biology. *Nature communications*, *6*(1), 6986.

Plate legends

Plate 1. Life cycle of *S. rigidula.*

The diagram of the life cycle of *S. rigidula* was created based on van den Hock and Flinterman (1968). (a) Sporophyte algae. (b) Enlarged view of the apical part of the sporophyte. (c) Unispore. When the sporophyte matures, it forms unispores on the algal body. (d) Unispore zoospore is released from mature unispores. (e) Unispore zoospore is released from mature unispores. (f) Female gametophyte. (g) Male gametophyte. (h) Plurilocular sporangium formed in the female gametophyte. (i) Plurilocular sporangium formed in the male gametophyte. (j) Female gamete is released from mature plurilocular sporangium. (k) Male gamete is released from mature plurilocular sporangium. (l) Zygote. Male and female gametes become fertilized and form a zygote.

Plate 2. Schematic diagram of cytokinesis in animal cells.

(a) Cells after mitosis. Astral and central MTs determine the plane of division. (b) Formation and contraction of the contractile ring. (c) Dividing cells are connected by intercellular bridges containing a midbody. (d) Completion of cytokinesis.

C, centrosome; CR, contractile ring; MD, midbody; MT, microtubule; N, nucleus.

Plate 3. Schematic diagram of cytokinesis in land plant cells.

(a) Cell in interphase (G2 phase). The PPB consisting of MTs determines the future division plane. (b) Formation of phragmoplast. Phragmoplast is composed of MTs and AFs. (c) Cell plate is formed within the phragmoplast. (d) Completion of cytokinesis.

AF, actin filament; CP, cell plate; PPB, pre-prophase band; N, nucleus.

Plate 4. Schematic diagram of cytokinesis in brown algae.

(a) Cell after mitosis. MT crossing region from centrosomes becomes the division plane. (b) Appearance of the actin plate. (c) Actin plate spreads across the division plane. (d) Completion of cytokinesis.

AP, actin plate; C, centrosome; MT, microtubule; N, nucleus.

Plate 5. Morphological observation of *S. rigidula.*

(a) Female gametophyte. (b) Apical region. (c) An apical cell with one nucleus. (d) Apical cell with two nuclei.

Scale bars, 50 μm (b), 20 μm (c, d).

Plate 6. Observation of cytokinesis in apical cells.

(a) Both the apical cell and the second cell from the apical cell have a single nucleus. (b) After 40 min. Nuclear division occurs in the second cell from the apex, and it has two nuclei. (c) After 180 min. Nuclear division occurs in the apical cell, which has two nuclei. A division plane was formed in the second cell from the apex (white arrow). (d) After 270 min. A division plane was formed in the apical cell (white arrowhead) and cytokinesis was completed in the second cell from the apex (white arrow). (e) After 660. Cytokinesis has been completed in the apical cell (white arrowhead). Scale bars, 50 μm. *; nucle.

Plate 7. Relationship between cytokinesis stages and membranes.

(a, d, g) Optical microscope images. (b, e, h) SYBR Green Ⅰ staining. (e, f, i) FM4-64FX staining. (a-c) A cell with one nucleus per cell with a membrane formed on the division plane. (d-f) A cell with two nuclei in one cell. (g-i) A cell with a forming membrane on its division plane.

Scale bars, 20 μm.

Plate 8. Graph showing nuclear number within a cell frequency by time zone.

The lights turn on at 8:00 and turn off at 22:00. The counting times of 10:00, 13:00, 16:00, and

19:00 were 2, 5, 8, and 11 h after the start of the light period. 0:00, 3:00, 6:00, and 9:00 were 2, 5, 8, and 11 h after the start of the dark period. Dark gray indicates the proportion of cells in the mononuclear stage, and light gray indicates the proportion of cells in the binuclear stage. The number of nuclei per cell in 100 randomly selected cells was counted each time.

Plate 9. Time-lapse observation of cytokinesis in an apical cell stained by FM4-64FX.

(a, d, g) Optical microscope images. (b, e, h) FM4-64FX staining. (c, f, i) Enlarged images of (b), (e), and (h). (a–c) FM4-64FX-labeled membrane is found on the sides of the cytokinetic plane. (d–f) One min later than (a–c). FM4-64FX-labeled membrane (arrowhead) accumulates in the center of the cytokinetic plane. (g–i) Two min later than (a–c). Area labeled by FM4-64FX (arrowheads) extends on the right side of the cytokinetic plane. Scale bars, 20 μm (a, b, d, e, g, h), 10 μm (c, f, i).

Plate 10. Time-lapse observation of cytokinesis in an apical cell stained with FM4-64FX.

(a, d, g) Optical microscope images. (b, e, h) FM4-64FX staining. (c, f, i) Enlarged images of (b), (e), and (h). (a-c) FM4-64FX-labeled membrane is found on the sides of the cytokinetic plane. (d-f) Three min later than (a-c). FM4-64FX-labeled membrane (arrowheads) accumulates in the

center of the cytokinetic plane. (g, h) Six min later than (a-c). FM4-64FX-labeled membrane was detected across the whole cytokinetic plane. Scale bars, 20 μm (a, b, d, e, g, h), 10 μm (c, f, i).

Plate 11. Ultrastructural observation of cytokinesis in an apical cell.

(a) Cytokinetic plane. Golgi vesicles (G) and flat cisternae (FC) form a line along the cytokinetic plane. (b) Magnified images of the furrows (arrow) on the left side of the cytokinetic plane in (a). (c, d) Magnified image of membranous sacs (MSs) found in (a). (e) Another section of the same cell as in (a-d). Large MS with convoluted membrane perforations is formed. (f) Magnified image of MS in (e). (g, h) Magnified images of the furrows (arrows) on the left and right sides of the cytokinetic plane in (e).

Ch, chloroplast. Scale bars, 2 μm (a, e), 500 nm (b, g, h), 200 nm (c, d), 1 μm (f).

Plate 12. Ultrastructural observations of cytokinesis in an apical cell treated with 0.5 μg mL^{-1} BFA for 6 h.

(a) A cytokinetic plane. Furrows are found on both sides of the cytokinetic plane (arrows). (b) Golgi apparatus (G) delaminated by BFA treatment. (c) Magnified image of the membranous sac (MS) of (a). Golgi vesicles (GVs) and flat cisternae (FCs) are observed around the MS. (d)

Another section of (a). (e) Magnified image of MSs of (d). GVs and FCs close to the MSs. (f) Cytokinetic plane in the same cell from (a) and (c). Several MSs appear on the division plane. The furrows (arrows) are found on both sides of the cytokinetic plane. Preplasmodesmata (arrowheads) are observed.

Ch, chloroplast; FC, flat cisterna; G, Golgi apparatus; GV, Golgi vesicle.

Scale bars, 2 μm (a, d, f), 1 μm (e), 500 nm (b, c).

Plate 13. Observation of actin and MTs using indirect immunofluorescence microscopy in apical cells.

(a, d, g, j) DAPI staining. (b, e, h, k) Actin. (c, f, I, l) MTs. (a-c) Interphase. (d-f) Metaphase. (g-i) Early telophase. MTs extending from the two centrosomes intersect in the intermediate region of the daughter nuclei. (m-r) Actin plate appears on the cytokinetic plane.

Scale bars, 20 μm.

Plate 14. Observation of actin and MTs using indirect immunofluorescence in apical cells under BFA.

(a, d, g, j) DAPI staining. (b, e, h, k) Actin. (c, f, I, l) MTs. (a-c) Interphase. (d-f) Metaphase. (g-

i) Early telophase. MTs extending from the two centrosomes intersect in the intermediate region of the daughter nuclei. (m-r) actin plate appears on the cytokinetic plane.

Scale bars, 20 μm.

Plate 15. Observation of actin plate and MTs in the formation in apical cells under BFA.

(a) DAPI staining. (b) Actin. (c) MTs (d, e, f) Green; Actin. Magenta; MTs. (a-c) Epifluorescence microscopic image. (d) Confocal laser scanning microscopic image of cell (a-c). (e, f) Different slice sections of the same cell with enlarged division planes in (d).

Scale bars, 20 μm.

Plate 16. Development of the actin plate and new cell division plane during cytokinesis in fixed apical cells.

(a, d, g, j) DAPI staining. (b, e, h, k) F-Actin staining with Alexa Fluor 488-phalloidin. (c, f, i, l) FM4-64FX-labeled membrane. (a-c) Apical cell before cytokinesis. Actin plate is not formed. (d-f) Beginning of actin plate formation. A small actin plate appears, and the membrane structure is formed in the same place as the actin plates (g-i) Expansion of the actin plate and new cell partition membrane. (j-l) Completion of cytokinesis. The actin plate spreads over the cytokinetic plane.

Scale bars, 20 μm.

Plate 17. Observation of actin plate during the progression of cytokinesis in fixed apical cells under BFA.

(a, d, g, j) DAPI staining. (b, e, h, k) F-Actin staining with Alexa Fluor 488-phalloidin. (c, f, i, l) FM4-64FX-labeled membrane. (a-f) Appearance of the actin plate in the center of the cytokinetic plane. The area of the actin plate is larger than that of the developing new membrane. (g-l) Actin plate is linked to one side of the cell wall. The developing new membrane shows a similar configuration as the actin plate. Scale bars, 20 μm.

Plate 18. Observation of the actin plate during cytokinesis in fixed apical cells under BFA by confocal laser scanning microscopy.

(a, d, g) DAPI staining. (b, e, h) F-actin staining with Alexa Fluor 488 phalloidin. (c, f, i) FM4-64FX-labeled membrane. (a-f) Expansion of actin plate and new cell partition membrane. (g-i) Completion of cytokinesis. Scale bars, 20 μm.

Plate 19. Schematic diagram of membrane formation during cytokinesis in *S. rigidula* and

other brown algae.

(a-e) Membrane formation during cytokinesis in many brown algae. (f-j) Membrane formation during cytokinesis in *S. rigidula*. (a) After mitosis. (b) Accumulation of Golgi vesicles (GVs) and flat cisternae (FCs) on the cytokinetic plane. (c) GVs and FCs begin to fuse with each other on the cytokinetic plane. (d) Advanced stage of membrane fusion. Membranous sacs (MSs) appear at the cytokinetic plane. (e) MSs become a continuous new cell partition membrane. (f) After mitosis. Furrow (Fu) is formed. (g) Accumulation of GVs and FCs on the cytokinetic plane. Fu is not invaginated. (h) GVs and FCs begin to fuse with each other on the cytokinetic plane. Fu is not invaginated. (i) Advanced stage of membrane fusion. MSs appear at the cytokinetic plane. Fu is not invaginated. (j) MSs reach Fu and become a continuous new cell partition membrane.

Plate 20. Gametophytes and sporophytes of *S. rigidula*.

(a-c) Apical dividing cells of sporophytes. (d-f) Apical dividing cells of female gametophytes.

Scale bars, 20 μm

Plate 21. Observation of actin and MTs using indirect immunofluorescence microscopy in apical cells of sporophytes.

(a, d, g) DAPI staining. (b, e, h) Actin. (c, f, i) MTs. (a-c) Interphase. (d-f) Early telophase. MTs extending from the two centrosomes intersect in the intermediate region of the daughter nuclei. (g-i) Actin plate appears in the cytokinetic plane.

Scale bars, 20 μm.

Plate 22. Observation of actin and microtubules using indirect immunofluorescence microscopy in the second cells from the tip of sporophytes.

(a, d, g) DAPI staining. (b, e, h) Actin. (c, f, i) MTs. (a-c) Interphase. (d-f) Early telophase. MTs extending from the two centrosomes intersect in the intermediate region of the daughter nuclei. (g-i) Actin plate appears in the cytokinetic plane.

Scale bars, 20 μm.

Plate 23. Time-lapse observation of the actin plate during cytokinesis in a living cell (No. 1).

Alexa Fluor 488-phalloidin was microinjected into a cell, which was then stained with FM4-64FX. (a, d, g, j, m) Optical microscopy images. (b, e, h, k, n) Fluorescence of Alexa Fluor 488-phalloidin. (c, f, i, l, o) FM4-64FX staining. (a-c) Observation at 0 min. The fluorescence of the probe is biased at the injection side (white arrowhead) and is particularly strong around the nearby

nucleus (white arrowhead). (d-f) After 30 min of observation. The actin plate begins to form before the new cell partition membrane (yellow arrowhead). (g-i) After 46 min of observation. The new cell partition membrane formed at the same position as the actin plate (yellow arrow). (j-l) After 52 min of observation. Expansion of the actin plate and new cell partition membrane (m-o) After 56 min of observation. The actin plate and new cell partition membrane spread across the division plane.

Scale bars, 20 μm.

Plate 24. Time-lapse observation of the actin plate during cytokinesis in a living cell (No. 2).

Alexa Fluor 488-phalloidin was microinjected into a cell, which was then stained with FM4-64FX. (a, d, g, j, m) Optical microscope images. (b, e, h, k, n) Fluorescence of Alexa Fluor 488-phalloidin. (c, f, i, l, o) FM4-64FX staining. (a-c) Observation at 0 min. The fluorescence of the probe is biased at the injection side (white arrowhead) and is particularly strong around the nearby nucleus (white arrow). The actin plate formed at the division plane (yellow arrowhead). (d-f) After 60 min of observation. The actin plate was present at the division plane (yellow arrowhead). (g-i) After 100 min of observation. The new cell partition membrane formed at the same location as the actin plate (yellow arrow). (j-l) After 120 min of observation. Expansion of the actin plate and new cell

partition membrane. (m-o) After 140 min of observation. The actin plate and new cell partition membrane spread across the division plane.

Scale bars, 20 μm.

Plate 25. Time-lapse observation of the actin plate during cytokinesis in a living cell (No. 3).

Alexa Fluor 488-phalloidin was microinjected into a cell, which was then stained with FM4-64FX. (a, d, g, j, m, p) Optical microscope images. (b, e, h, k, n, q) Fluorescence of Alexa Fluor 488-phalloidin. (c, f, i, l, o, r) FM4-64FX staining. (a-c) Observation at 0 min. The fluorescence of the probe is biased at the injection side (white arrowhead) and is particularly strong around the nearby nucleus (white arrow). The actin plate formed at the division plane (yellow arrowhead). (d-f) After 10 min of observation. The actin plate formed at the division plane (yellow arrowhead). (g-i) After 30 min of observation. The new cell partition membrane formed at the same location as the actin plate (yellow arrow). (j-l) After 50 min of observation. A faint fluorescence of Alexa Fluor 488-phalloidin and FM4-64FX was detected throughout the division plane. (m-o) After 60 min of observation. Alexa Fluor 488-phalloidin and FM4-64FX fluorescence were detected throughout the division plane. (p-r) After 70 min of observation. The actin plate and new cell partition membrane spread across the division plane.

Scale bars, 20 μm.

Plate 26. Observation of the actin plate during cytokinesis using confocal laser scanning microscopy.

(a-c) Epifluorescence microscopy images. (d-k) Confocal laser scanning microscopy images of the same cell as in a-c. (a) Optical microscopy images. (b, d, f, h, j) Fluorescence of Alexa Fluor 488-phalloidin. (c, e, g, i, k) FM4-64FX staining. (d, e) Observed section. (f, g) Focus plane changed 2.5 μm from (d, e). (h, i) Focus plane changed 4.0 μm from (d, e). (j, k) Focus plane changed 5.0 μm from (d, e). The actin plate and the membrane were present in the same form inside the cell.

Scale bars, 20 μm.

Plate 27. Time-lapse observation of MTs during cytokinesis in a living cell (No. 1).

HiLyte 488-conjugated tubulin was microinjected into a cell, which was then stained with FM4-64FX. (a, d, g, j, m) Optical microscopy images. (b, e, h, k, n) Fluorescence of HiLyte 488-conjugated tubulin. (c, f, i, l, o) FM4-64FX staining. (a-c) Observation at 0 min. Yellow arrowhead; microtubules extending toward the plasma membrane. White arrowhead;

microinjection site. (d-f) After 45 min of observation. Microtubules were associated with the division plane (white arrow). The furrow of the plasma membrane was observed (yellow arrows). (g-i) After 60 min of observation. (j-l) After 65 min of observation. New cell partition membrane formed in the division plane. (m-o) After 70 min of observation. When the membrane spread across the division plane, the connection between MTs and the division plane disappeared. Scale bars, 20 μm.

Plate 28. Time-lapse observation of MTs during cytokinesis in a living cell (No. 2).

HiLyte 488-conjugated tubulin was microinjected into a cell, which was then stained with FM4-64FX. (a, d, g, j, m, p) Optical microscopy images. (b, e, h, k, n, q) Fluorescence of HiLyte 488-conjugated tubulin. (c, f, i, l, o, r) FM4-64FX staining. (a-c) Observation at 0 min. White arrowhead; microinjection site. Microtubules were associated with the division plane (white arrow). (d-f) After 30 min of observation. Yellow arrowhead; microtubules extending toward the plasma membrane. Microtubules were associated with the division plane (white arrow). Furrow of the plasma membrane was observed (yellow arrows). (g-i) After 50 min of observation. (j-l) After 60 min of observation. New cell partition membrane formed in the division plane. (m-o) After 70 min of observation. (p-r) After 80 min of observation. When the membrane spread across

the division plane, the connection between microtubules and the division plane disappeared.

Scale bars, 20 μm.

Plate 29. Observation of MTs during cytokinesis.

Cells were microinjected with rhodamine-conjugated tubulin and stained with PlasMem Bright Green. (a-c) and (d-f) are images of different cells. (a, d) Epifluorescence microscopy images. (b, e) PlasMem Bright Green staining. (c, f) Fluorescence of rhodamine-conjugated tubulin. Rhodamine-conjugated tubulin fluorescence was present at the centrosome and the division plane, indicating nonspecific labeling.

Scale bars, 20 μm.

Plate 30. Time-lapse observation of MTs and actin plate during cytokinesis in a living cell (No. 1).

HiLyte 488-conjugated tubulin and rhodamine-conjugated actin were microinjected into a cell. (a, d, g, j, m) Optical microscopy images. (b, e, h, k, n) Fluorescence of HiLyte 488-conjugated tubulin. (c, f, i, l, o) Fluorescence of rhodamine-conjugated actin. (a-c) Observation at 0 min. MTs elongate toward the division plane (white arrow). Rhodamine-conjugated actin was observed in

granular form near the microinjection site. White arrowhead; microinjection site. (d-f) After 20 min of observation. Microtubules were associated with the division plane (white arrow). Fluorescence of HiLyte 488-conjugated tubulin is visible in the division plane. (g-i) After 30 min of observation. The actin plate formed (yellow arrow). (j-l) After 35 min of observation. (m-o) After 50 min of observation. The actin plate expanded, the distance between the centrosomes widened, and the connection between the division plane and the microtubule plus end was lost. Scale bars, 20 μm.

Plate 31. Time-lapse observation of MTs and actin plate during cytokinesis in a living cell (No. 2).

HiLyte 488-conjugated tubulin and rhodamine-conjugated actin were microinjected into a cell. (a, d, g, j, m) Optical microscopy images. (b, e, h, k, n) Fluorescence of HiLyte 488-conjugated tubulin. (c, f, i, l, o) Fluorescence of rhodamine-conjugated actin. (a-c) Observation at 0 min. Rhodamine-conjugated actin was observed in granular form near the microinjection site. White arrowhead; microinjection site. (d-f) After 30 min of observation. Microtubules were associated with the division plane (white arrow). Fluorescence of HiLyte 488-conjugated tubulin is visible in the division plane. Rhodamine-conjugated actin fluorescence was observed at the division

plane. (g-i) After 50 min of observation. The actin plate formed (yellow arrow). (j-l) After 70 min of observation. (m-o) After 90 min of observation. The actin plate expanded, the distance between the centrosomes widened, and the connection between the division plane and the microtubule plus end was lost.

Scale bars, 20 μm.

Plate 32. Time-lapse observation of MTs and actin plate during cytokinesis in a living cell (No. 3).

HiLyte 488-conjugated tubulin and rhodamine-conjugated actin were microinjected into a cell. (a, d, g, j, m) Optical microscopy images. (b, e, h, k, n) Fluorescence of HiLyte 488-conjugated tubulin. (c, f, i, l, o) Fluorescence of rhodamine-conjugated actin. (a-c) Observation at 0 min. Rhodamine-conjugated actin was observed in granular form near the microinjection site. At the start of observation, the actin plate was observed at the division plane (yellow arrow). White arrowhead, microinjection site. (d-f) After 20 min of observation. Microtubules were associated with the division plane (white arrow). The actin plate was enlarged. (g-i) After 60 min of observation. Fluorescence of HiLyte 488-conjugated tubulin was visible in the division plane. The actin plate was enlarged. (j-l) After 80 min of observation. The actin plate was located at the center

of the division plane. (m-o) After 120 min of observation. The actin plate expanded, the distance between the centrosomes widened, and the connection between the division plane and the microtubule plus end was lost.

Scale bars, 20 μm.

Plate 33. Time-lapse observation of the actin plate and MTs during cytokinesis in a living cell.

Alexa Fluor 555-phalloidin and HiLyte 488-conjugated tubulin were microinjected into a cell. (a, d, g, j, m) Optical microscopy images. (b, e, h, k, n) Fluorescence of HiLyte 488-conjugated tubulin. (c, f, i, l, o) Fluorescence of Alexa Fluor 555-phalloidin.

Scale bars, 20 μm.

Plate 34. Schematic diagram of cytoskeleton dynamics during cytokinesis in *S. rigidula*.

(a) Immediately after mitosis. (b) Aggregation and fusion of vesicles to form the new cell partition membrane. (c) Completion of cytokinesis. (d-i) Detailed step of b. (d) The actin plate formed at the region where MTs intermingled. (e) Vesicles were transported to the division plane. (f) Vesicles accumulated in the actin plate formation area. (g) The vesicles fused at the actin plate to

form a new cell partition membrane. (h) Expansion of the actin plate and new cell partition membrane. MTs were observed along the developing actin plate and new cell partition membrane. (i) Actin plate and membrane spread across the division plane. When the membrane and actin plate spread across the division plane, the association between the microtubule plus end and the division surface was lost.

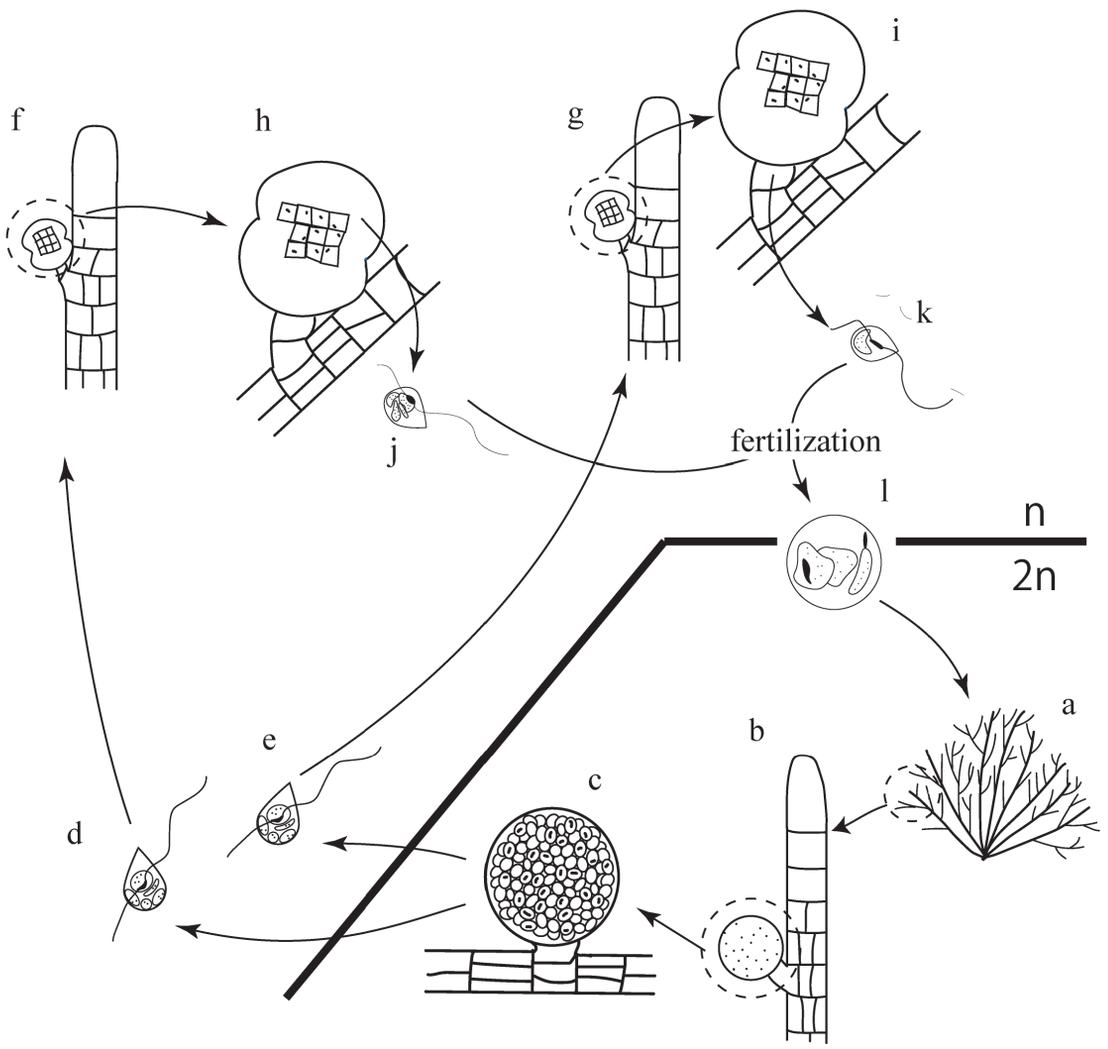


Plate 1

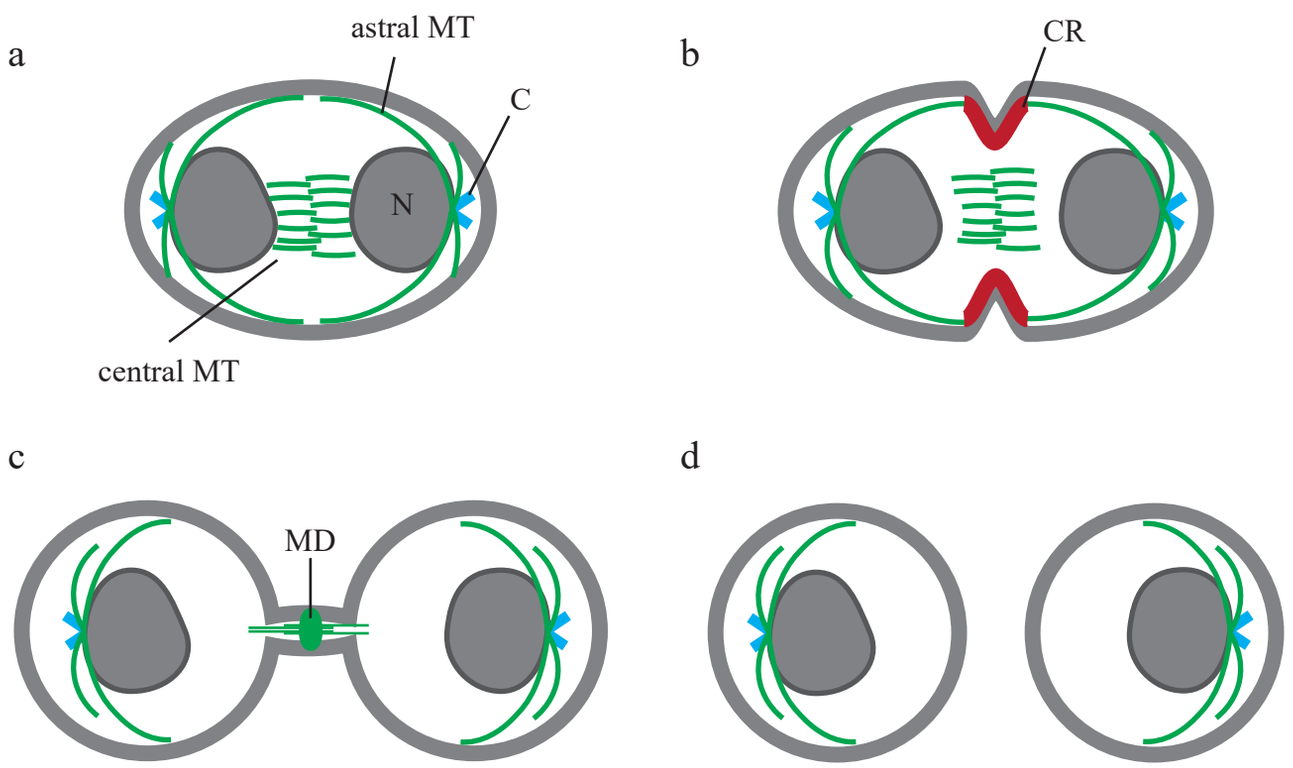


Plate 2

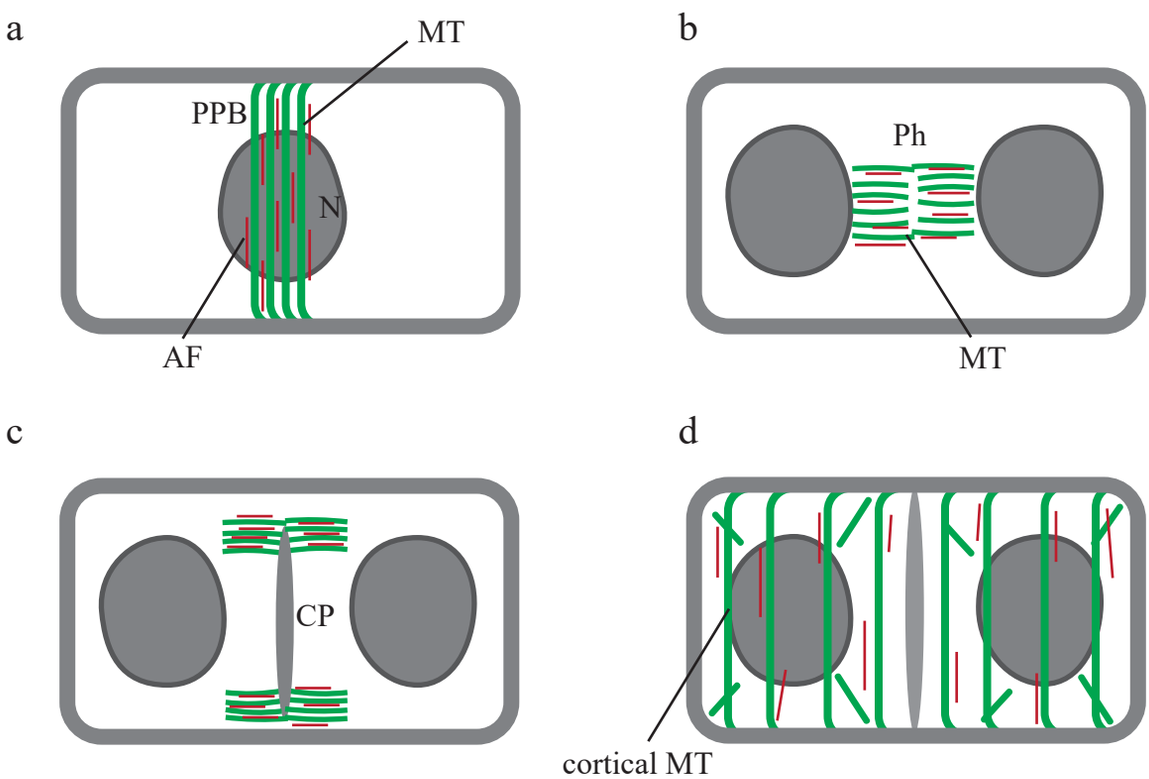
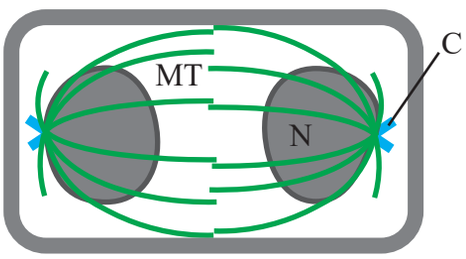
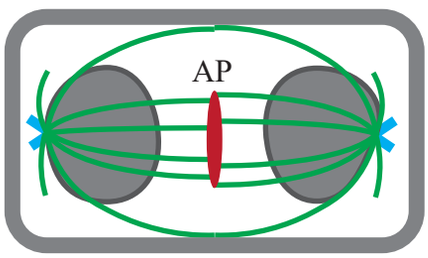


Plate 3

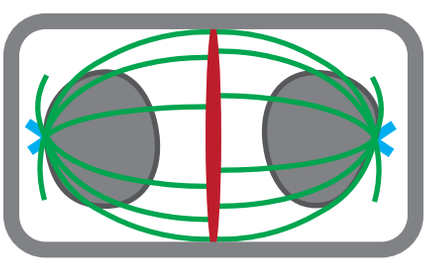
a



b



c



d

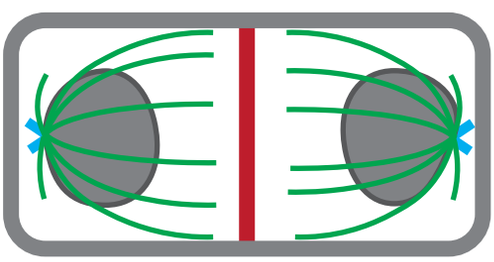


Plate 4

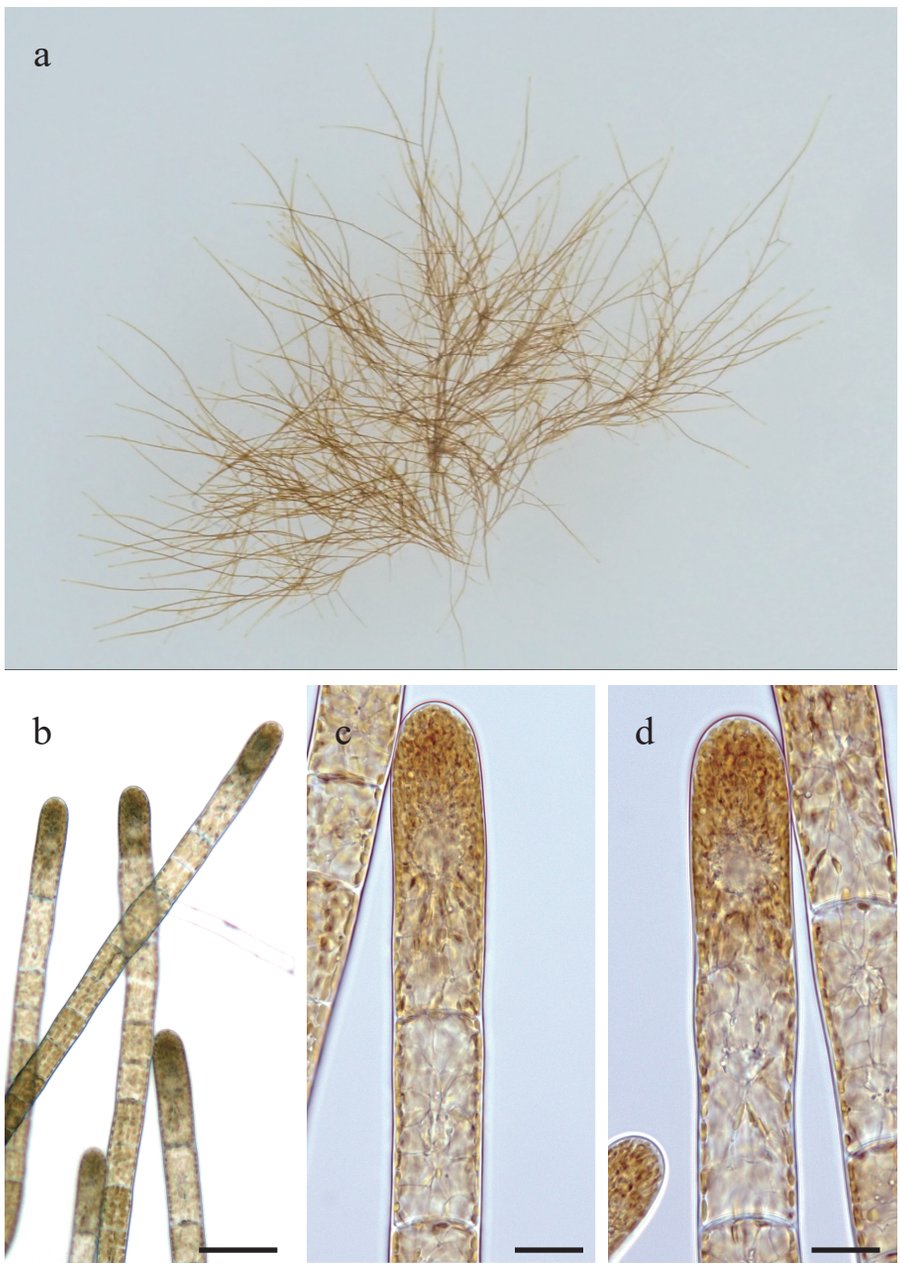


Plate 5

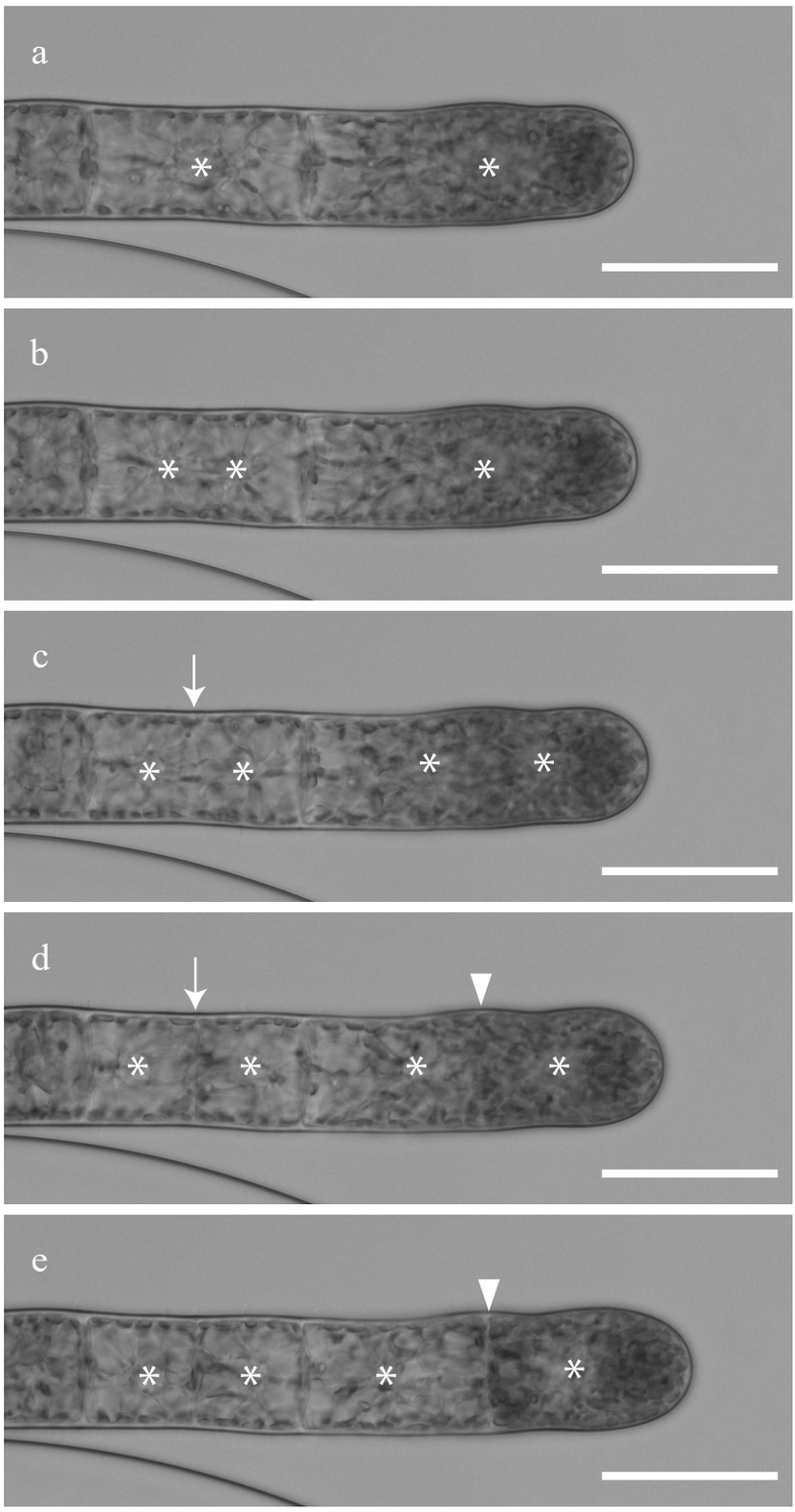


Plate 6

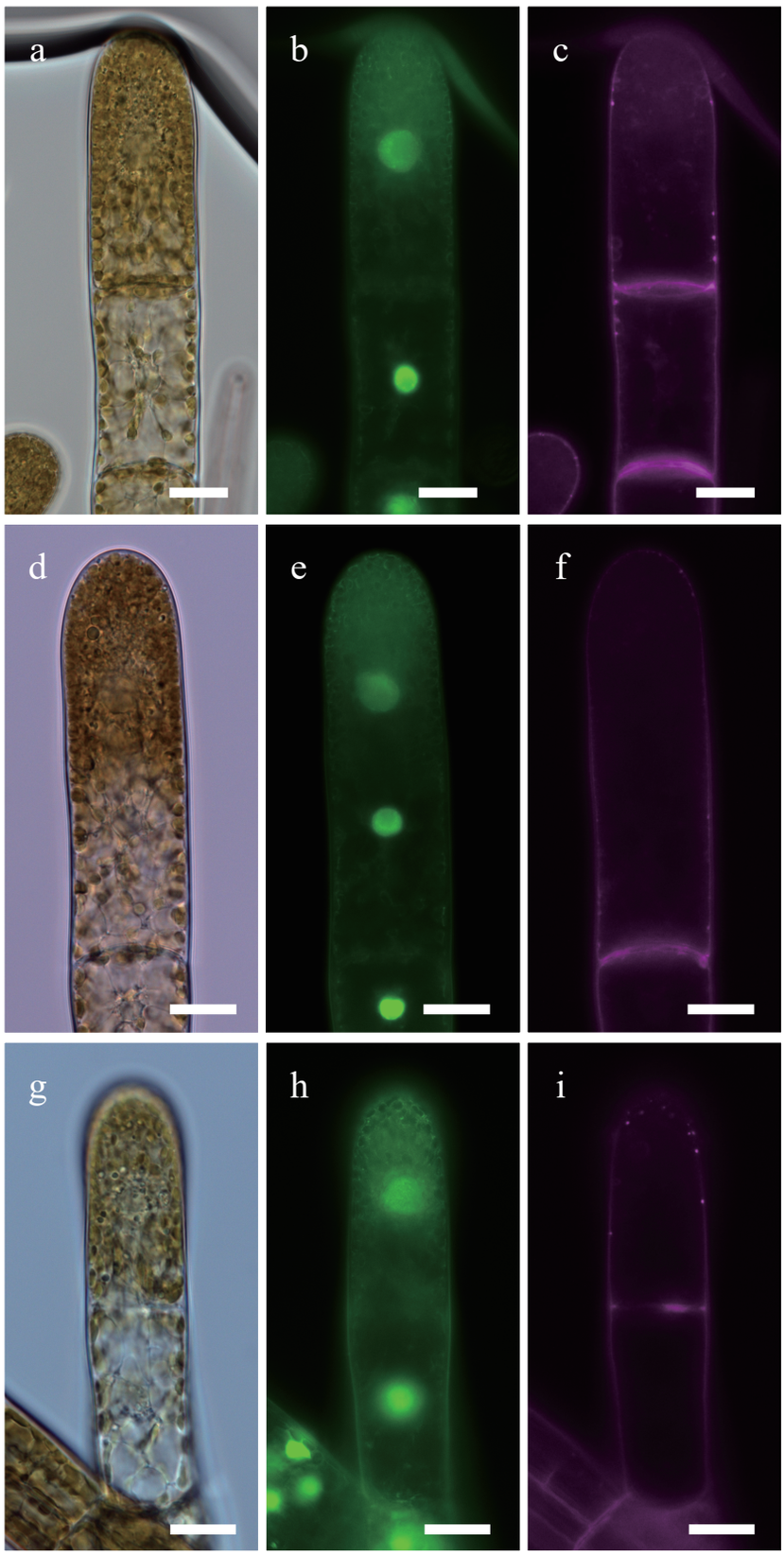


Plate 7

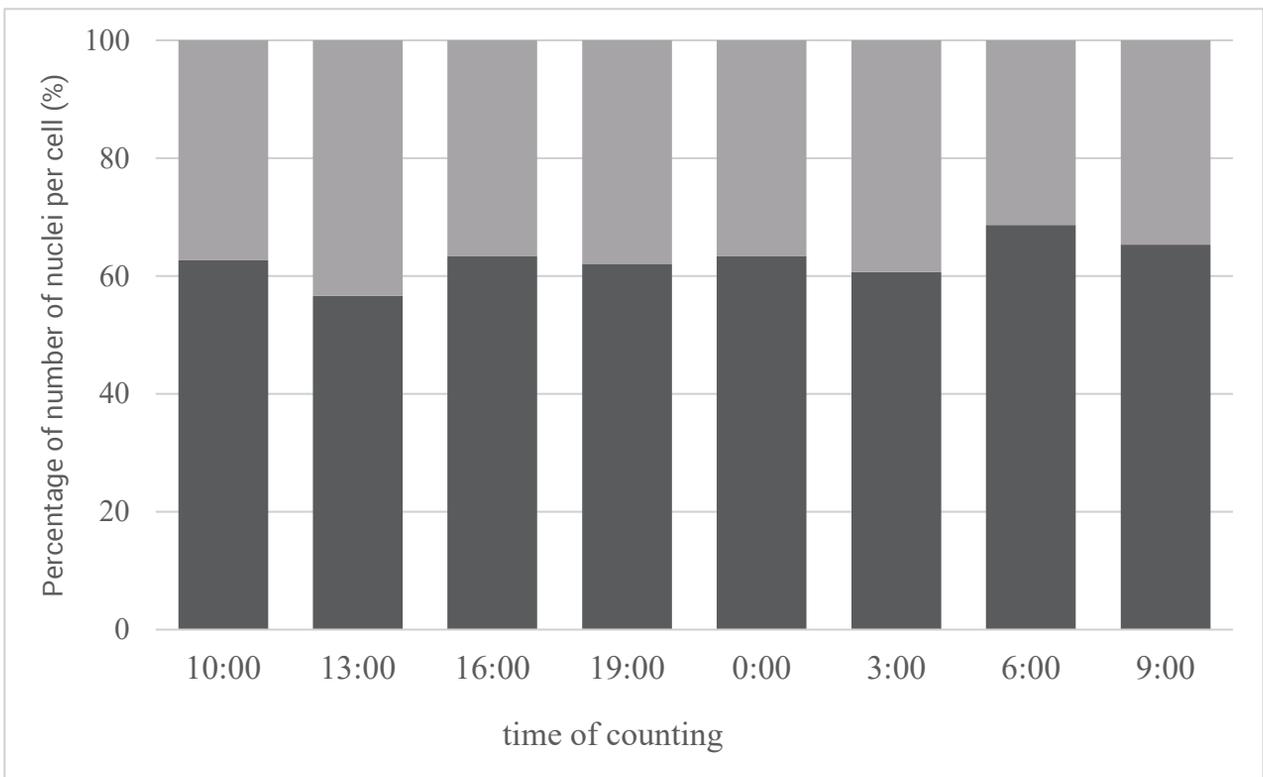

Percentage of number of nuclei per cell (%)
100
80
60
40
20
0
10:00
13:00
16:00
19:00
0:00
3:00
6:00
9:00
time of counting

Plate 8

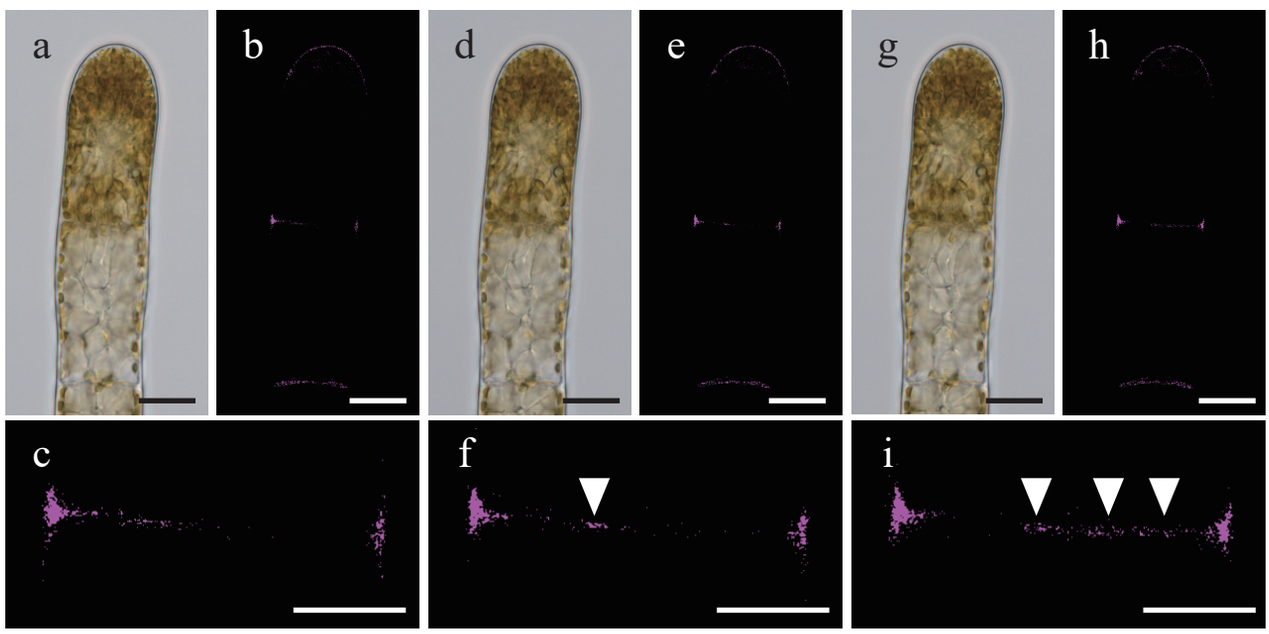


Plate 9

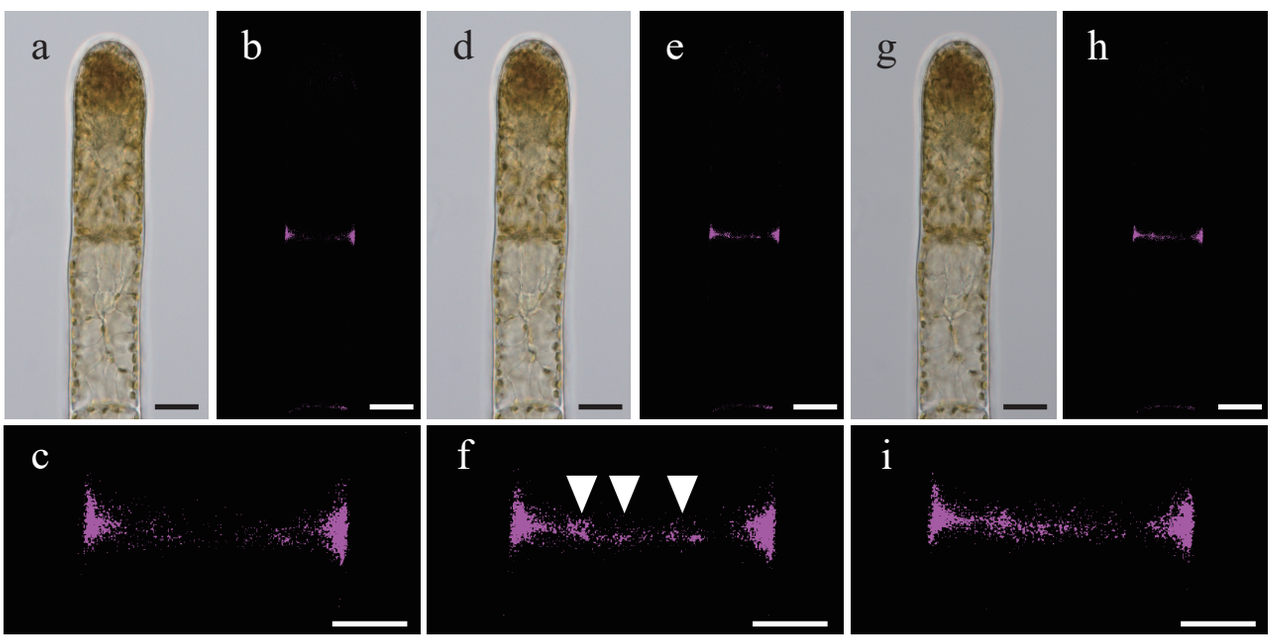


Plate 10

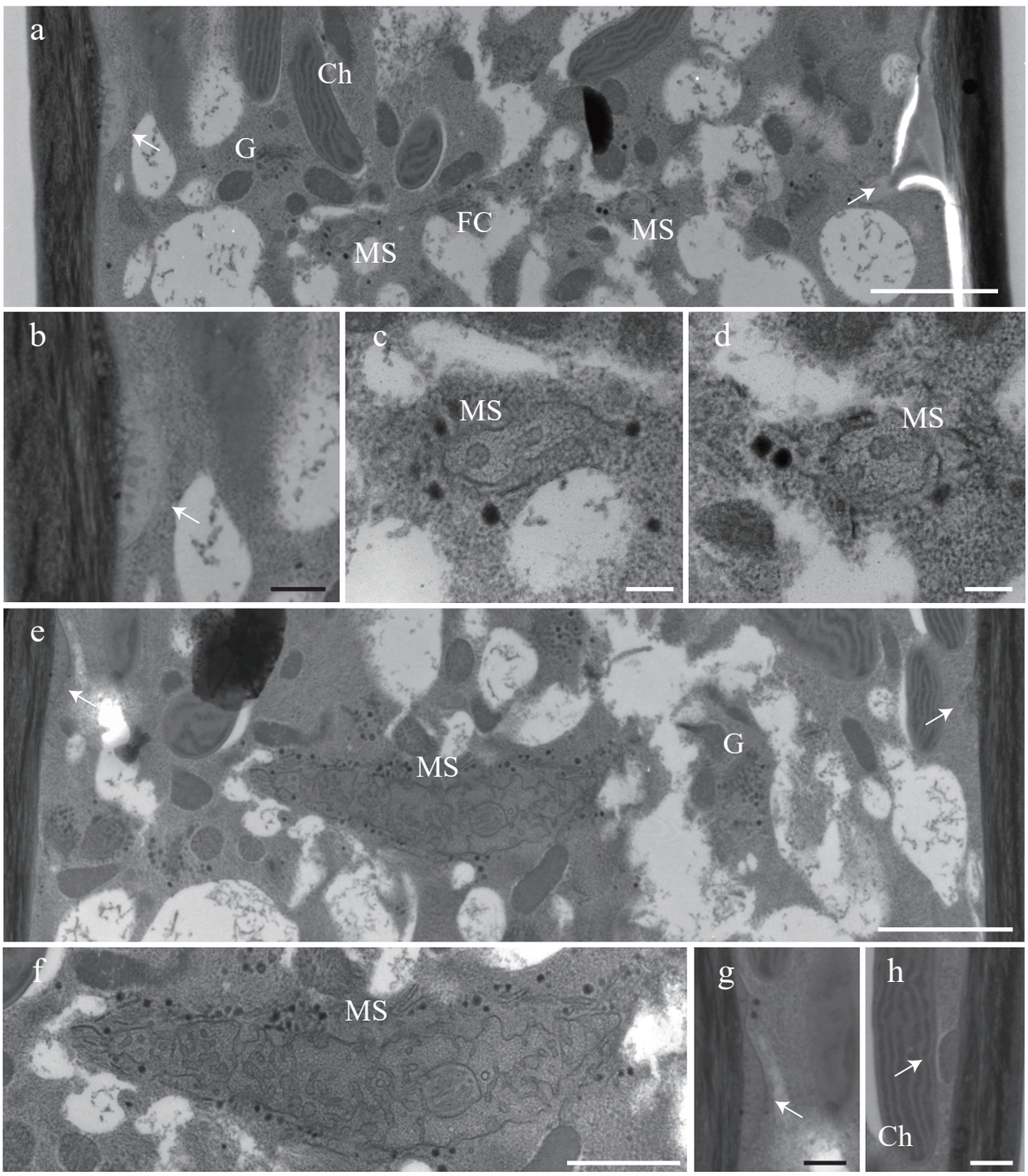


Plate 11

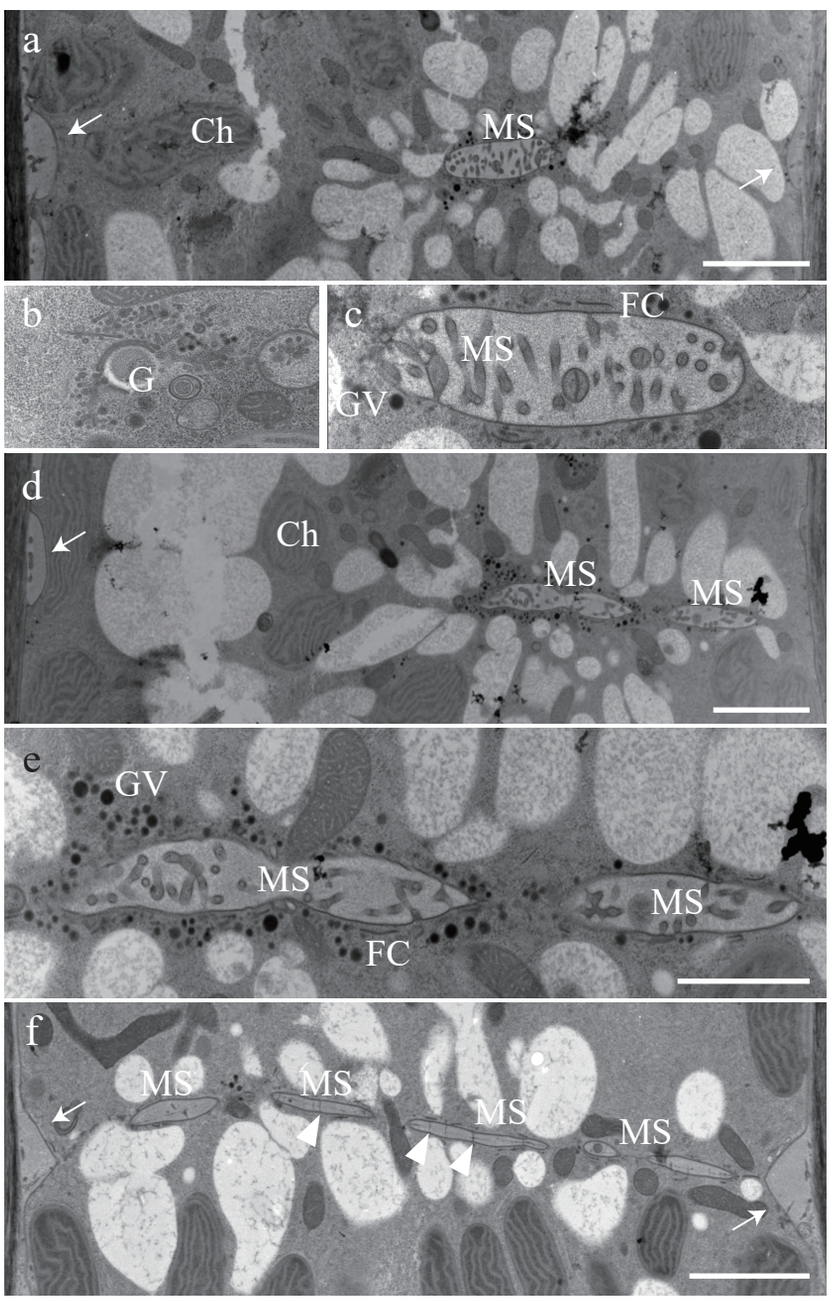


Plate 12

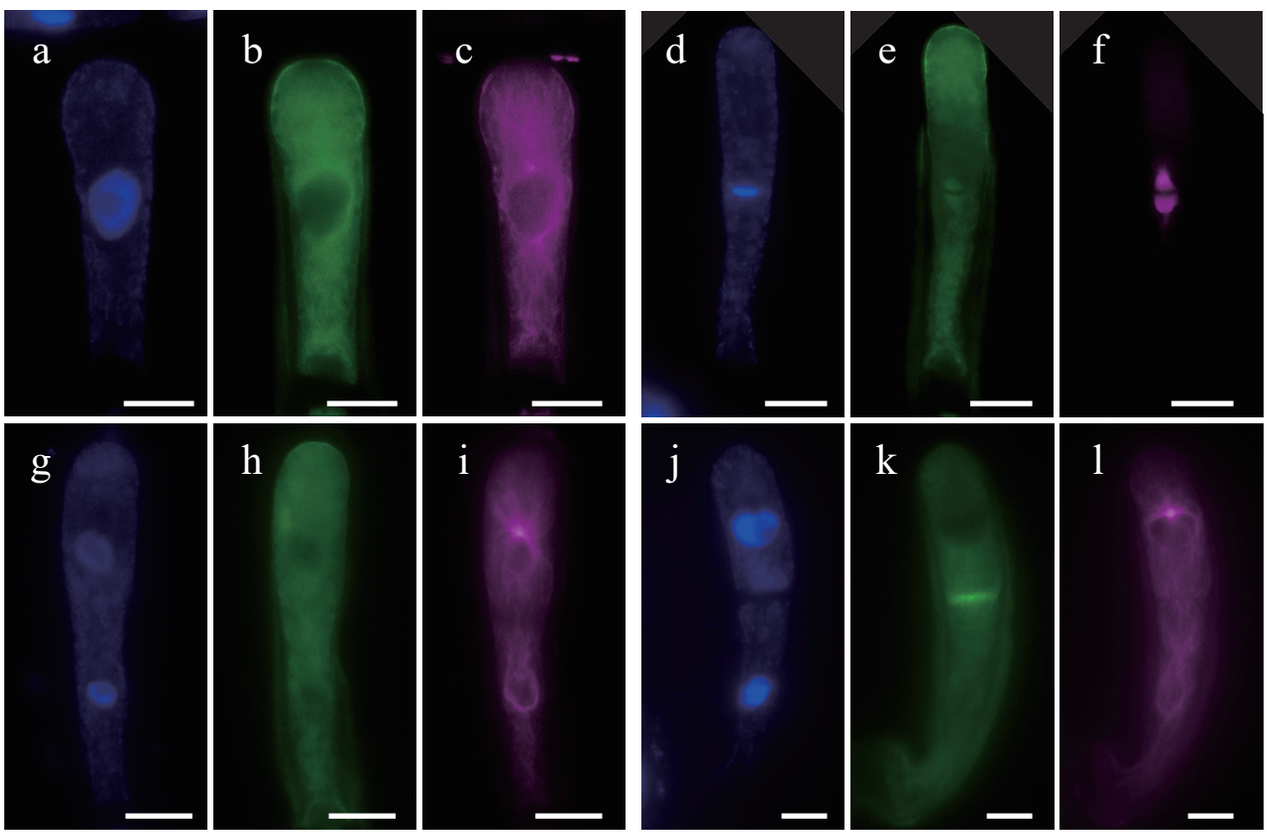


Plate 13

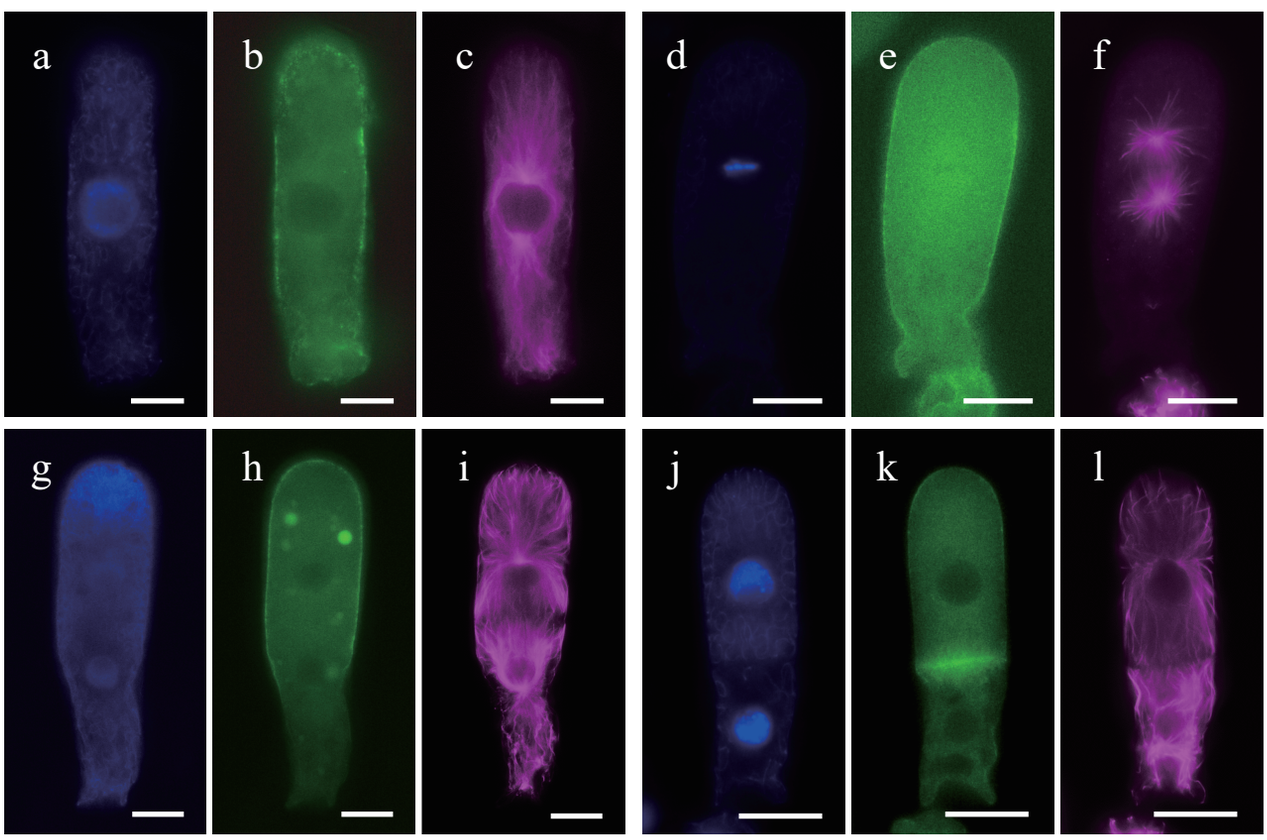


Plate 14

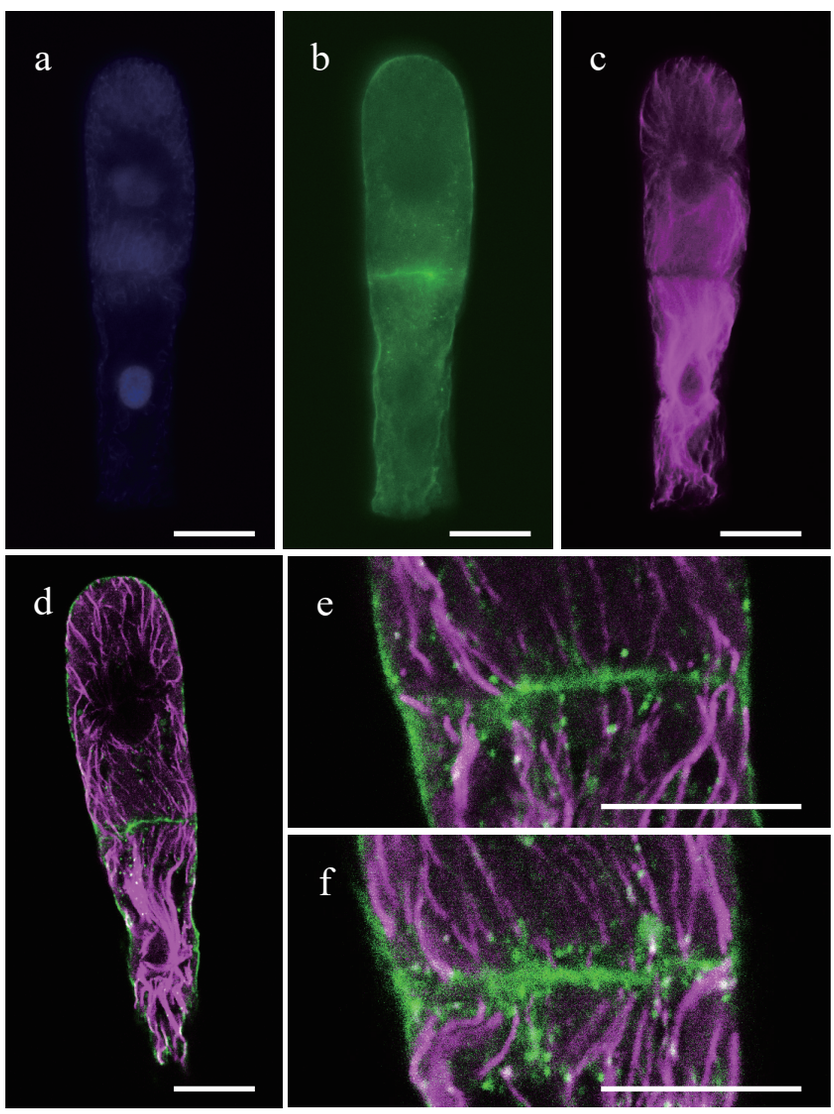


Plate 15

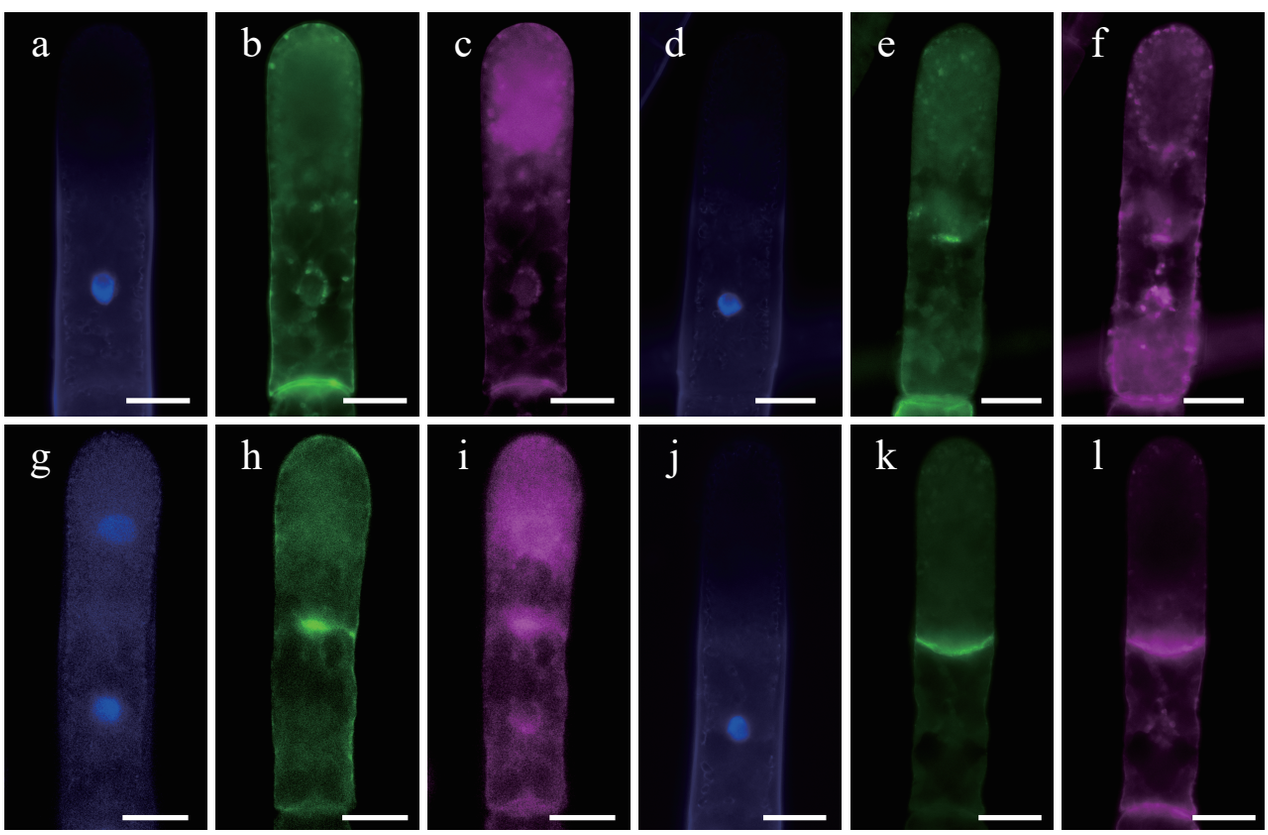


Plate 16

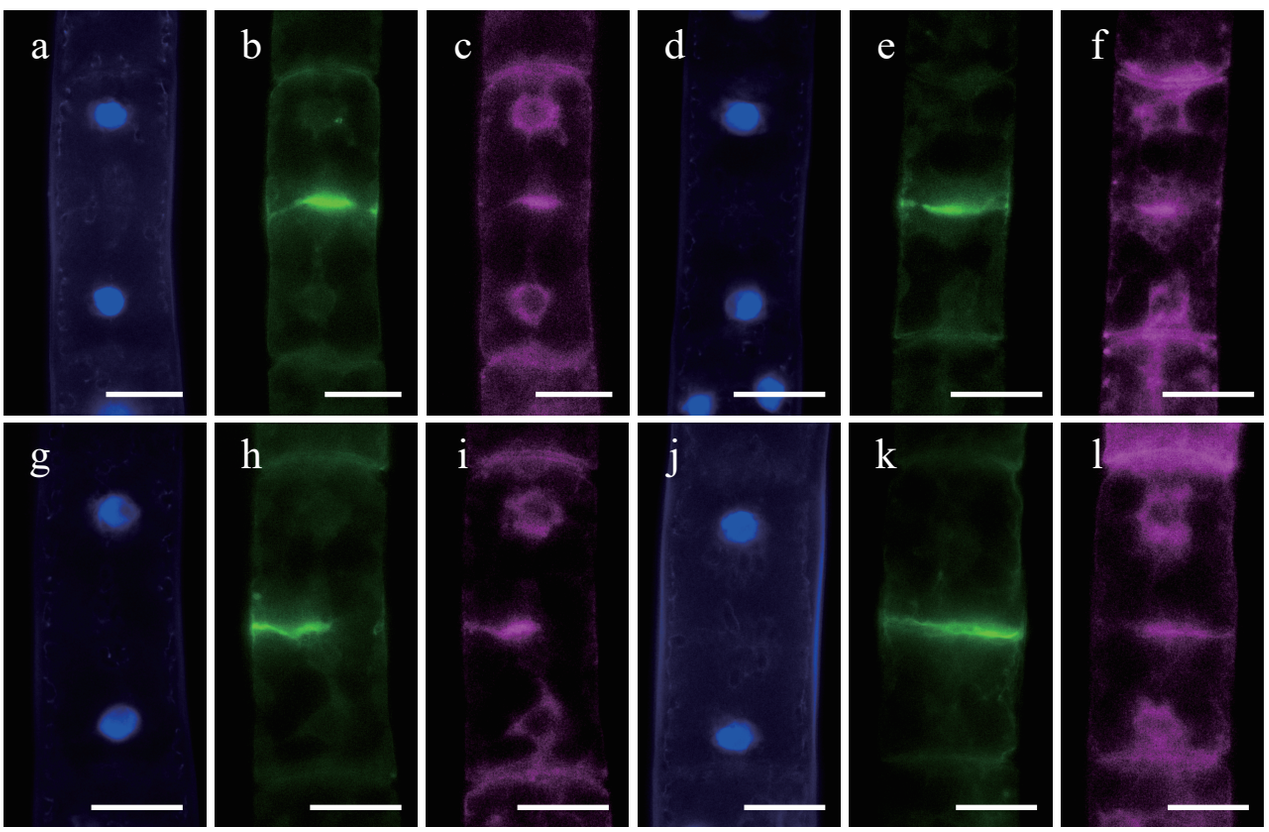


Plate 17

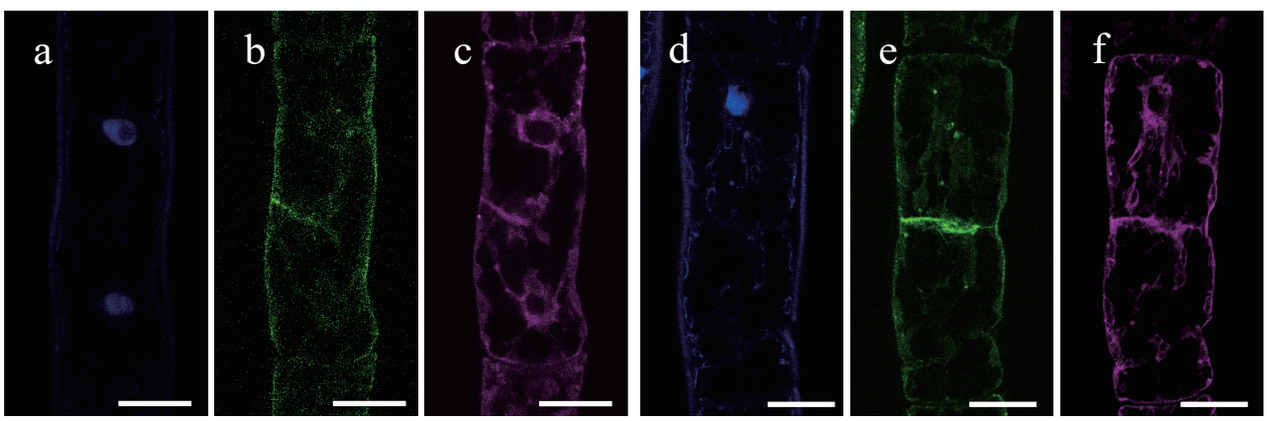


Plate 18

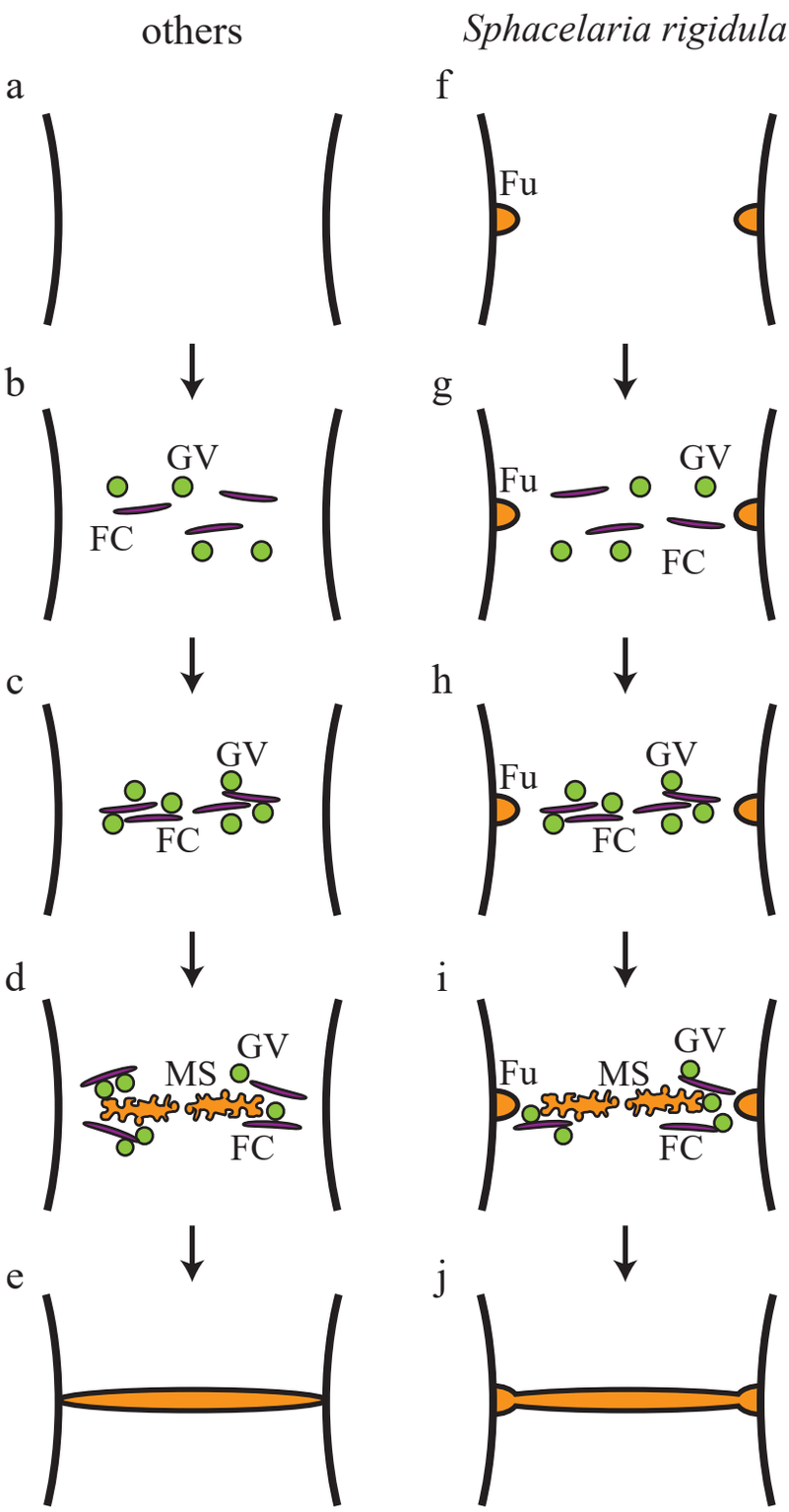


Plate 19

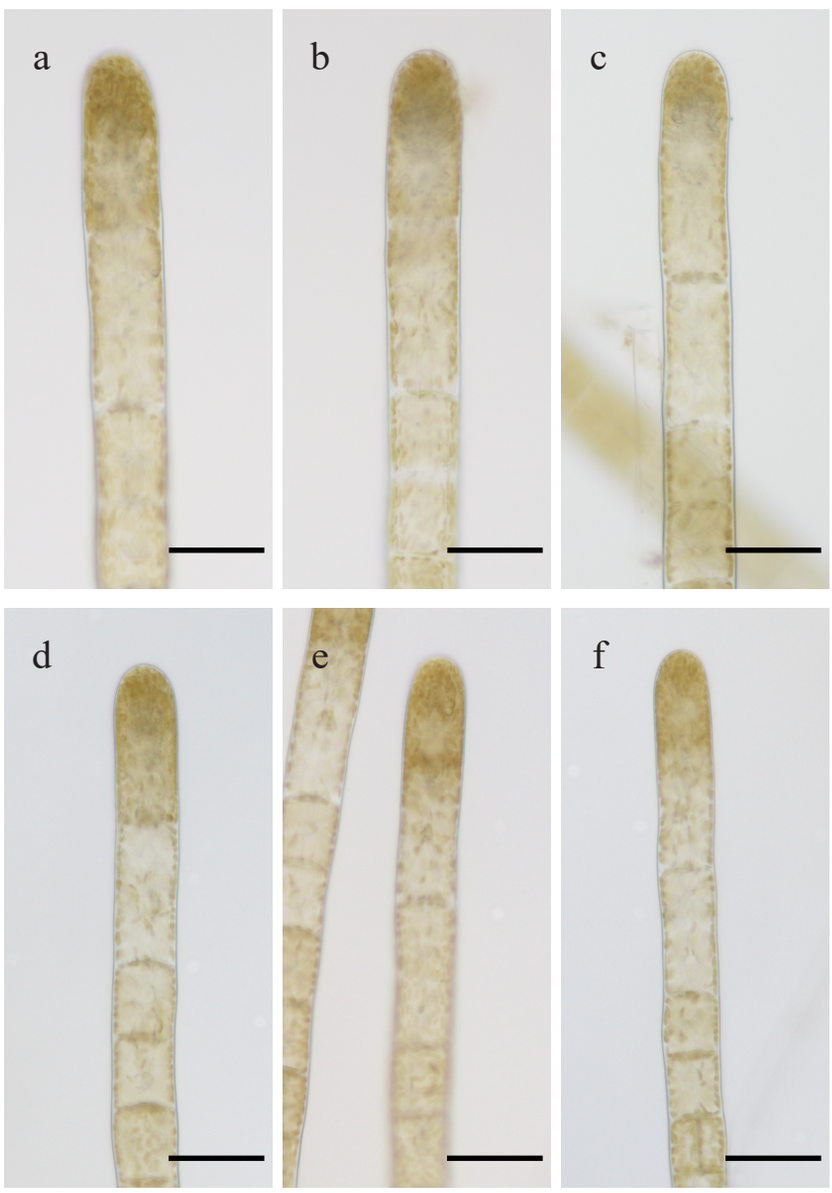


Plate 20

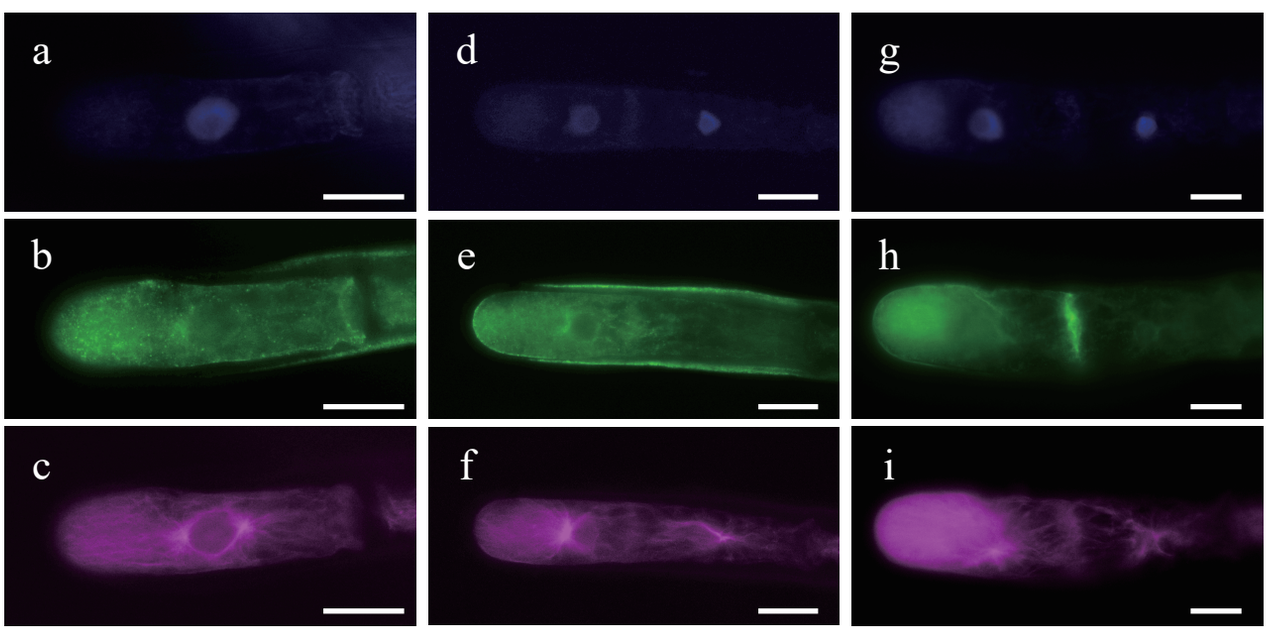


Plate 21

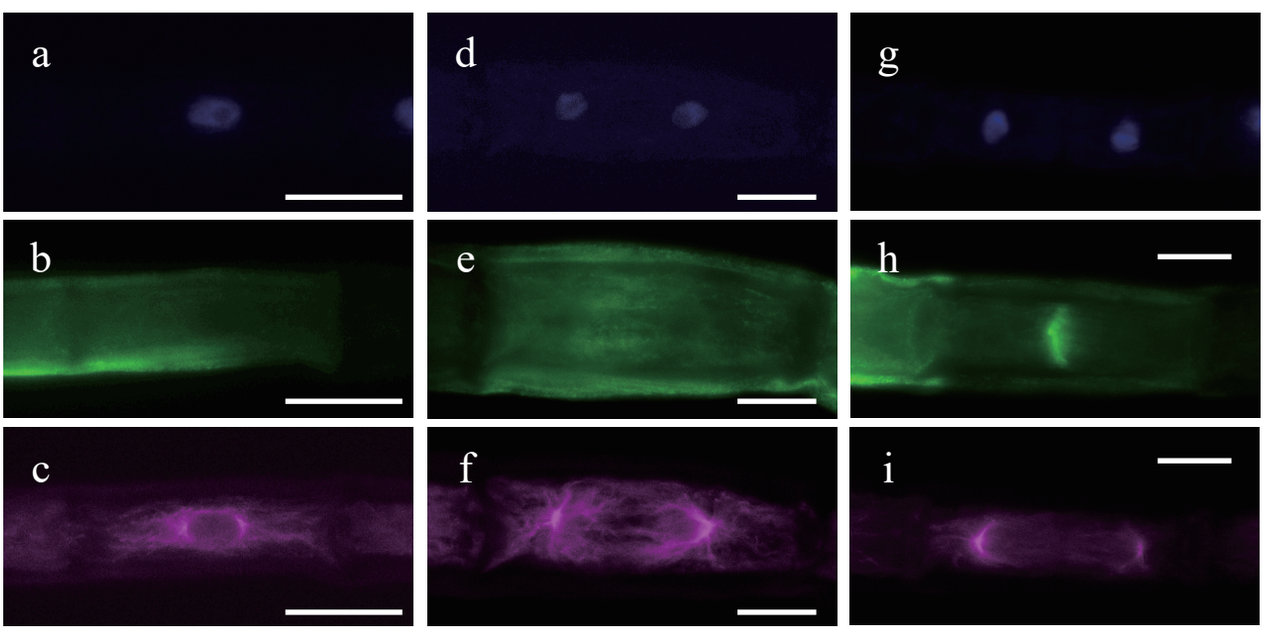


Plate 22

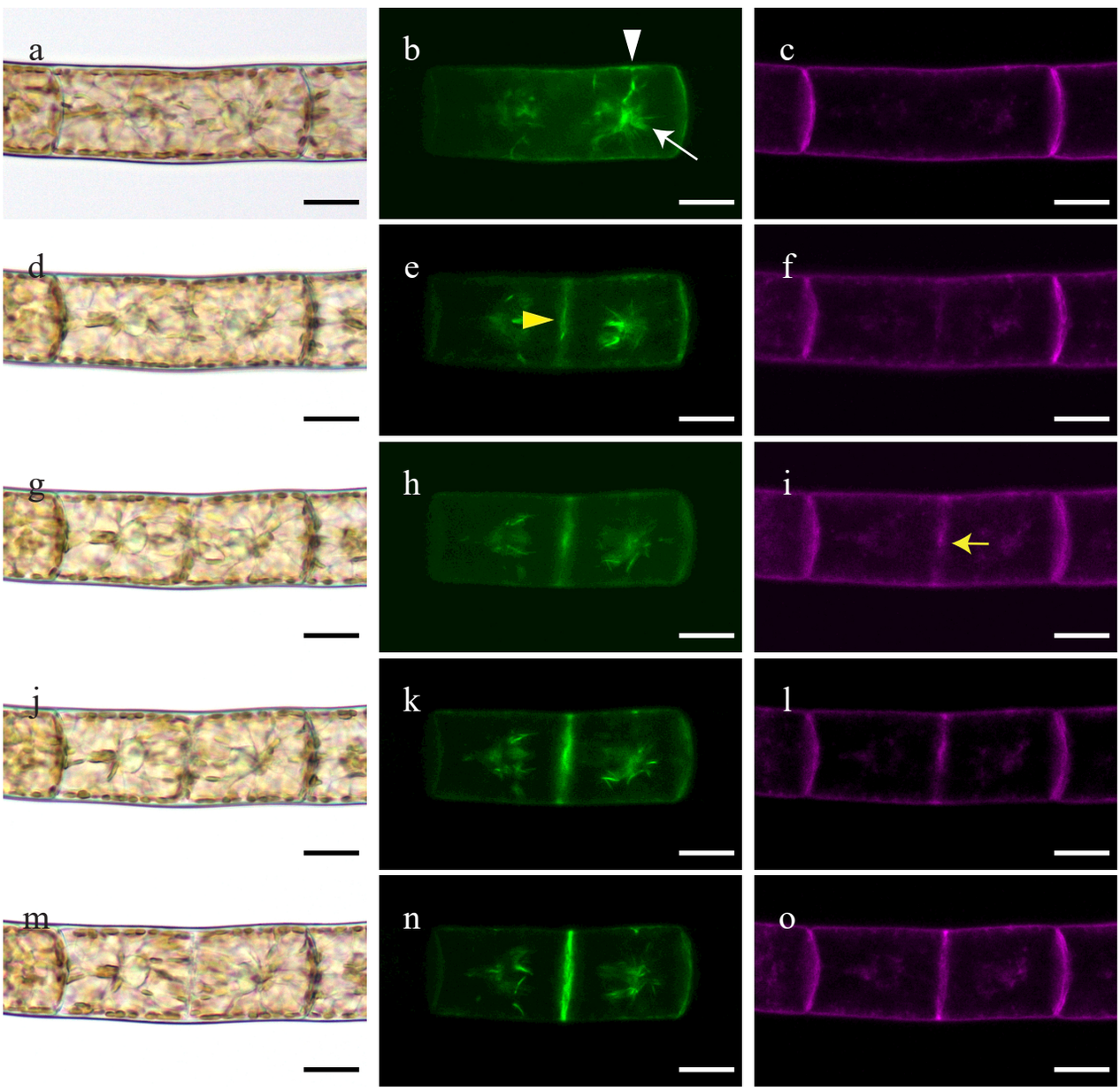


Plate 23

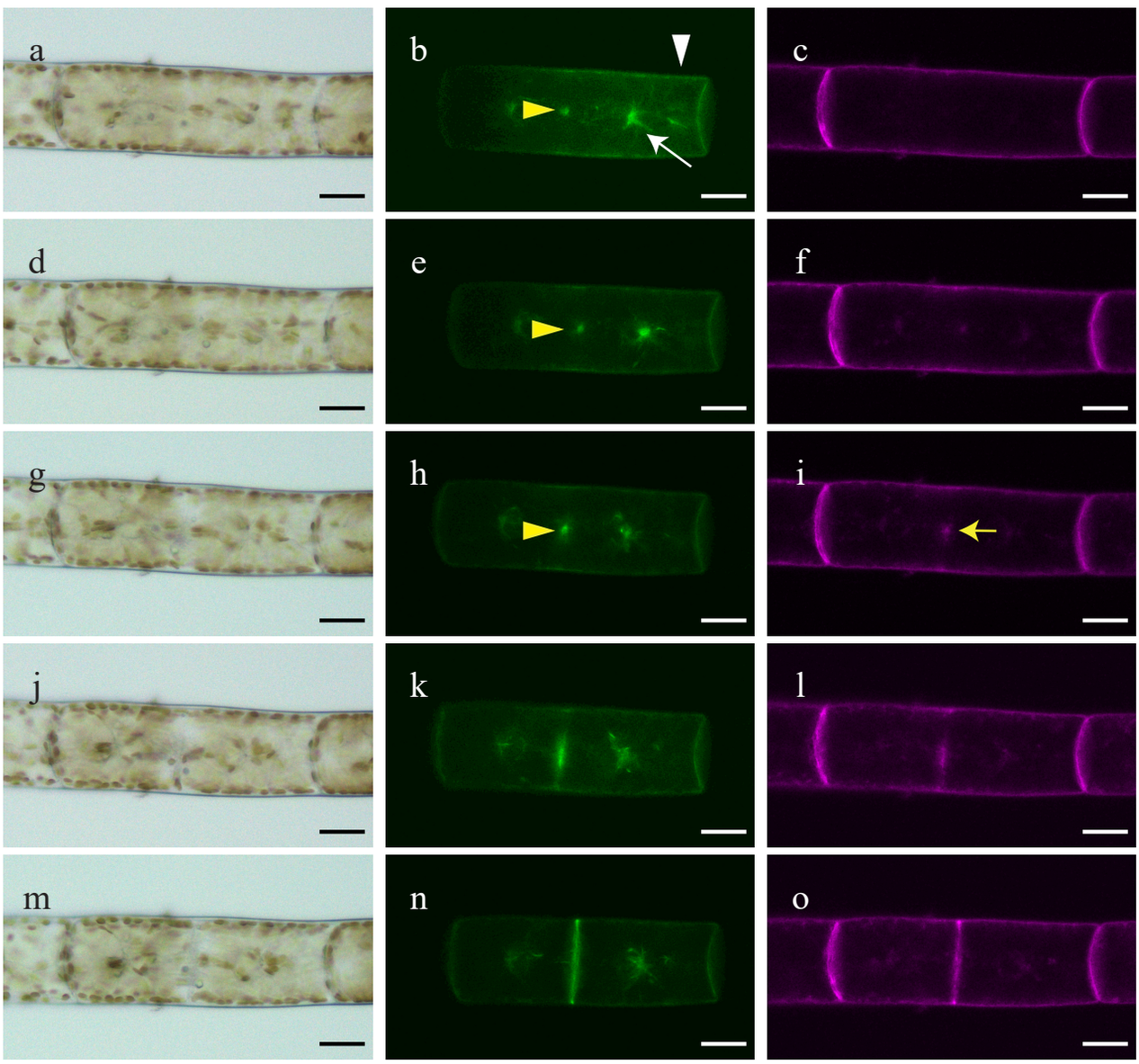


Plate 24

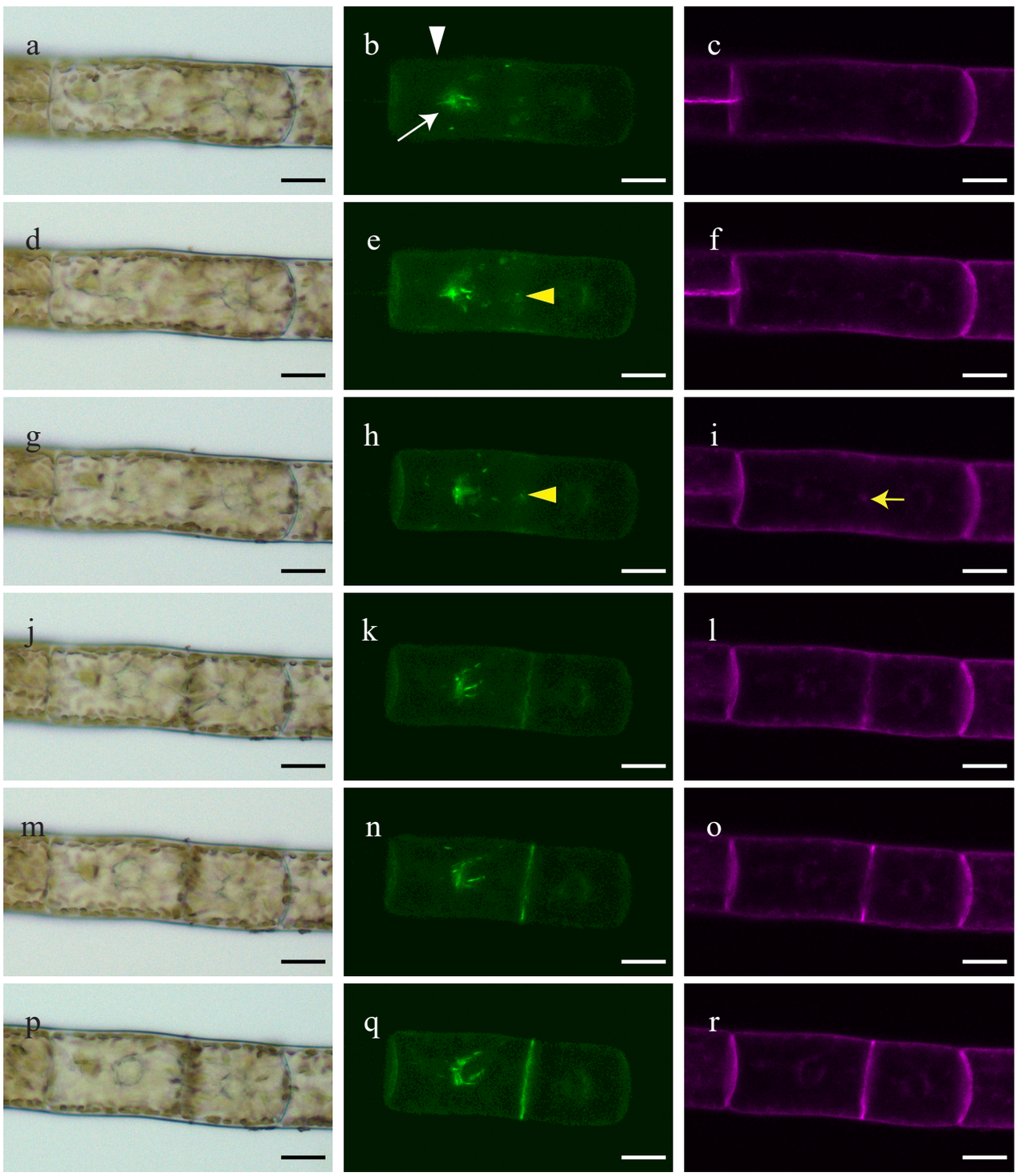


Plate 25

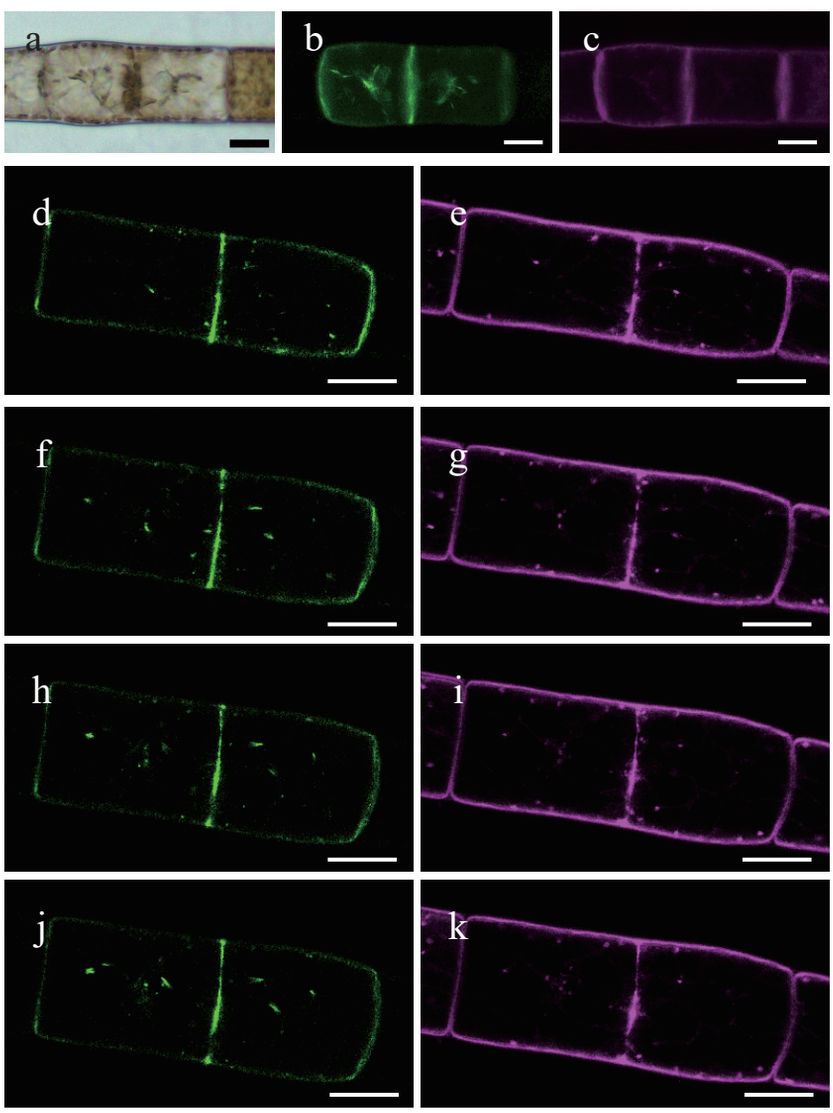


Plate 26

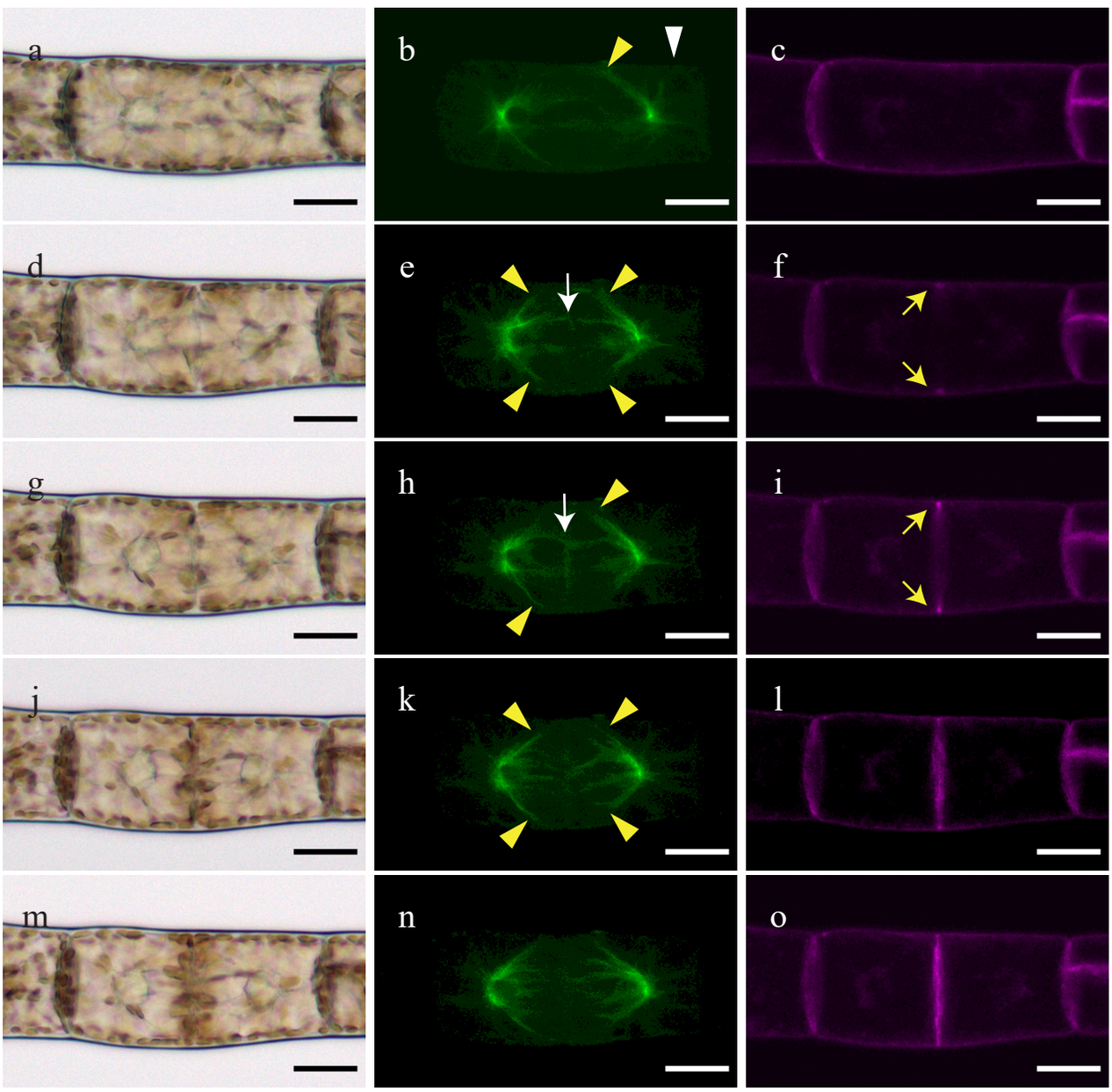


Plate 27

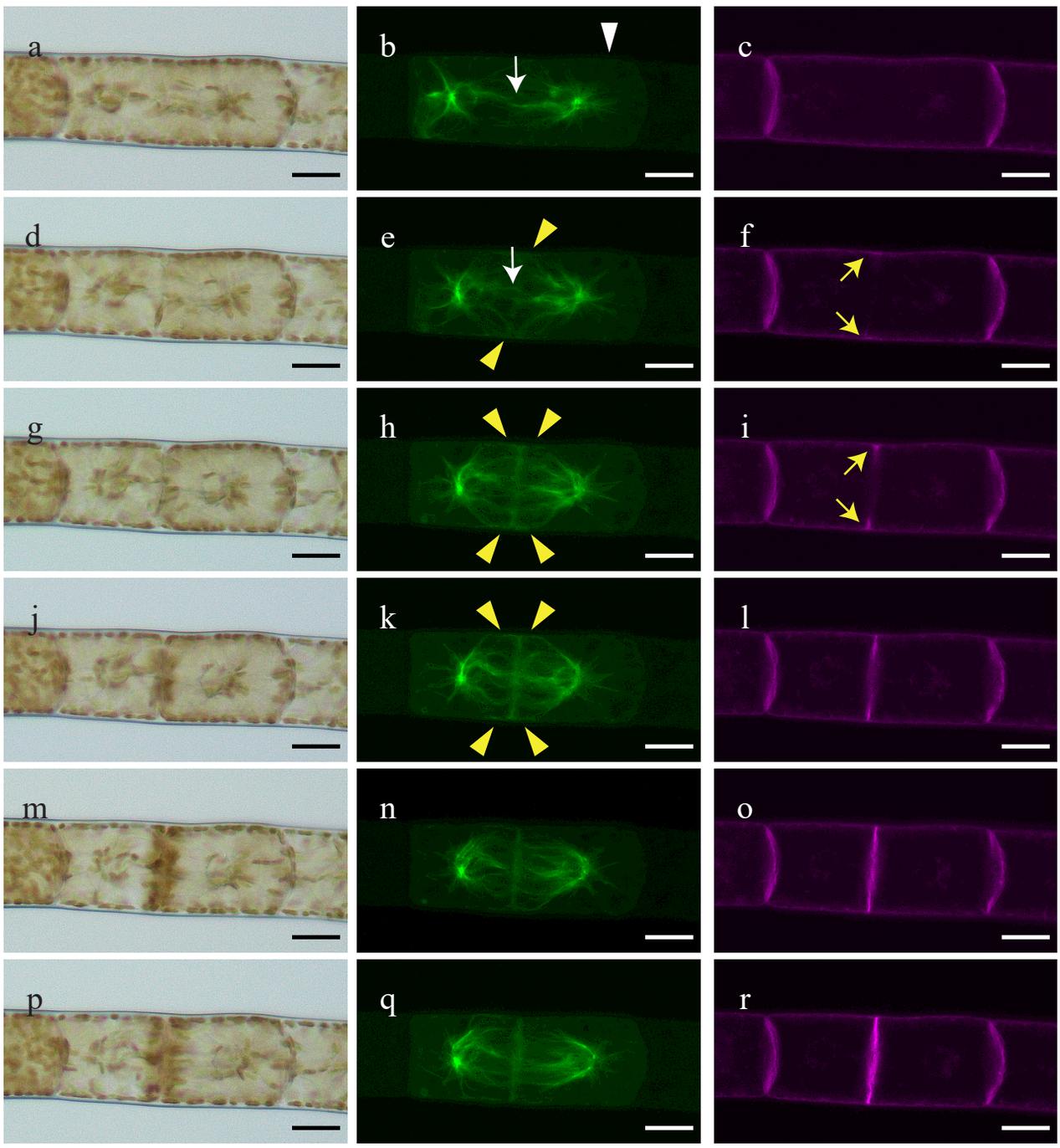


Plate 28

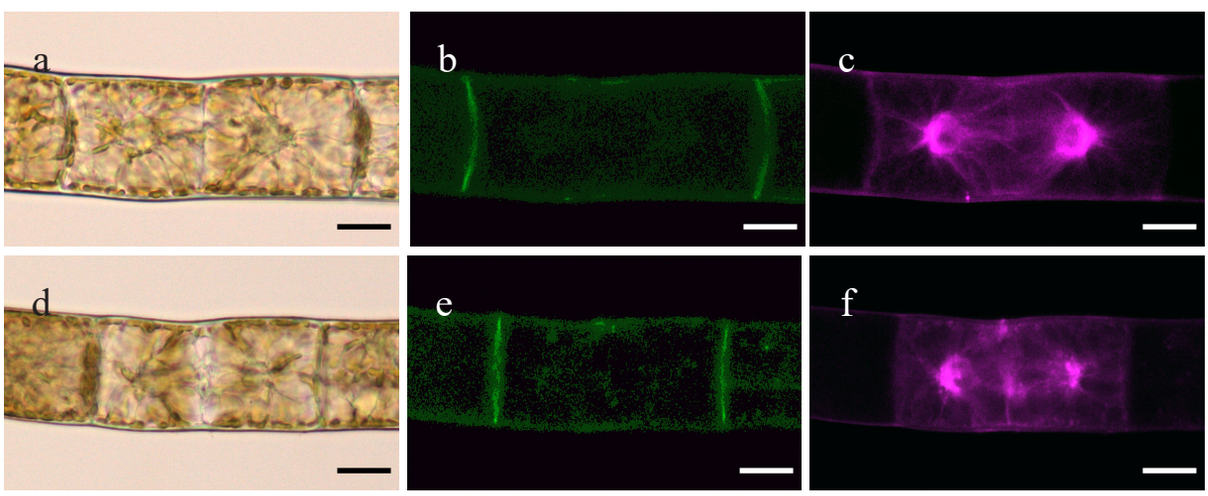


Plate 29

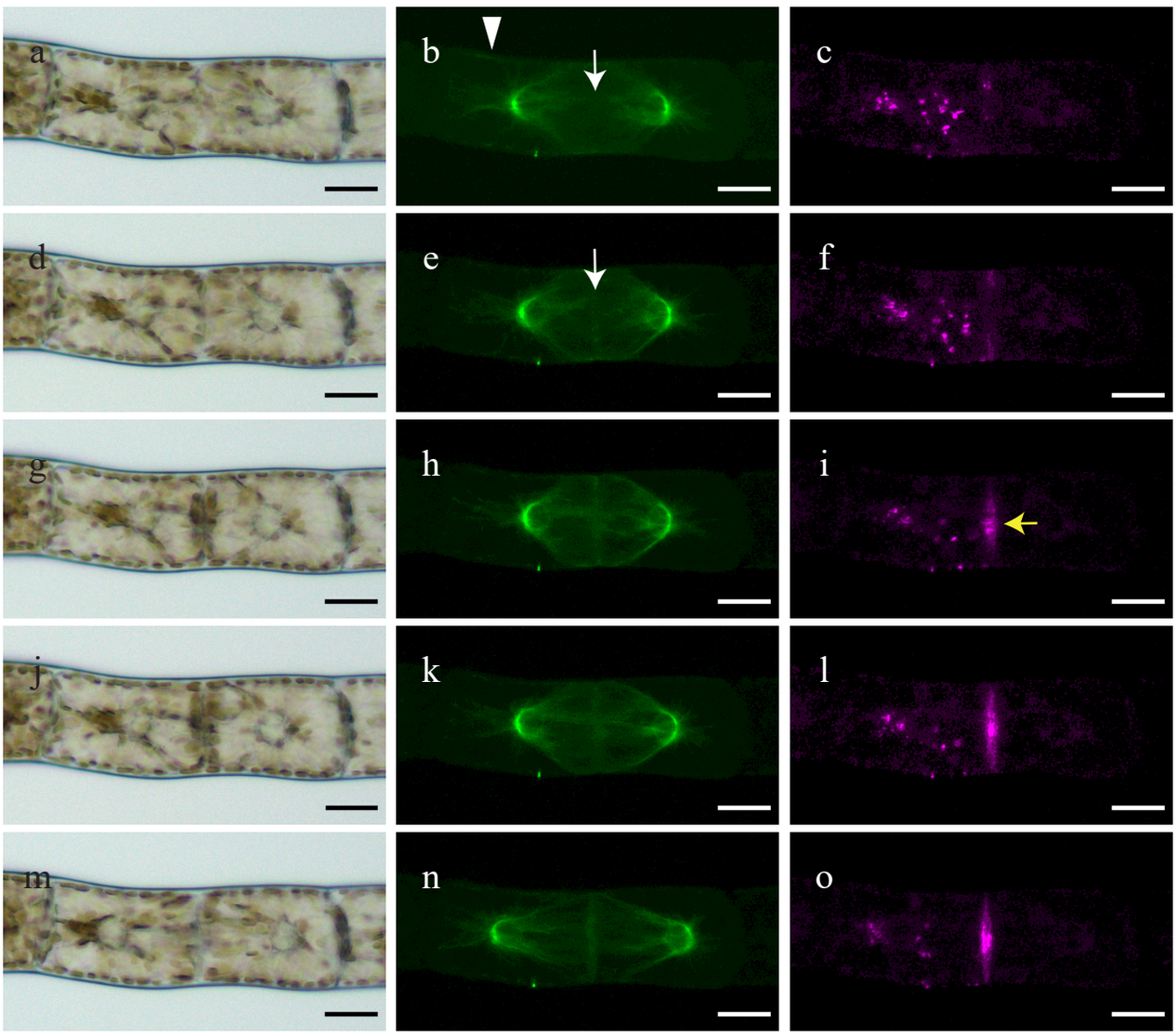


Plate 30

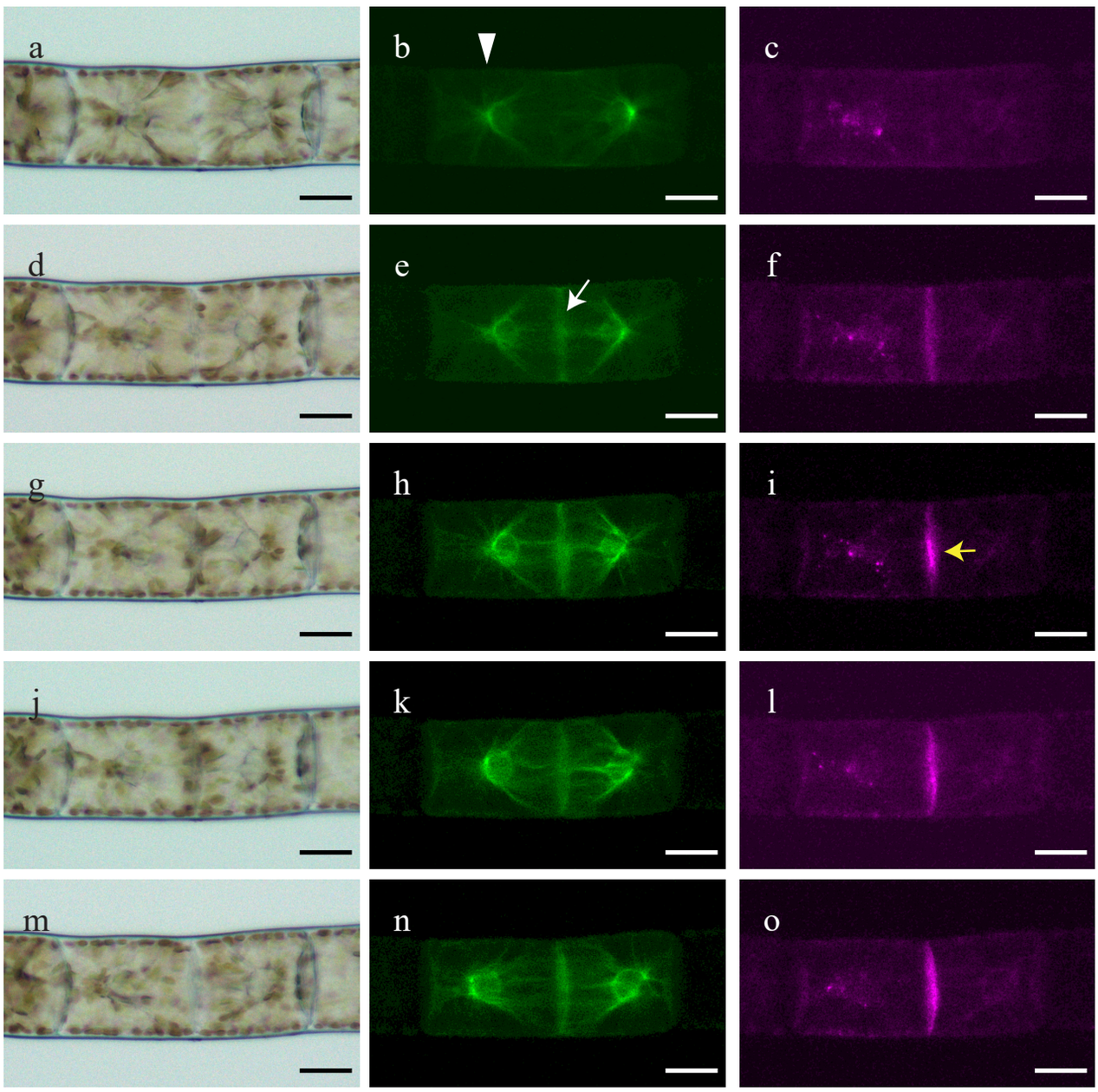


Plate 31

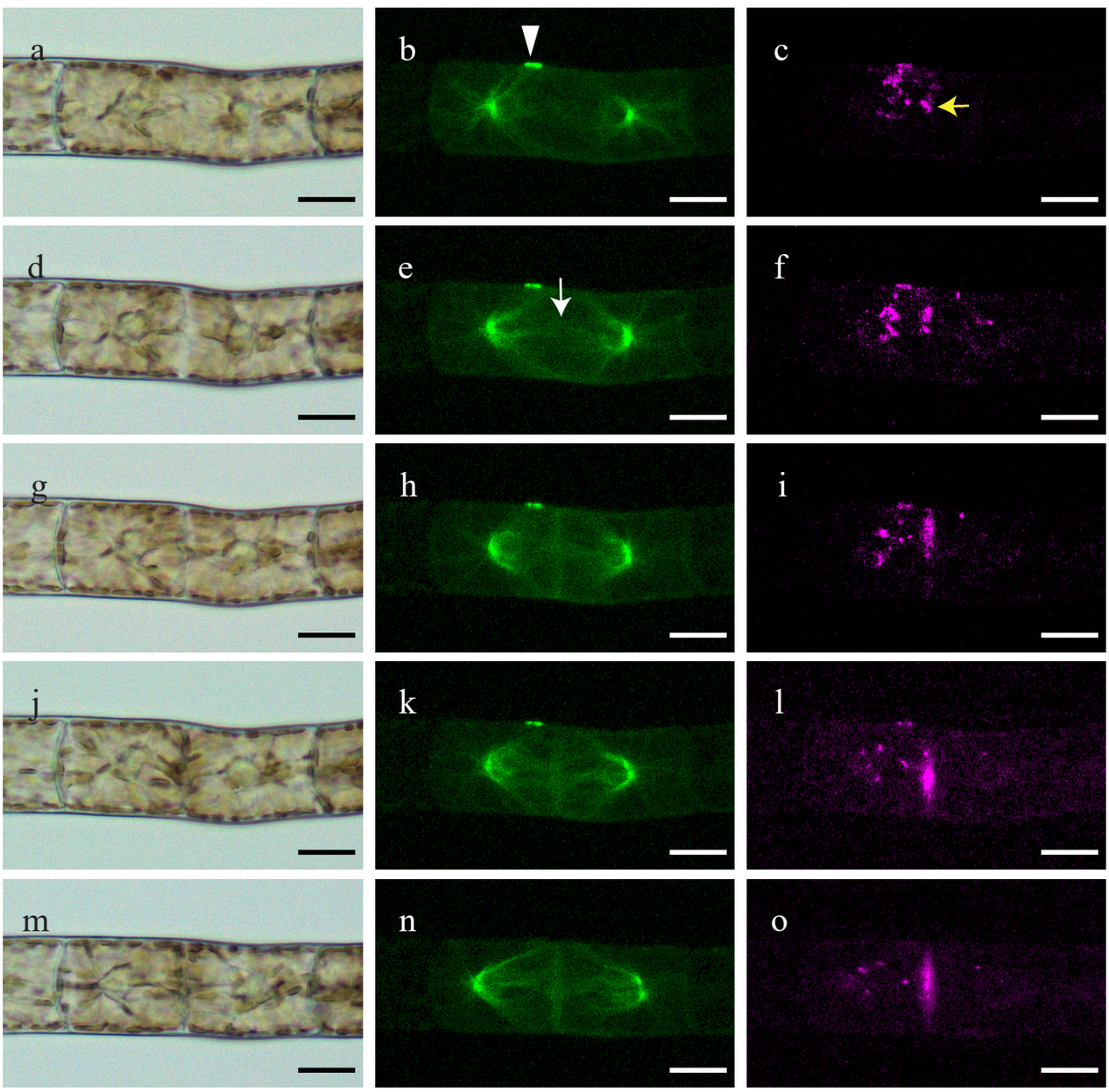


Plate 32

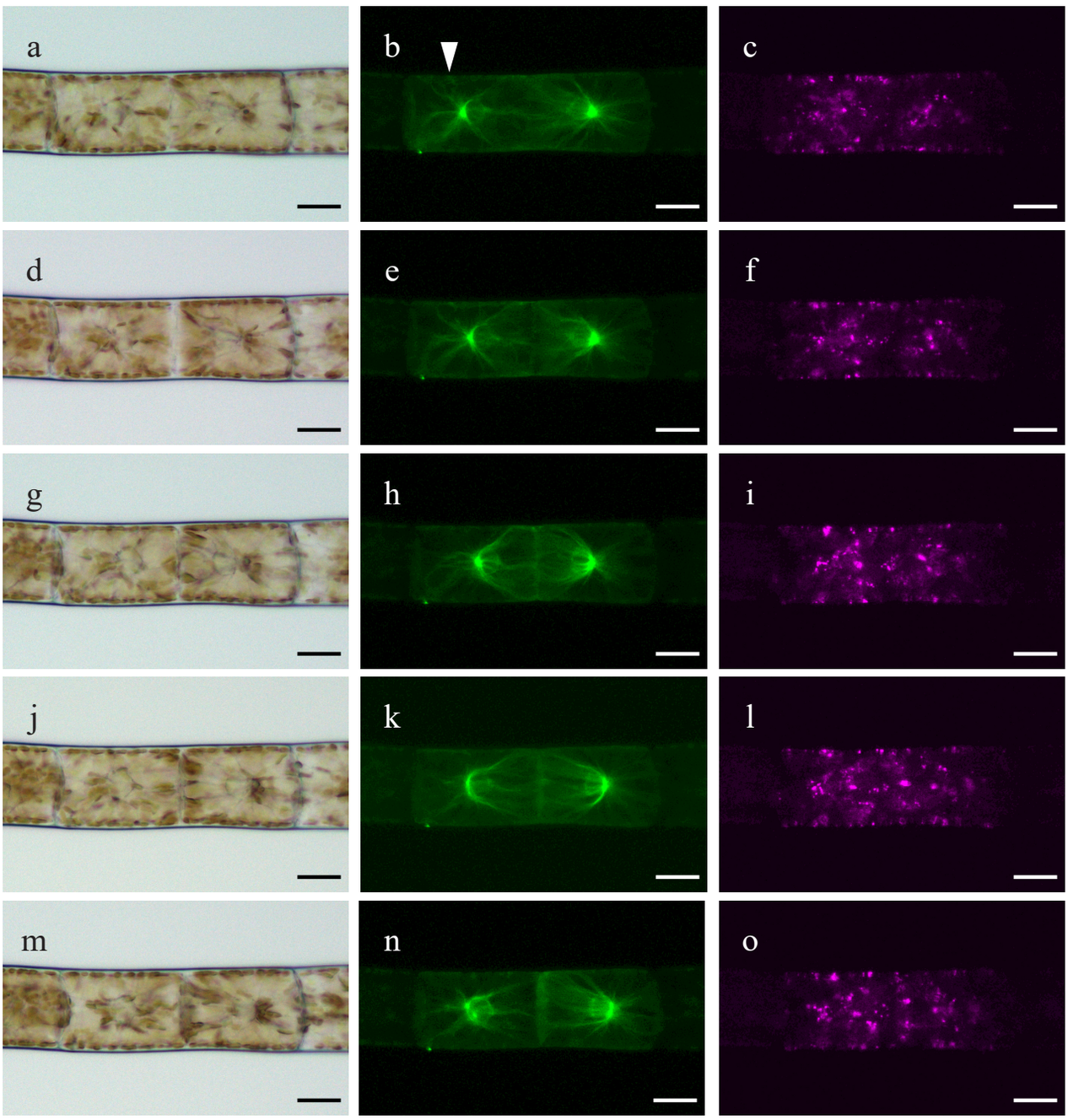


Plate 33

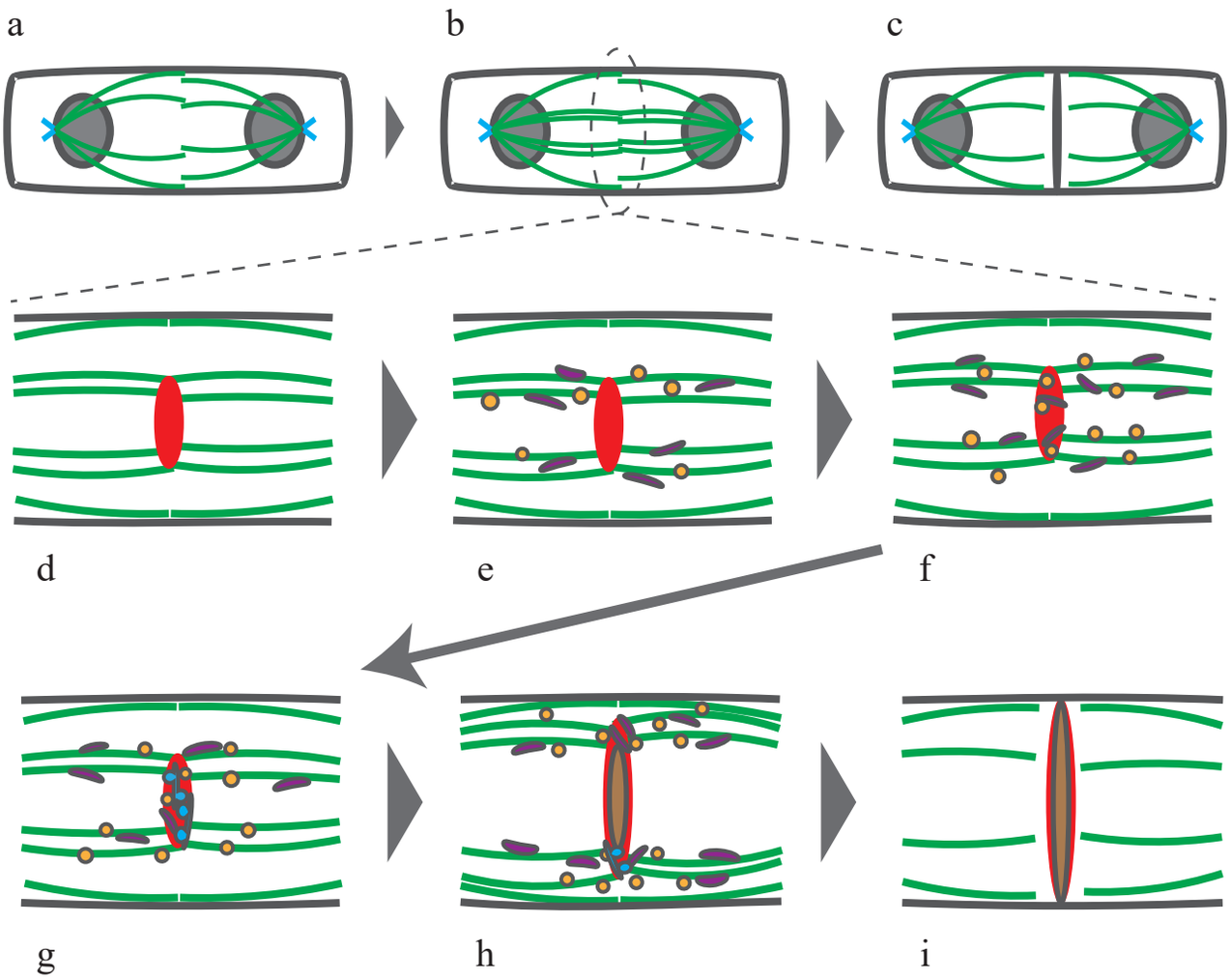


Plate 34